Engineering Research Center

For

Environmentally Benign Semiconductor Manufacturing

Annual Report

February 2007

Section 1

Core Projects

List of Core Projects

1. An Integrated, Multi-Scale Framework for Designing Environmentally-Benign Copper, Tantalum and Ruthenium Planarization Processes (P915; Thrust A)
   Philipossian (UA), Boning (/MIT), and Beaudoin (Purdue)

2. Environmentally Benign Electrochemically Assisted Chemical Mechanical Planarization (P908; Thrust A)
   Raghavan (UA), Philipossian (UA), and Boning (MIT)

3. EHS Impact of Electrochemical Planarization Technologies (P910, Thrust A)
   Alen West (Columbia)

4. Low Environmental-Impact Processing of sub-50 nm Interconnect Structures (P914, Thrust A)
   Gleason (MIT) and Muscat (UA)

5. Environmentally Benign Vapor-Phase and Supercritical CO_2 Processes for Patterned Low- k Dielectrics (P911, Thrust A)
   Gleason (MIT), Ober (Cornell), and Watkins (U Massachusetts)

6. Non-PFOS/non-PFAS Photoacid Generators: Environmentally Friendly Candidates for Next Generation Lithography (P905, Thrusts D)
   Ober (Cornell) and Sierra (UA)

7. CMOS Biochip for Rapid Assessment of New Chemicals (P904, Thrust C)
   Mathine (UA) Bahl (UA), and Runyan (UA)

8. Environmentally-Friendly Cleaning of New Materials and Structures for Future Micro- and Nano-Electronics Manufacturing (P919; Thrusts B and C)
   Nishi (Stanford), Raghavan (UA), and Shadman (UA)

9. Low-Water and Low-Energy Rising and Drying of Patterned Wafers and Nano-structures (P918, Thrust C)
   Shadman (UA). Vermeire (ASU)

10. Reductive Dehalogenation of Perfluoroalkyl Surfactants in Semiconductor Effluents (P909, Thrust C)
    Sierra (UA), Jacobsen (UA), and Wysocki (UA)

11. Destruction of Perfluoroalkyl Surfactants in Semiconductor Process Waters using Boron Doped Diamond Film Electrodes (P913, Thrust C)
    Farrell (UA), Sierra (UA), and Raghavan (UA)

12. ESH Assessment: Materials, Structures and Processes for Nano-scale MOSFETs with High-Mobility Channel (Thrust B)
    Saraswat and McIntyre (Stanford)

An Integrated, Multi-Scale Framework for Designing Environmentally-Benign Copper, Tantalum and Ruthenium Planarization Processes

Personnel:

PIs:

- Ara Philipossian: Chemical and Environmental Engineering (UA)
- Duane Boning: Electrical Engineering and Computer Science (MIT)
- Steve Beaudoin: Chemical Engineering (Purdue)

Other Research Personnel:

- Yun Zhuang: Chemical and Environmental Engineering (UA)
- Fransisca Sudargho: Chemical and Environmental Engineering (UA)
- Leonard Borucki: (Araca Incorporated)
- Ed Paul: Visiting Scientist (MIT)

Graduate Students:

- Yasa Sampurno: Chemical and Environmental Engineering (UA)
- Rumin Zhuang: Chemical and Environmental Engineering (UA)
- Hong Cai: Materials Science and Engineering (MIT)
- Daniel Truque: Electrical Engineering and Computer Science (MIT)
- Xiaolin Xie: Physics (MIT)
- Bum Soo Kim: Chemical Engineering (Purdue)
- Caitlin Kilroy: Chemical Engineering (Purdue)
- Gautam Kumar: Chemical Engineering (Purdue)

Undergraduate Students:

- Anita Lee: Chemical and Environmental Engineering (UA)
- Geoff Steward: Chemical and Environmental Engineering (UA)
- Jessica Torres: Chemical Engineering (Purdue)

Objectives:

This objective is to perform fundamental scientific investigations of copper, tantalum, and ruthenium CMP processes over several length scales and levels of complexity. A deeper and more comprehensive understanding of the physical and chemical processes will help to reduce consumption and wastes associated with the processes.

Background:

Future integrated circuits will critically depend on the ability to planarize and form inlaid structures using chemical-mechanical polishing (CMP). CMP is essential not only in the advanced interconnect structures using copper and low-k dielectrics, but also in front end device formation involving shallow trench isolation (STI) and in alternative transistor formation processes (e.g. inlaid metal gates). However, existing CMP processes are known to suffer from a number of environmental, performance and cost concerns. These include an excessive consumption of costly slurry and pad materials, generation of

by-product wastes containing substantial solids, consumption of water, and substantial processing times requiring significant energy. Performance limitations include imperfect feature planarization (dishing and erosion), over-polish or endpoint control challenges, wafer-level uniformity and repeatability difficulties, and throughput limitations. As the industry also explores new materials (e.g. ruthenium) and interconnect technologies, the polishing and planarization process must undergo further evolution to meet environmental as well as performance requirements.

A powerful and fundamental approach to significantly reducing consumption and wastes associated with copper, tantalum and ruthenium processes is to develop a deeper and more comprehensive understanding of the physical and chemical processes that control polishing and to use this understanding to drive changes in consumables and polishing protocols. This approach offers the inherent advantage of simultaneously addressing issues of productivity, performance, and environmental concerns. For this vision to be realized, several key enabling technologies need to be developed and integrated. In this research, we are focusing on two key areas which we believe provide maximum leverage for evolution of polishing technology, particularly for future advanced interconnect: (1) Fundamental understanding of individual and combined mechanisms contributing to consumable wear, and the integration of these mechanisms to develop topography evolution models for the sub-100Å regime for dishing and erosion; and (2) development of real-time sensing and detection, coupled with modeling of pattern evolution, for optimal and flexible control of the process.

We are structuring our research along two primary tasks: Task 1, which focuses on fundamental understanding of copper, tantalum, and ruthenium polishing processes, and Task 2 which focuses on in-situ metrology (coupled with modeling) to improve the control and operation of the processes.

Task 1: Fundamental Understanding of Copper, Tantalum, and Ruthenium CMP Processes

There are two subtasks in this task. The summary for each subtask is as follows:

Subtask 1.1: Effect of Conditioning Force on Pad Topography and Removal Rate during Copper CMP

In CMP processes, diamond conditioners provide rate stability by counteracting the degrading influences of abrasive wear and plastic deformation on pad surface, and by preventing the buildup of debris and byproducts from wafer polishing. Since varying conditioning forces create different pad topography and therefore different polishing rates, optimum conditioning force may be achieved when both the requirements of reduction of consumables and high polishing performance are satisfied. The EHS impact of CMP would decrease if such a conditioning force can be determined.

The objective of this subtask is to determine how conditioning force affects pad topography, coefficient of friction (COF), pad temperature and removal rate. We further aim to study pad surface evolution, and by modeling of removal rate and kinetic rate constants, we hope to correlate pad surface profile descriptors with kinetic rate constants.

Method of Approach:

Experiments were performed using a 200-mm Fujikoshi polisher modified at the University of Arizona for real-time shear force analysis. Experimental data were collected and compared at two conditioning forces of 2.5 and 4.9 lb-f on a 4-inch Mitsubishi Materials Corporation TRD disc with 200-grit diamonds sweeping at 0.33 Hz and rotating at 30 RPM. Wafer sliding velocities of 0.37, 0.94 and 1.22 m/s were chosen to avoid resonance with the sweep period and to produce uniform conditioning. Polishing pressures were set at 1, 2 or 3 PSI. The pad and the slurry were D100 and iCue 600Y75, respectively (manufactured by Cabot Microelectronics Corporation). During polishing, shear force and pad temperature data at the wafer leading edge were acquired in real-time. Active diamond counts at the two conditioning forces were determined by a novel method. To quantify the pad topography evolution, pad coupons were extracted after certain polishing conditions and then measured with surface profilometry. Mean peak spacing, mean peak curvature and surface roughness were defined and compared. A Langmuir-Hinshelwood model was used to explore removal rate data in detail. Pad surface data were then used to calculate Langmuir-Hinshelwood model parameters. By studying the pad topography and the removal rate under the two conditioning forces, physical theory connecting conditioning force with removal in copper polishing could be verified.

Highlights of Results and Accomplishments:

At both conditioning forces, removal rates show non-Prestonian behavior. At moderate values of pV, copper removal rate depends on the conditioning force (Fig. 1).

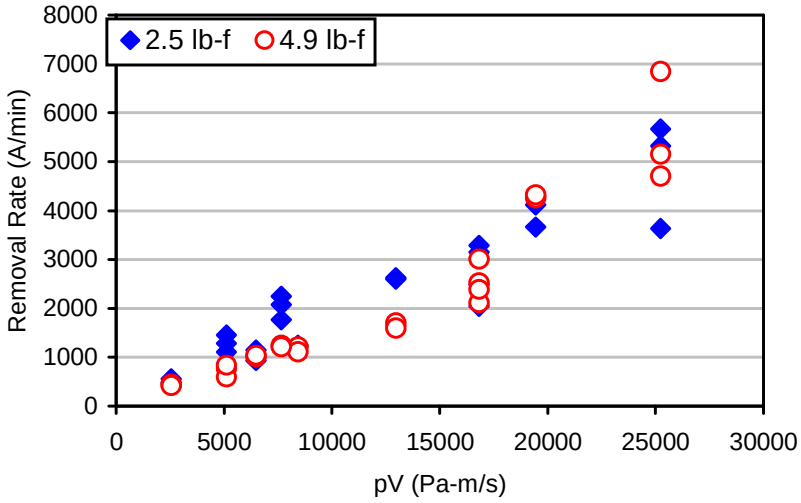

Figure 1. Removal rates at 2.5 and 4.9 lb-f conditioning forces.

COF ranges between 0.4 and 0.6, indicating that the mechanism is that of boundary lubrication (Fig. 2). COF is similar at the two conditioning forces as per the Wilcoxon signed-rank test.

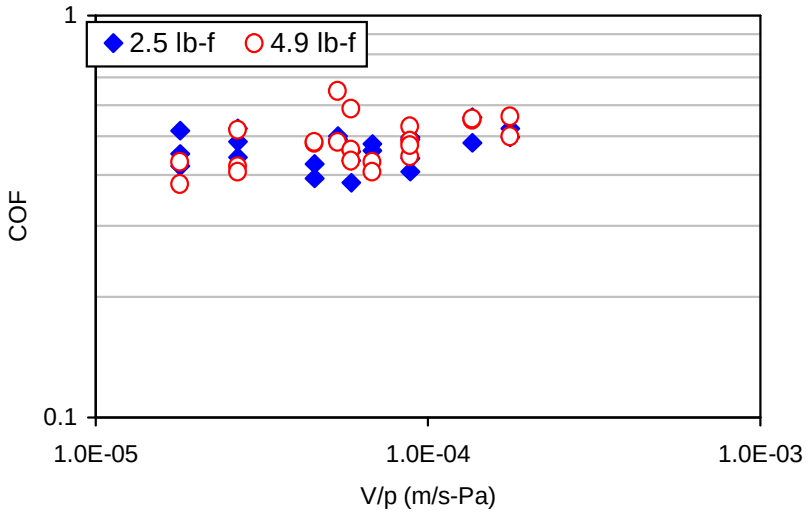

Figure 2. COF at 2.5 and 4.9 lb-f conditioning forces.

As values of pV increase, average pad temperature increases from around 25 to 32 degree Celsius. Pad temperature is generally higher at 2.5 lb-f conditioning force than at 4.9 lb-f conditioning force. For removal rate, at both conditioning forces, simulation agrees well with experimental data and successfully captures the non-Prestonian behavior as well as the large scatters at higher values of pV (Figs. 3 and 4).

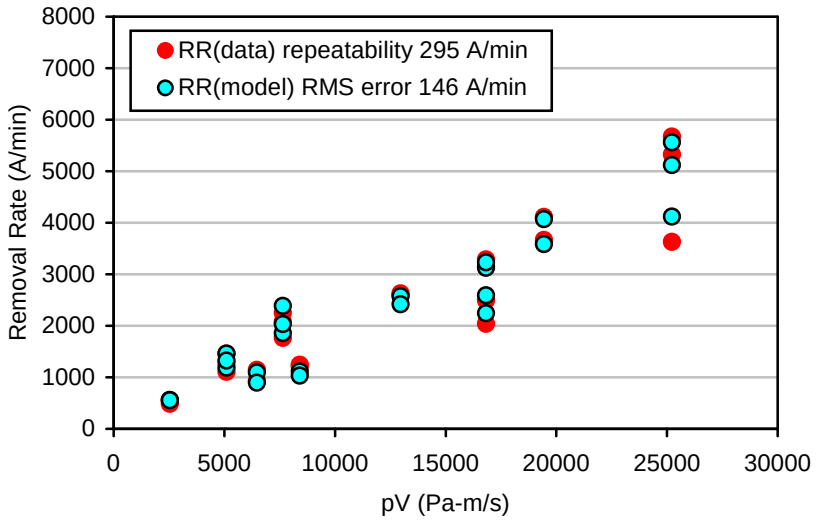

Figure 3. Comparison of simulated removal rates with experimental data at 2.5 lb-f conditioning force.

Figures 5 and 6 show the simulated chemical rate and mechanical rate constants at 2.5 and 4.9 lb-f, respectively. Simulated chemical rate is considerably larger at 2.5 lb-f conditioning force than at 4.9 lb-f. Mechanical rate is slightly higher at 2.5 lb-f conditioning force at some pV conditions. By comparing the ratio of chemical rate

constant to mechanical rate constant, it indicates that the polishing is more mechanically limited at 2.5 lb-f than that at 4.9 lb-f conditioning force.

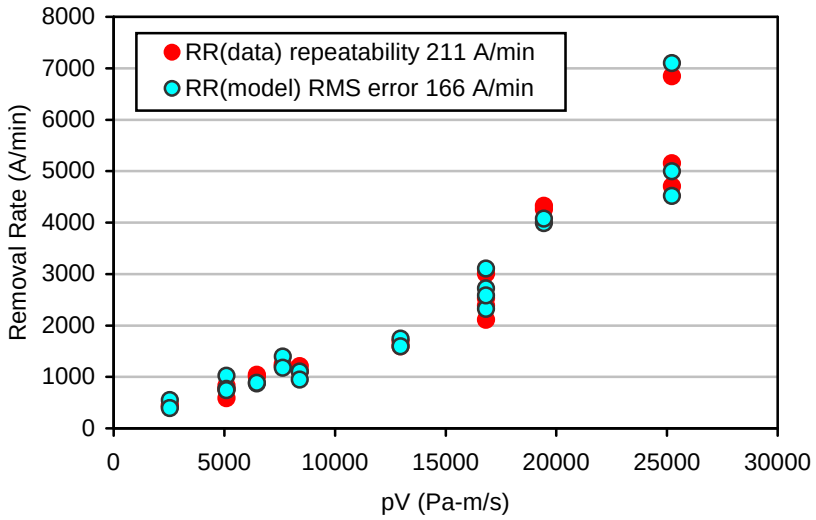

Figure 4. Comparison of simulated removal rates with experimental data at 4.9 lb-f conditioning force.

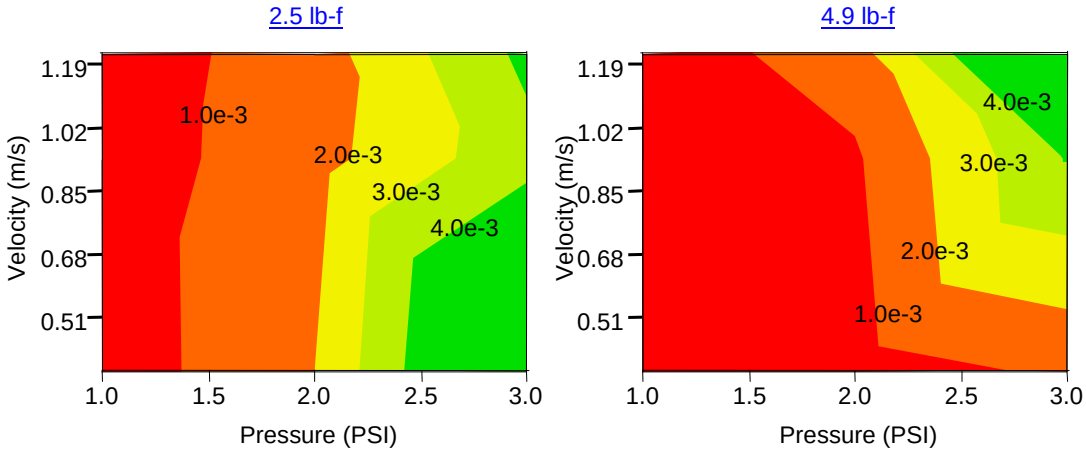

Figure 5. Simulated chemical rate constants at 2.5 and 4.9 lb-f conditioning forces.

Mean peak spacing, mean peak curvature and surface roughness are extracted from pad surface profilometry analysis (Fig. 7). Mean peak spacing decreases as the conditioning force increases. This is consistent with an increase in the active diamond count. At the higher conditioning force, diamonds cut the pad surface deeper; as a result, the peaks become sharper rendering a higher mean peak curvature. In addition, the surface height probability density function (PDF) has a wider tail and the value of lambda is larger, indicating that the surface becomes rougher.

With the extracted pad surface data, a conditioning theory is used to independently calculate the flash heating parameter β and the proportionality constant c_p of mechanical rate constant expression. The calculated values are very close to those

extracted from the Langmuir-Hinshelwood model. This reveals a strong correlation between the pad surface profile and the kinetic rate constants and therefore indicates the physical meaning of the fitting parameters c_p and β in the Langmuir-Hinshelwood model. In this study, the physical theory connecting conditioning force with pad topography and removal rate in copper polishing is successfully verified.

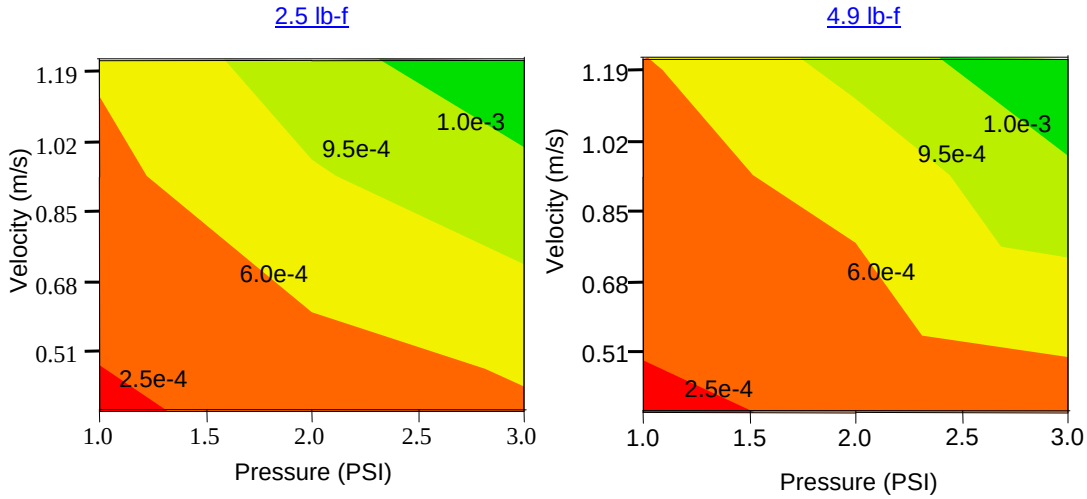

Figure 6. Simulated mechanical rate constants at 2.5 and 4.9 lb-f conditioning forces.

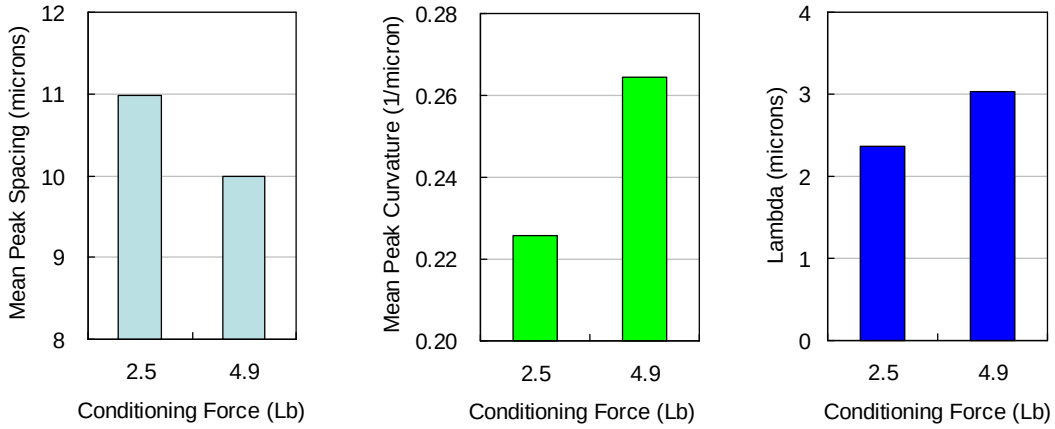

Figure 7. Pad surface profilometry analysis at 2.5 and 4.9 lb-f conditioning forces.

Industrial Interactions and Technology Transfer:

- Cliff Spiro and Mike Lacy: Cabot Microelectronics Corporation
- Naoki Rikita: Mitsubishi Materials Corporation

ESH Impact:

- Potential for 2X increase in conditioner and pad life due to 2X reduction in diamond disc down-force. This will reduce consumption of pads and diamonds and increase tool uptime by lowering the number of 'pit-stops'.

Conference Presentations:

- Rumin Zhuang, Leonard Borucki, Yun Zhuang, Mike Lacy, Cliff Spiro and Ara Philipossian, "Effect of Conditioning Force on Pad Topography and Removal Rate during Copper CMP", *11th International Symposium on Chemical-Mechanical Planarization*, Lake Placid, NY, August 13 – 16, 2006.
- Rumin Zhuang, Leonard Borucki, Yun Zhuang, Mike Lacy, Cliff Spiro and Ara Philipossian, "Effect of Conditioning Force on Pad Topography and Removal Rate during Copper CMP", *2006 International Conference on Planarization/CMP Technology*, Foster City, CA, October 12 – 13, 2006.

Next Year Plan:

- Investigating the effect of diamond grit size and conditioning force on pad surface through macro-scale/micro-scale characterization and incremental loading test.
- Determining pad hardness and pad porosity's impact on polishing performance.

Subtask 1.2: Investigation of Electrochemical Reactions on Copper Surface

A fully quantitative representation of CMP would require information about the presence and residence time of slurry particles at the pad-wafer interface. To obtain information about particle residence time at the pad-wafer interface, it is necessary to understand the particle-wafer adhesion forces. In order to model the measured adhesion forces effectively, it is essential to understand the electrochemical reactions occurring on the wafer surface, so that the compositionally appropriate layer on the wafer surface can be considered in the force calculations. The objective of this subtask is to investigate the electrochemical reactions on copper surface so that slurry particle interactions with copper surface can be characterized.

Method of Approach:

There are two approaches that are most commonly used to describe particle adhesion to surfaces, a thermodynamic approach and a force-based approach. The force approach is most appropriate for the CMP systems considered here. Figure 8 is a schematic showing an asymmetric particle adhering in the vicinity of a rough substrate. The interactions of interest in this case include van der Waals (vdW) and electrostatic (ES) interactions. Chemical bonds are important in many systems, but are not encountered in these proposed studies. Hydrophobic interactions may also be important in aqueous systems, but they are not significant for particles at CMP conditions compared to the other forces. vdW forces are present in all systems, and in the absence of chemical bonding, these forces are the most significant component of the adhesive force when a particle is in contact with or within up to 15 nm of a surface. While ES forces are often described in terms of electrostatic double layers, there are many CMP-relevant cases of particle adhesion where fully-formed double layers do not exist. For this reason, full ES forces, and not simply ES double layer forces, must be considered to describe particle-wafer interaction during CMP. Beaudoin and his students have developed a method for measuring and modeling particle-substrate interactions that is partially illustrated in Fig. 8. With this approach, particles of interest are mounted on the tip of atomic force

microscope cantilevers and their adhesion forces against substrates of interest are measured directly, in liquids of interest. Following the force measurements, a second AFM cantilever is used to measure the roughness of the particle and substrate, after which a combined FIB/SEM apparatus is used to prepare cross-sections of the particle. The cross-sections, combined with the roughness data, are used to prepare a 3-D model of the particle. The measured substrate roughness is used to develop a 3-D model of the polished surface. Both surfaces are discretized into nanoscale elements, and the vdW and ES forces between the two surfaces are calculated as a function of particle-substrate separation distance. Figure 9 shows a comparison between predicted and measured adhesion forces for a micron-scale silica particle adhering with a TEOS-sourced oxide surface in DI water. A very important aspect of Beaudoin's work with particle adhesion is that the modeling results are scaleable, which means that models can be validated for micron-sized particles and the forces that would be exerted by nanoscale particles can be accurately predicted. Hence, the method of approach for this work is to mount micron-scale particles on AFM cantilevers, measure their adhesion forces against substrates of interest in CMP, model these forces, and then scale the models to the nanoscale to describe the interaction forces for nanoscale particles.

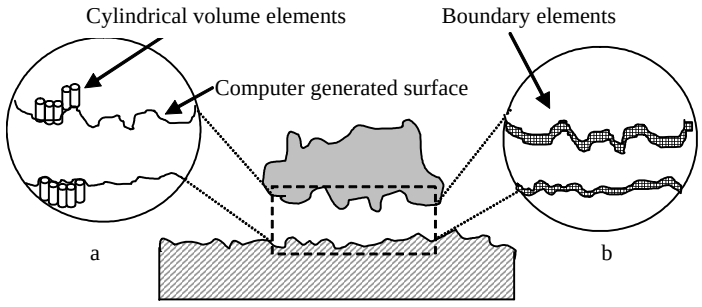

Figure 8. Schematic of existing computation of vdW and ES forces.

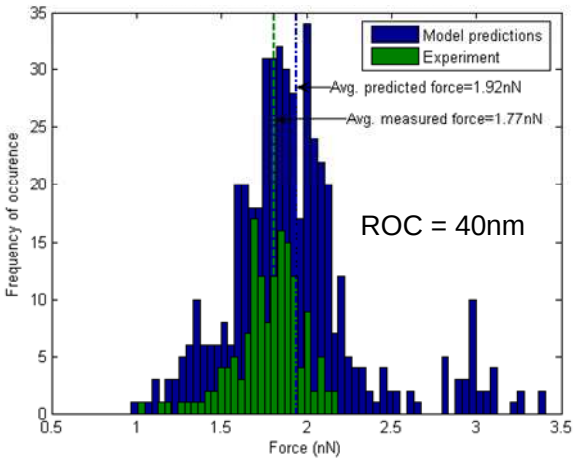

Figure 9. Measured (300 measurements) and modeled (1000 predictions) adhesion between Si_3N_4 cantilever with 40 nm radius of curvature (ROC) on tip and chrome (with surface oxide) substrate in DI water.

Highlights of Results and Accomplishments:

There are a number of accomplishments to report. The most exciting are real-time analyses of Cu electrochemistry which may allow a window into the interfacial processes occurring during polishing. Figure 10 shows a home-made guillotine electrode apparatus designed and fabricated in our lab. With this apparatus we can track the electrochemical processes occurring on Cu surfaces in real time, in direct simulation of the electrochemistry that occurs on a Cu wafer after a slurry particle abrades the surface.

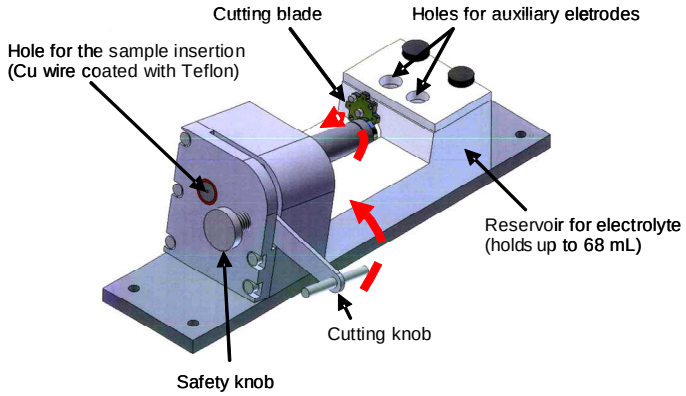

Figure 10. Home-made guillotine electrode for real-time observation of Cu electrochemistry at CMP-relevant conditions.

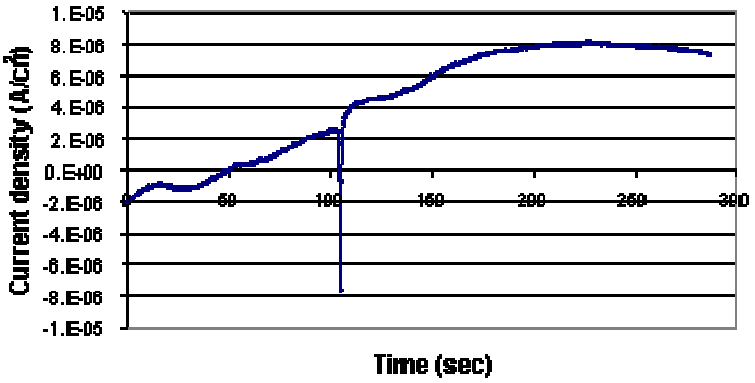

Figure 11. Electrochemical reactions on Cu surface within guillotine electrode (commercial Cu slurry with 5 wt% H_2O_2)

In Fig. 11, a Cu wire (with no Teflon coating) was immersed in commercial Cu slurry containing 5% H_2O_2 in the guillotine electrode and the current (electrochemical reaction rate) was monitored. Figure 11 shows that initially, Cu dissolves, but after about 50 seconds, passivation of the Cu becomes dominant. However, when the wire is cut there is an instantaneous spike in the current due to dissolution, and then an instantaneous return to the passivation driven system. In planned work, the sides of the Cu wire will be Teflon-coated, such that the only electrochemistry being monitored is at the wire tip. This will dramatically enhance the resolution of the studies of Cu behavior during CMP.

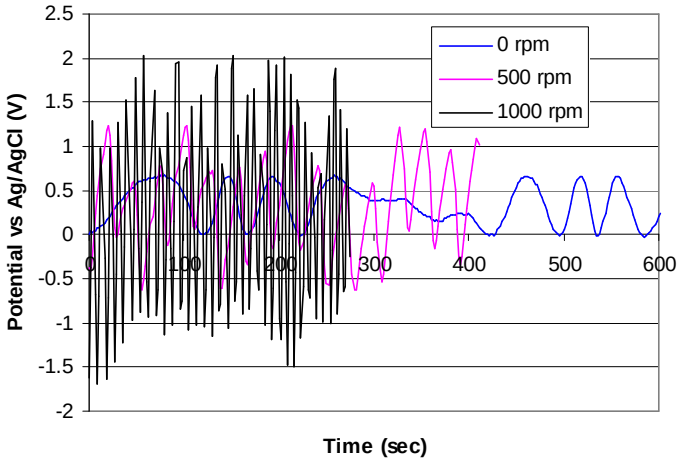

Figure 12. Potential oscillations on Cu surface resulting from mass transfer and surface reaction effects in aqueous 2.25 M HCl and 0.43 M H_2O_2.

A balance of mass transfer and surface reaction effects will dictate the surface reactions occurring during CMP. We have studied this phenomenon in detail in a model system, with a goal of developing a modeling framework that can describe these effects. In Fig. 12, the potential oscillations occurring during the dissolution/passivation of Cu in a solution of 2.25 M HCl and 0.43 M H_2O_2 are shown. These were obtained using a Cu disk in a rotating disk apparatus. As the rotational speed of the disk increases, the rate of mass transfer of reactants/products to and from the disk surface increases. As shown in Fig. 12, the frequency and amplitude of the oscillations increase with increasing mass transfer, suggesting that wider swings of dissolution/passivation occur with increasing mass transfer rates, and that they occur more quickly. A preliminary model has been developed in our lab that describes these mass transport and reaction phenomena.

Conference Presentations:

- Beaudoin, S., "Particle Adhesion over Multiple Length Scales", *Fifth International Surface Cleaning Workshop, Northeastern University/NSF Center for Microcontamination Control*, November, 2006.
- Butterbaugh, J., and Beaudoin, S., "Particle Adhesion and Removal", *FSI International Knowledge Services Seminar Series*, Tel Aviv, Israel, October 2006.
- Beaudoin, S., "Particle Adhesion and Removal", *FSI International Knowledge Services Seminar Series*, Grenoble, France, October 2006.
- Beaudoin, S., "Particle Adhesion and Removal", *FSI International Knowledge Services Seminar Series*, Dresden, Germany, October 2006.
- Beaudoin, S., "Particle Adhesion during Microelectronic Manufacturing", *Eighth International Symposium on Ultraclean Processing of Silicon Surfaces*, Antwerp, Belgium, September 2006.
- Kumar, G., Smith, S., and Beaudoin, S., "Adhesion of Particles to Surfaces – Scaling from the Micron to the Nanometer Size", *Adhesion Society Annual Meeting*, February 2006.

Next-Year Plan:

In the next year, we will complete the modeling studies of the mass transfer and reaction effects on Cu electrochemistry, and will use these to model Cu surface composition during CMP. We will continue particle adhesion studies to Cu surfaces. Combined with modeling results, we will develop new models for effects of Cu reactions and particle-wafer interactions on CMP. We will also repeat the process used for the Cu system to describe Ru polishing.

Task 2: In-situ Metrology Coupled with Modeling to Improve Control and Operation of CMP Processes

There are three subtasks in this task. The summary for each subtask is as follows:

Subtask 2.1: Feasibility of Real-time Detection of Abnormality in Inter Layer Dielectric Slurry during Chemical Mechanical Planarization Using Frictional Analysis

Agglomeration of abrasive particles, large abrasive particles as well as solidified particles generated along the slurry supply system are the main causes of the defect formation during chemical mechanical planarization (CMP). Mechanical abrasion by large abrasive particles is the major mechanism creating micro-scratches. If critical defects are formed in the wafer surface, the wafer may be discarded. Otherwise, it requires further re-processing, which consumes more consumables, generates more wastes, and decreases overall throughput.

Numerous studies have focused on detecting changes in the large particle tail of the slurry particle size distribution (PSD). The rate of formation of particle agglomerations from small particles is measured *in-situ* along the slurry supply system. However, separate study indicated that abrasive particles in injected slurry tend to agglomerate during polishing process due to fluctuations in local particles or salt concentration under dynamic processing conditions. Hence, real-time methodologies are needed to give an advance warning as to detecting the presence of defect causing particles during polishing process.

The objective of this subtask is to investigate the feasibility of utilizing shear force measurement to detect the presence of large particles in slurry in order to reduce scratch defects during chemical mechanical planarization.

Method of Approach:

Polishing tests were performed using a 100-mm wafer polisher with capability to measure shear force in real-time during polishing. Prior to wafer polishing, a Rohm and Haas IC1020 M-groove pad was conditioned with a 100-grit diamond disc for 30 minutes with DI water. Two slurries were used to polish 100-mm blanket silicon wafers with 6000 Å thermally grown silicon dioxide: Fujimi PL-4217 slurry with 12.5% weight percent of 0.1 μm abrasive silica, Fujimi PL-4217 slurry with 12.5% (weight percent) of 0.1 μm abrasive silica contaminated with 0.5% (weight percent) of 0.9 μm alumina. Each wafer was polished for 75 seconds. The polishing pressure was 28 kPa and the pad-wafer sliding velocity was 1.12 m/s. Shear force data was collected at 1000 Hz during

polishing. Fast Fourier Transformation (FFT) was implemented to convert the fluctuating component of shear force from time domain to frequency domain.

Highlights of Results and Accomplishments:

For the Fujimi PL-4217 slurry contaminated with alumina, it can be calculated that there is about 1 alumina particle for every 20,000 silica particles. Table 1 shows that the removal rate is not affected by the presence of alumina particles. On the other hand, coefficient of friction and shear force variance are significantly affected by the presence of infinitesimal amount of alumina particles in the slurry, thereby suggesting that these particles actually participate in the polishing.

Table 1. Removal rate, COF, and variance of shear force for pure and contaminated Fujimi PL-4217 slurries.

Slurry	Removal Rate (Å/min)	COF	Variance of Shear Force (lb_f^2)
Pure PL-4217	1636 (54)	0.27 (0.01)	1.35 (0.40)
Contaminated PL-4217	1632 (140)	0.46 (0.01)	4.29 (0.54)

Values in parentheses are standard deviations

Figure 13 shows the comparison of the raw shear force data for the pure Fujimi PL-4217 slurry and contaminated slurry. Higher shear forces are observed for the contaminated slurry confirming that the alumina particles are transported effectively to the pad-wafer region. Larger alumina particles abrade the wafer surface more aggressively than silica particles, resulting in higher shear forces. The contaminated slurry also induces larger shear force variations than the pure Fujimi PL-4217 slurry as summarized in Table 1. The presence of larger abrasive particles leads to an unequal distribution of applied load on the wafer surface, contributing to a less stable polishing process. Such significant increase in shear force variance as well as COF associated with the contaminated slurry shows it is feasible to implement frictional measurement technique to detect slurry abnormality in real-time during CMP process.

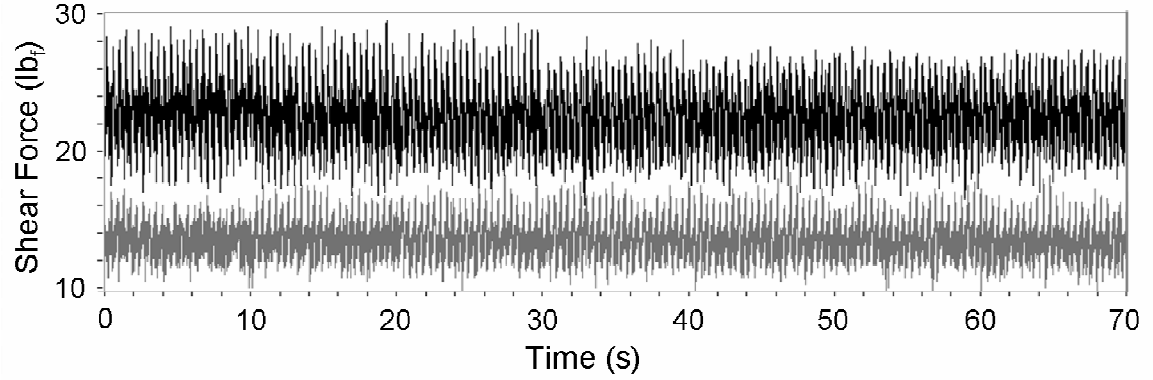

Figure 13. Comparison of raw shear force data for pure Fujimi PL-4217 slurry (grey curve) and contaminated Fujimi PL-4217slurry (black curve).

Fast Fourier Transformation (FFT) was implemented to convert the fluctuating component of shear force from time domain to frequency domain. To exclude the peaks resulting from the intrinsic vibration of the tool, the spectral amplitude of the polishing run is subtracted by the spectral amplitude of the baseline process in which the polisher was run with the wafer completely disengaged from the pad. Figure 14 shows that the pure and contaminated Fujimi PL-4217 slurries induce similar stick-slip signature. However, the contaminated slurry results in higher spectral amplitudes than the pure Fujimi PL-4217 slurry as shown in Table 2.

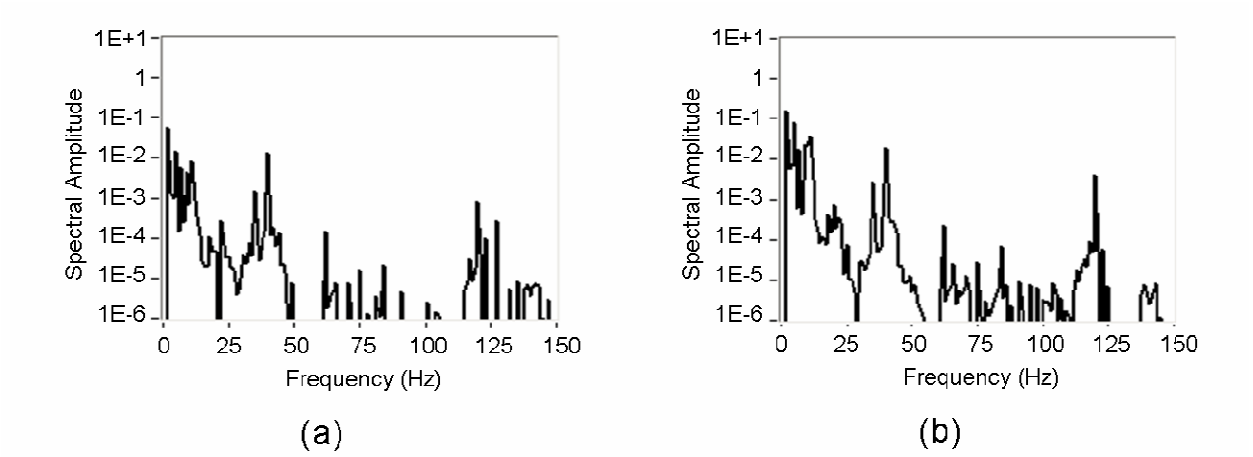

Figure 14. Shear force spectral analysis for (a) pure and (b) contaminated Fujimi PL-4217 slurries.

Table 2. Spectral amplitudes for pure and contaminated Fujimi PL-4217 slurries.

	Spectral Amplitude		
Slurry	**0 - 15 Hz**	**30 - 50 Hz**	**115 - 130 Hz**
Pure PL-4217	0.82 (0.21)	0.15 (0.01)	0.02 (0.00)
Contaminated PL-4217	3.45 (0.47)	0.24 (0.01)	0.04 (0.01)

Values in parentheses are standard deviations

When particles make contacts with wafer surface, it can be assumed that large and small particles roll at the same linear velocity since the wafer surface drags the particles at equal sliding velocity. Hence, the interaction between the wafer surface and large particles induces lower rolling frequencies compared to small particles in order to achieve the same linear velocity. Such interaction may explain why the shear force spectral amplitude in the low frequency range of 0 – 15 Hz is significantly higher for the contaminated slurry than the pure Fujimi PL-4217 slurry as shown in Table 2.

Figure 15 shows the normalized shear force spectral amplitudes for the pure and contaminated Fujimi PL-4217 slurries. The normalized shear force spectral amplitude at certain frequency is calculated by dividing the shear force spectral amplitude at this frequency by the total spectral amplitude from 0 to 500 Hz. Therefore, Fig. 15 shows the

shear force spectral amplitude distribution in different frequencies. Table 3 summarizes the shear force spectral amplitude distribution in three frequency ranges. Results indicate that large particles in the contaminated Fujimi PL-4217 slurry lead to a higher spectral amplitude distribution in the low frequency range of 0 – 15 Hz (91.5% vs. 81.0% for the pure Fujimi PL-4217 slurry).

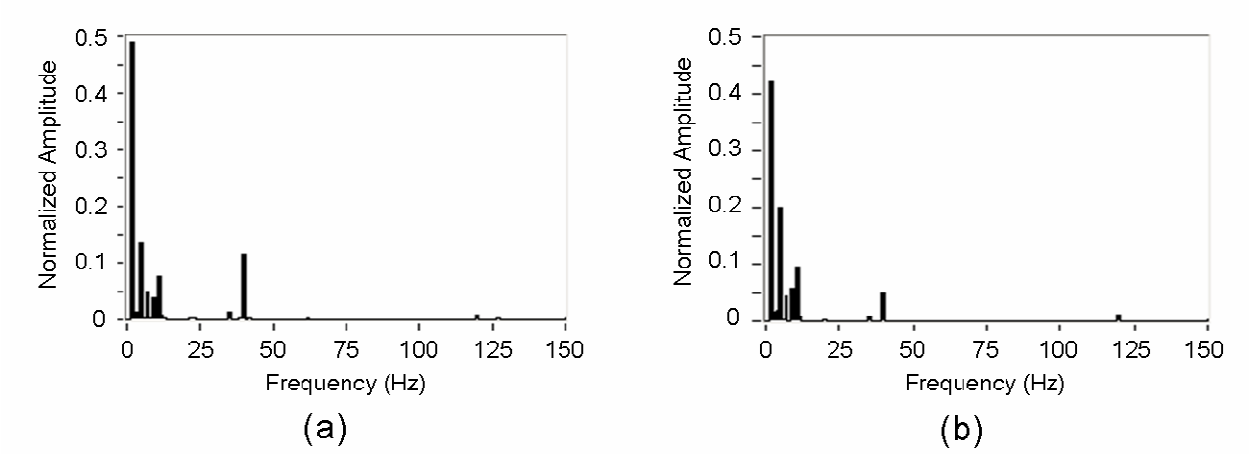

Figure 15. Normalized shear force spectral amplitudes for (a) pure and (b) contaminated Fujimi PL-4217 slurries.

Table 3. Normalized spectral amplitude for pure and contaminated Fujimi PL-4217 slurries.

	Normalized Spectral Amplitude (%)		
Slurry	**0 - 15 Hz**	**30 - 50 Hz**	**115 - 130 Hz**
Pure PL-4217	81.0 (4.3)	15.7 (3.4)	1.7 (0.6)
Contaminated PL-4217	91.5 (1.1)	6.4 (0.7)	1.1 (0.3)

Values in parentheses are standard deviations

Industrial Interactions and Technology Transfer:

- Michael Goldstein: Intel Corporation

ESH Impact:

This study shows it is feasible to utilize real-time shear force measurement to detect the presence of large particles in slurry during chemical mechanical planarization. It lays the groundwork for slurry quality monitor, which helps to improve manufacturing throughput and reduce consumable usage and waste generation.

Conference Presentation:

- Yasa Sampurno, Yun Zhuang, Fransisca Sudargho, Michael Goldstein, and Ara Philipossian, "Detection of Slurry Abnormality during ILD CMP Using Real-Time Frictional Force Measurement and Analysis", *2006 International Conference on Planarization/CMP Technology*, Foster City, CA, October 12 – 13, 2006.

Next-Year Plan:

Slurries with different types and concentrations of particles will be used for ILD and copper CMP to investigate abrasive particle's effect on the frictional, thermal, and kinetic attributes of polishing processes.

Subtask 2.2: Pad Asperity Modeling

A key issue in order to improve the performance of CMP, especially to reduce dishing and erosion is to better understand the effect of pad surface and bulk properties. In past models of pad surface topography evolution using semi-empirical pattern density and step-height dependencies, we have ignored the detailed characteristics of pad asperity height and size distributions. To enable an integrated model that incorporates the experimental observation and characterization of pad properties (investigated elsewhere in this project), we have developed a model that explicitly accounts for the statistical properties of the pad surface. The approach is shown schematically in Fig. 16.

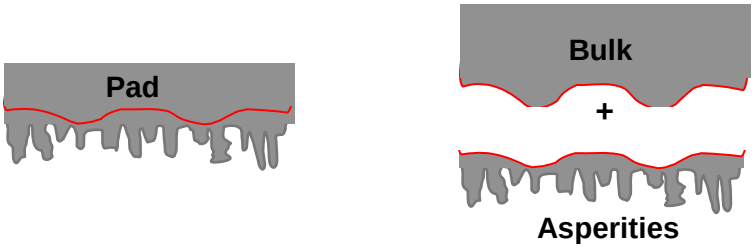

Figure 16. Decomposition of pad into bulk region (governed by contact wear pressure-displacement dependencies) and surface asperities (governed by statistical distributions of asperities size and heights).

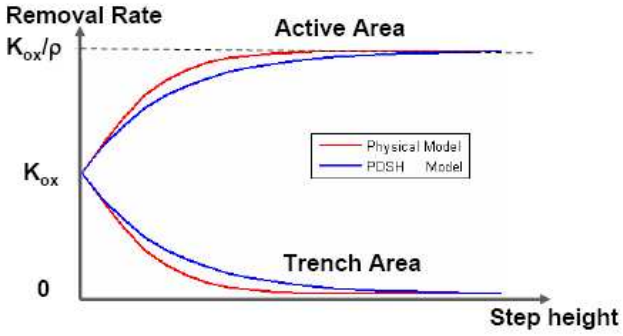

Figure 17. Removal rate vs. step-height, derived using an exponential distribution for asperity height, in comparison to the older pattern-density-step-height (PDSH) model.

The bulk pad distributes the overall down force across the chip surface; the regional pressures are calculated using a contact wear model. The pad surface, on the other hand, is represented using the distribution of pad asperity heights and sizes, resulting in a more physically based representation of removal rate versus step height, as shown in Fig. 17.

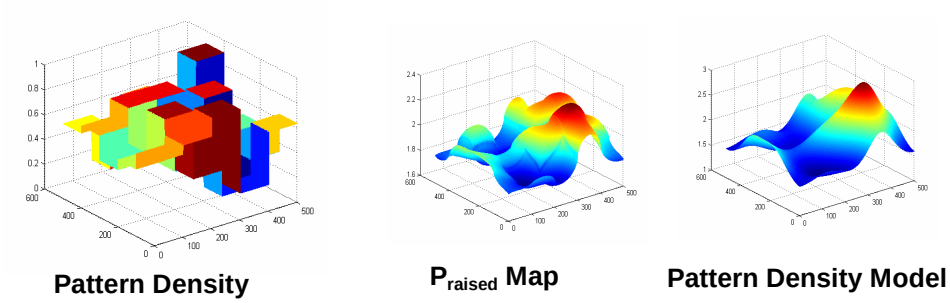

Figure 18. Chip-scale topography resulting from varying pattern densities across the chip (shown at left); for the new physically-based pad asperity model (center) versus the older empirical pattern density model (right).

The prediction of the resulting chip-scale topography evolution, as shown in Fig. 18, is improved compared to the older pattern density model. The new model helps to resolve the unclear dependency of the "contact height" (point at which recessed regions between features experience removal or dishing), by noting that a small fraction of "tall" and small asperities can result in appreciable removal when a conventional continuum pad elastic model would suggest no dishing would occur. The model also enables coupling with the direct physical observations of pad-wafer contact area under different loading conditions, as well as confocal microscope or other measurements of pad surface heights.

Subtask 2.3: Plating/CMP Modeling and Process Co-Optimization

A major result this year is the completion of an integrated chip-scale model for multilevel copper interconnects, and demonstration of the application of the model for co-optimization of the process. Three components of this accomplishment are (1) improvements to the electrochemical deposition (ECD) model; (2) extensions and to the CMP model for asperity and multilevel effects and integration with the ECD model; and (3) application to reduction of plating thickness, using the model to design a new "in-pattern" dummy fill pattern.

The chip-scale copper ECD model is physically based, considering copper ion depletion effects, and surface additive adsorption and desorption. The plating model is able to predict the initial topography for subsequent CMP modeling with sufficient accuracy and computational efficiency. A compatible chip-scale CMP model has been developed that integrates contact wear and density-step-height approaches, so that a consistent model framework can be used for copper bulk polishing, copper over-polishing, and also barrier layer polishing stages. A variant of this CMP model is developed which explicitly considers the pad topography properties. Finally, ECD and CMP parts are combined into an integrated model applicable to single level and multilevel metallization cases, so that the topography remaining in a lower level can be handled when predicting the upper level metal dishing and erosion.

The integrated multilevel copper metallization model is applied to the co-optimization of the plating and CMP processes. An alternative in-pattern (rather than between-pattern) dummy fill strategy is proposed, as shown in Fig. 19. The key idea is to

design dielectric posts and segments that sit within large copper regions, to improve both the plating process (by increasing sidewall surface area to increase plated thickness), and the CMP process (posts to hold up the polishing pad and reduce asperity-induced dishing). The integrated ECD/CMP model is applied to the optimization of the in-pattern fill, to achieve improved ECD uniformity and final post-CMP topography, as seen in the thickness maps and histograms in Figs. 20 and 21. An important result of the co-optimization is that the copper seed and plating thickness is reduced to 4000 Å, from the 8500 Å in the non-optimized process, with corresponding substantial savings in both ECD and CMP process time, cost, and waste production.

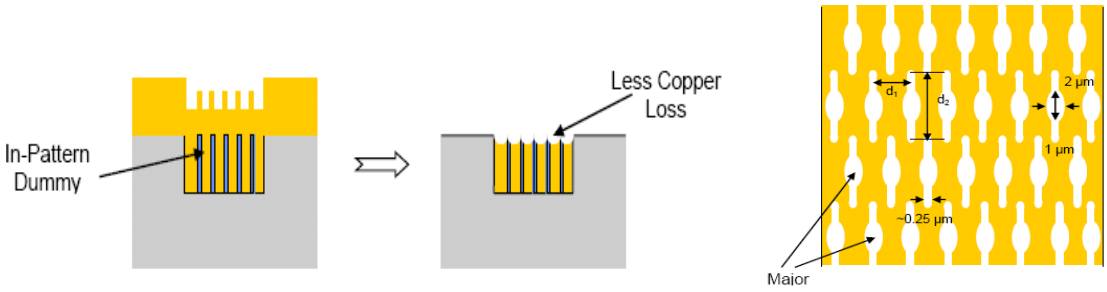

Figure 19. Use of "in-pattern" dummy fill, to reduce the dishing problem in wide copper areas.

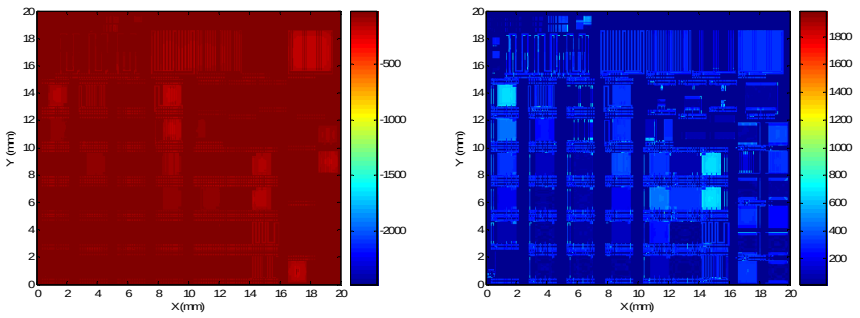

(a) (b)

Figure 20. Chip-scale model results with in-pattern dummy, showing improved envelope (erosion) and step height (dishing), for MIT/SEMATECH 854 M1 test mask, using abrasive-free slurry model.

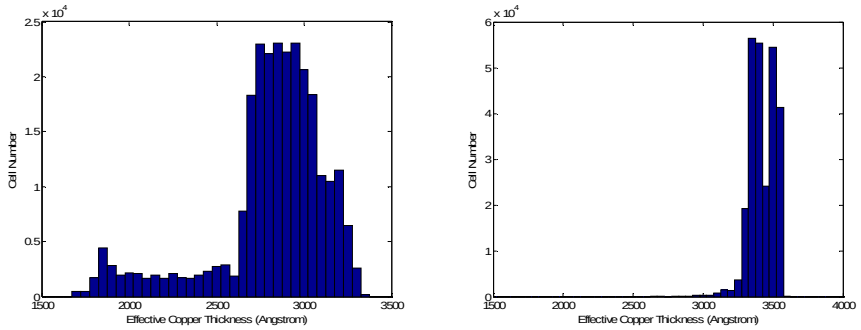

(a) (b)

Figure 21. Histogram plots for effective copper thickness at dummy filled areas, using abrasive-free slurry model.

Industrial Interactions and Technology Transfer:

- Chris Borst: Albany Nanotech
- Laertis Economikos: IBM Corporation
- Maria Peterson: JSR Microelectronics, Inc.

Conferences Presentations:

- X. Xie, D. Boning, F. Meyer, and R. Rzehak, "Analysis of Nanotopography and Layout Variations in Patterned STI CMP", *2006 International Conference on Planarization/CMP Technology*, Foster City, CA, October 2006.
- Somani, D. Boning, P. Gschwend and R. Reif, "Environmental Impact Evaluation Methodology for Emerging Silicon-Based Technologies", *International Symposium on Electronics and the Environment*, San Francisco, May 2006.

Next-Year Plan:

- Adapt and integrate pattern evolution models with endpoint and diagnostic signal analysis from novel force-spectra measurement systems. This will enable improved detection by relating signal features with modeled topography states (copper clear; barrier clearing) for arbitrary product layout.

Environmentally Benign Electrochemically-Assisted Chemical-Mechanical Planarization (E-CMP)

Personnel:
PIs:

- Srini Raghavan: Materials Science and Engineering (UA)
- Duane Boning: Electrical Engineering and Computer Science (MIT)
- Ara Philipossian: Chemical and Environmental Engineering (UA)

Other Research Personnel:

- Ed Paul: Visiting Scientist (MIT)

Graduate Students:

- Ashok Muthukumaran: Materials Science and Engineering, UA
- Daniel Truque: Electrical Engineering and Computer Science (MIT)
- Xiaomin Wei: Chemical and Environmental Engineering (UA)

Objectives:

The main objectives of this project are to investigate and model copper and tantalum barrier layer ECMP processes.

Background:

Electrochemically-assisted chemical mechanical polishing (E-CMP) is a new process technology that has the potential to address both environmental and performance concerns existing in convention CMP processes for advanced copper/low-k interconnect. In most existing conventional CMP processes, substantial solids (slurry particles) are used, together with sophisticated chemistries, to polish-back and planarize copper, barrier, and insulating layers. The high rate of chemical and consumable usage (slurry, pad and water) and concern about copper and solids effluent have drawn substantial attention in conventional CMP. E-CMP offers substantially reduced consumption and effluents and cost and environmental benefits.

We are structuring our research along two primary tasks: Task 1, which focuses on experimental investigation of Cu and Ta E-CMP processes, and Task 2 which focuses on modeling, optimization and control of ECMP processes.

Task 1: Experimental Investigation of Cu and Ta E-CMP Processes

During the last few years, electrochemical mechanical planarization (E-CMP) technique has been actively explored for bulk copper removal in the fabrication of Cu-low k structures. However, development and implementation of a full-sequence E-CMP process, which includes the removal of the barrier layer as well, is in the infant stage. The removal of Ta based materials by conventional CMP is done using silica slurries with high (about 10 weight %) solids content at alkaline pH values and is mostly ‘mechanical’ in nature. ECMP is typically done using chemically active formulations with no or very small amount of solids and since Ta is a refractory metal, such formulations, which are not highly corrosive, are in very early stage of development. Some studies have shown that hydroquinone sulfonic acid can be used as an oxidizer for tantalum CMP [1, 2].

Sulfonic acids have found use in electrochemical etching and polishing of Ta [3, 4]. Additionally, aryl sulfonic acids such as dihydroxy benzene disulfonic acid (aka Tiron) form strong complexes with refractory metals. Based on the literature information, it was decided to develop a hydroxy benzene sulfonic acid system for the E-CMP of tantalum and explore conditions that would provide a 1:1 selectivity between Ta and Cu.

Method of Approach:

Electrochemical and polishing studies on tantalum and copper samples were conducted in a modified electrochemical abrasion cell (EC-AC) tool. This tool was re-designed for better control of low down-force pressure (about 0.5 PSI) and to accommodate sample of size 6 cm in diameter. The counter electrode is a stainless steel 316L disc (diameter about 3 cm), to which a perforated polishing pad is affixed at the bottom. The center of the pad/electrode was offset from the center of the wafer sample such that 70% of the sample was polished. Electrochemical data were obtained using an EG&G PARC 273A potentiostat.

Polishing of tantalum film was carried out in sulfonic acid based solution at various current densities under different pH conditions. After polishing, the solution was collected for analyzing tantalum concentration using inductively coupled plasma-mass spectroscopy (ICP-MS). The removal rate of tantalum was calculated from tantalum concentration in solution. To study the selectivity for sulfonic acid based chemistry, polishing of electroplated copper films (thickness 6000 Å) was also carried out under the same conditions. Removal rate of copper was calculated from thickness measurements using a four point probe.

Highlights of Results and Accomplishments:

Preliminary tests indicated that a small amount (0.05 to 0.1%) of colloidal silica particles is needed to provide decent tantalum removal rates in 2,5-dihydroxy benzene sulfonic acid solutions. Figure 1(a) shows the removal rate of tantalum in 0.3 M sulfonic acid based chemistry containing 0.1% SiO_2 as a function of pH at different current densities. At pH 4, the removal rate of tantalum is 50 and 70 Å/min for corresponding current densities of 0.1 and 0.25 mA/cm^2. At a pH of 10, the removal rate is increased by abou

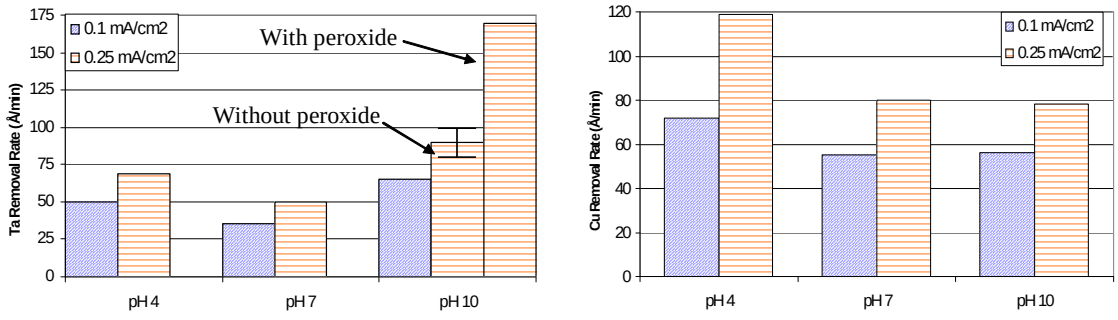

(a) (b)

Figure 1. Removal rate of (a) tantalum and (b) copper in 0.3M sulfonic acid based chemistry containing 0.1% SiO_2 as a function of pH at different current densities.

Initial experiment on the addition of 1.2 M H_2O_2 to 0.3 M sulfonic acid based chemistry containing 0.1% SiO_2 at pH 10 shows a significant increase in the removal rate of tantalum to 170 Å/min for 0.25 mA/cm^2. Further experiments will be carried out to study the effect of peroxide under different ECMP conditions.

Figure 1(b) shows the removal rate of copper under same conditions. Higher removal rate of copper was observed at pH 4 and then the rate drops off as the pH is increased. At pH 4, for a current densities of 0.1 and 0.25 mA/cm^2, the removal rate of copper is 70 and 120 Å/min. At pH 10, the removal rate of copper is reduced to 55 and 80 Å/min at 0.1 and 0.25 mA/cm^2, respectively.

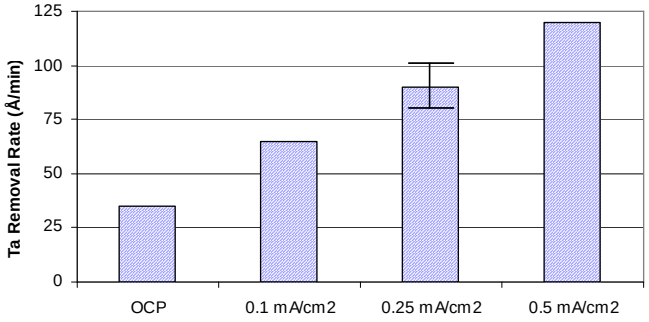

Figure 2. Removal rate of tantalum as a function of applied current densities in 0.3 M sulfonic acid based chemistry containing 0.1% SiO_2 at pH 10.

Figure 2 shows removal rate of tantalum as a function of applied current densities in 0.3 M sulfonic acid based chemistry containing 0.1% SiO_2 at pH 10. Under open-circuit potential (OCP) condition, the removal rate of tantalum is 30 Å/min. When a current density of 0.1 mA/cm^2 was applied, the removal rate was found to be 65 Å/min. At higher current density of 0.25 mA/cm^2 which corresponds to overpotential of 1 V, the removal rate has increased to 90 ± 10 Å/min. Further increase in the current density to 0.5 mA/cm^2, does not significantly increase the removal rate of tantalum.

Table 1: Current efficiency (%) as a function of pH in 0.3 M sulfonic acid solution containing 0.1% SiO_2

Applied current density (mA/cm^2)	Estimated removal rate of tantalum (Å/min)	Actual removal rate of tantalum (Å/min)			Current efficiency (%) after correcting for OCP removal rate		
		pH 4	pH 7	pH 10	pH 4	pH 7	pH 10
OCP	-	23	12	30	-	-	-
0.1	23	52	35	65	120*	102*	142*
0.25	56	71	52	100	84	68	119*
0.5	112	-	-	119	-	-	77

(*: Please see text for explanation of current efficiencies higher than 100%)

Current efficiency (%) values for various experimental conditions are shown in Table 1. The current efficiencies were calculated after correcting for OCP removal rates.

For example, at pH 4, the removal rate of tantalum under OCP condition is about 23 Å/min. At an applied current density of 0.1 mA/cm^2, the removal rate of tantalum calculated from solution analysis is 52 Å/min. After correcting for OCP removal rate, the current efficiency based on three electron transfer was found to be 120%; assuming that there are no errors in solution analysis, this higher than 100% efficiency indicates that there may be some mechanical removal of metallic Ta. Similarly, the current efficiency values calculated at pH 10 were also found to be more than 100% for the aforementioned reason. It may be noted that the corrosion current density determined from the polarization curve at pH 10 was found to be 70 $\mu A/cm^2$.

Industrial Interactions and Technology Transfer:

- Renhe Jia: Applied Materials, Inc.

ESH Impact:

Goals	Usage Reduction		Waste Reduction	
	Chemicals	Abrasives	Solid	Liquid
Using full sequence ECMP	N/A	> 90% reduction	> 99%	N/A

Publications:

- V. Lowalekar, "Oxalic Acid Based Chemical Systems for Electrochemical Mechanical Planarization of Copper", *Ph. D. Dissertation*, University of Arizona, 2006.
- A. Muthukumaran, V. Lowalekar and S. Raghavan, "Evaluation of Inhibitors for ECMP of Copper Using Electrochemical Quartz Crystal Microbalance (EQCM) Technique", *Mater. Res. Soc. Symp. Proc.*, 914, 213-16, 2006.

Conference Presentation:

- A. Muthukumaran, V. Lowalekar and S. Raghavan, "Evaluation of Inhibitors for ECMP of Copper Using Electrochemical Quartz Crystal Microbalance (EQCM) Technique", *MRS spring symposium*, April 2006.

Next-Year Plan:

- Develop chemical systems for the removal of other barrier layers (TaN, Ru).

References:

[1] Phillip W. Carter, Jian Zhang, Steven K. Grumbine, Thesauro Rege, Francesco De, "Compositions and methods for tantalum CMP", *United States Patent Application 20060030158*, (2006).

[2] Melvin K. Carter, Robert J. Small, Xiaowei Cass Shang, Donald W. Frey, "*CMP method for copper, tungsten, titanium, polysilicon, and other substrates using organosulfonic acids as oxidizers*", *United States Patent Application 2005090109*, (2005).

[3] Leonard Johannes Joseph Janssen, Richard Johannes Van Der Net, "Method

for the electrolytic polishing of a metal in the presence of an electrolyte composition, as well as a molded element obtained by using such a method", *European Patent WO0171068,* (2001).
[4] Soji Tsuchiya, Toshikuni Kojima, "*Electrochemical etching of tantalum*", *Japanese Patent 03053099*, (1991).

Task 2: Modeling, Optimization and Control of E-CMP Processes.

The key process capability that E-CMP must provide is the planarization and formation of embedded damascene copper features; it is thus critical that our investigations of new E-CMP capabilities evaluate and improve patterned wafer performance, in addition to reducing environmental and process cost. Existing E-CMP technology provides attractive process control capability, but also has important limitations. In present E-CMP systems, control of the total charge can be achieved in zonal regions so that effective profile control can be achieved (e.g. to make edge removal faster or slower than in the center). Understanding the interaction of mechanical pad properties with the electrochemistry will be pursued, in order to model and optimize feature-scale step-height reduction and minimize dishing and erosion. In addition, modeling (including geometric as well as electrochemical modeling) of the pad/wafer interactions at the wafer, chip, and feature scale will be undertaken, as shown in Fig. 3, so that the coupled wafer uniformity and die uniformity can be optimized. Finally, novel approaches for endpoint detection and control, particularly at the copper clearing and/or barrier removal steps should be possible due to expected discontinuities in both the current/voltage relationship and in electrolyte properties and will be explored, as the technology development in the other subtasks reaches this point.

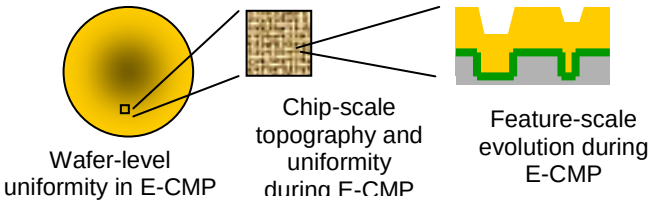

Figure 3. Multi-scale modeling to understand wafer, chip, and feature level uniformity and performance in E-CMP.

Highlights of Results and Accomplishments:

The primary focus for the initial work in the modeling and control subtask has been to understand existing E-CMP technology, equipment, consumables, and process technology. The key accomplishment is initial development of a wafer-level dynamic model for material removal in E-CMP, appropriate for wafer-level optimization and control. This is based in part on an internship with IBM at Albany Nanotech in summer 2006. In addition, a model for surface film formation and removal dynamics in E-CMP, appropriate for use in feature-scale evolution modeling, has been explored.

The wafer level dynamic E-CMP model is based on time evolving current density distributions across the wafer, resulting from electrical contact and current flow through both surface films and the electrolyte. The wafer is discretized as finite-elements, and the potential and current density distributions are calculated based on the applied voltage zones and metal film thicknesses across the wafer, as pictured in Fig. 4. The copper

removal rate is proportional to the current density, and thus the copper thickness (and conductance) can be calculated as a function of position on the wafer and polish time. Using a time-stepping simulation, the model is able to capture the wafer level non-uniformity and time-dependence of E-CMP removal. The model is also able to model the time-varying voltage zones used in E-CMP, and can be used to find optimal voltage zone control schemes to achieve improved wafer-level uniformity.

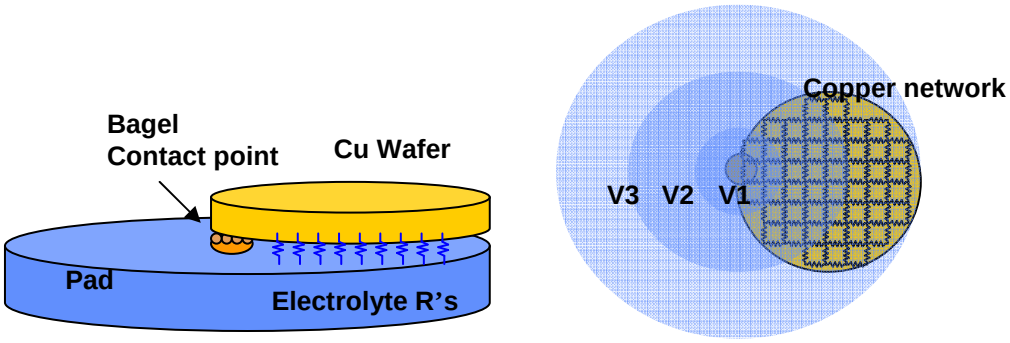

Figure 4. Wafer-level modeling of copper removal rates in E-CMP. Current flows from edge contact through both copper/barrier thin films on wafer surface, and through electrolyte.

Industrial Interactions and Technology Transfer:

- Chris Borst: Albany Nanotech
- Laertis Economikos: IBM Corporation

ESH Impact:

- Improvement in E-CMP for bulk copper removal can reduce the thickness of plated copper needed by about 25% (with corresponding plating and polishing time and waste reduction).

Next-Year Plan:

- Develop a prototype chip-scale E-CMP model of pattern and topography evaluation on the wafer surface, which can be integrated with wafer-level and feature-level models. The model will aid in evaluation of potential performance benefits of copper and barrier E-CMP.

EHS Impact of Electrochemical Planarization Technologies

Personnel:
PIs:

- Alan West, Department of Chemical Engineering, Columbia University

Graduate Students:

Kristin Shattuck, Chemical Engineering, Columbia University

Objectives:

The objective of this project is to investigate the feasibility of utilizing electrochemical planarization (e-CMP) technologies as a replacement or compliment to chemical mechanical planarization (CMP) in order to reduce waste generation and toxicity. Objectives include: studies of copper e-CMP, with an emphasis on understanding mechanisms, and the screening of electrolytes for studies of liner e-CMP.

Background:

The International Technology Roadmap for Semiconductors (ITRS) identifies resource conservation as a concern, and it is well known that CMP processes are a major source of waste generation in wafer processing. Furthermore, the introduction of low-k materials will require major changes in CMP, as identified in the ITRS (2003, items 7 and 8). Specifically, the ability to achieve acceptable polishing rates with chemical-mechanical planarization (CMP) may be compromised by the introduction of low-k materials that do not have the requisite properties to withstand large mechanical forces. There have thus been significant recent efforts to develop electrochemical-mechanical planarization (e-CMP) technologies as a replacement of or complement to CMP.

In e-CMP, oxidation occurs via an electrochemical reaction and there may be no need for the bath to contain oxidizing agents for the case of Cu ECMP. Furthermore, electrochemical oxidation rates can be significantly greater than chemical oxidation rates achievable by CMP, eliminating possibly the need for abrasive particles in the electrolyte, even though a polishing pad will still be required to achieve planarization. These simplifications in bath chemistry may reduce waste generation/treatment associated with metal-overburden removal. Extension of ECMP to barrier removal is vital to gaining industry acceptance of the technology, but little is known yet about the likely makeup of, for example, a Ta/TaN ECMP chemistry or a Ru ECMP chemistry.

While ECMP-bath waste may be easier to treat, there has been almost no consideration yet of the volume of ECMP waste that will be generated in comparison with competing low-down-force CMP processes. Furthermore, the overall EHS impact of ECMP will not be known until it is established whether ECMP will be a complete or partial replacement of CMP.

Method of Approach:

In order to begin studying e-CMP, our research team needed to obtain an apparatus which could be used for polishing blanket and patterned wafers. It was decided that the best approach would be to design a bench top e-CMP device that could be used to study and isolate specific parameters of the process. Because of anticipated constraints imposed by low dielectric materials, in all studies a down force of < 1.0 PSI will be used.

The holder for the substrate is able to accept a variety of wafer fragment sizes (max: 4 cm x 4 cm) as well as 2" diameter wafers. The pad, which is located directly below the substrate, will be perforated in order to allow current and electrolyte to flow to the substrate surface. We are partnering with industrial experts to select pads to be tested. In order to prevent bubbles from effecting planarization, the cathode will be placed an appropriate distance away from the electrolyte flow to the substrate. The motion of the substrate will be 5 cm in the x direction and 1 mm in the y direction. The motion will be controlled by rheostats and maintained at a constant velocity. The device will be mainly used to characterize bath chemistries for Cu e-CMP and then barrier e-CMP.

To quantify the characteristics of each bath chemistry, the following tools will be used: electrochemical impedance spectroscopy (EIS), profilometry, scanning electron microscopy (SEM), four-point probe, and possibly scanning probe measurements. When the device has been able to demonstrate the anticipated trends using Cu foil electrodes, then polishing on wafers will begin. Those tools will be used to examine metal removal rates, selectivity, and planarization efficiency. Mathematical models intended to test mechanisms proposed by the experimental studies will also be developed and tested.

In parallel with and subsequent to Cu e-CMP studies, bath chemistries will also be used for barrier e-CMP. The major focus of these studies will be characterization of removal rates in select electrolytes and the measurement of Cu/liner selectivity. Selectivity measurements will be made by studying each material separately as well as galvanic couples of the materials.

Highlights of Results and Accomplishments:

This project commenced in June 2006. Experiments were performed using a Cu rotating disk electrode (RDE) and an e-CMP device, which was designed and built this year as well. The e-CMP bench-top device was built in-house. The device is shown in Figure 1a and 1b. The design features two dimensional linear motion that is controlled by two rheostats connected to DC motors. The movement is approximately 5 cm in the x direction and 1 mm in the y direction. The design is able to accommodate both 2" wafers, as well as wafer fragments. The polishing pad is located within the electrolyte, on a perforated support to ensure current flow and electrolyte flow to the wafer surface. This device can operate in both contact and non-contact modes. In order to control the low down force requirement (<0.3 PSI), a small micrometer is mounted on the surface of the top plate which encloses the xy stage and the long shaft which carries the wafer. The apparatus is mounted on springs which support the entire weight of the upper portion. When the pad is submerged within the electrolyte, the upper portion is lowered onto the springs at a distance of ~ 1 mm from the surface of the pad. The micrometer is then used to slowly lower the wafer onto the pad surface. By designing our own e-CMP device,

we are able to control a number of the key parameters that otherwise would be difficult to study using a conventional CMP tool.

In parallel with the development of the e-CMP tool, electrochemical characterization of the impact of bath chemistry on Cu electrodissolution was carried out using electrochemical impedance spectroscopy and linear sweep voltammetry applied to Cu rotating disk electrodes. Emphasis was placed on phosphate-based electrolytes containing BTA. Figure 2 for example shows the impact of BTA on the dissolution rate at a pH of approximately four.

After completion of the e-CMP device, preliminary experiments have been performed to observe the effect of a CMP pad, operating in both contact and non-contact modes. It can be seen in Figure 3 that when the pad is contacting the electrode surface, the current density increased. This could be due presumably to the removal of the passivation layer created by the presence of BTA in the electrolyte.

Electrochemical methods were used to rapidly screen for the impact of BTA at different applied potentials at solution pH on the electrochemical dissolution rate. Results are shown in Figure 4, where I is the current density with BTA present and I_{no} is the current density with no BTA present. It is hypothesized that the ratio of current densities can be related to planarization efficiency, but this has not yet been demonstrated. The removal rates of Cu under these conditions were also measured directly using profilometry and four-point probe measurements. Since an electrolyte that exhibits desirable planarization may also roughen the material, surface roughness measurements have also commenced.

(a) (b)

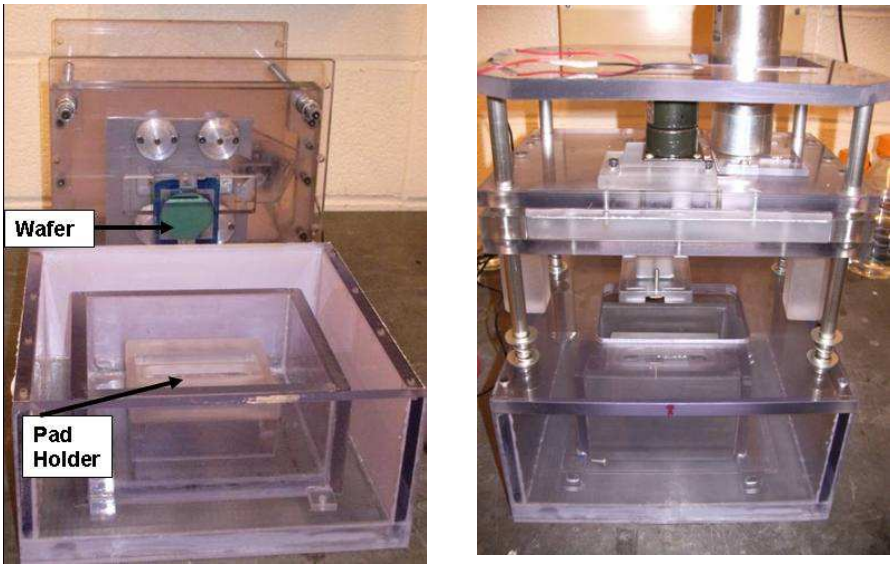

Figure 1. Benchtop e-CMP Device
(a) Cross Section
(b) Side View

Figure 2. Effect of BTA concentration
At pH 4.3: No BTA & 0.01 M BTA, using RDE

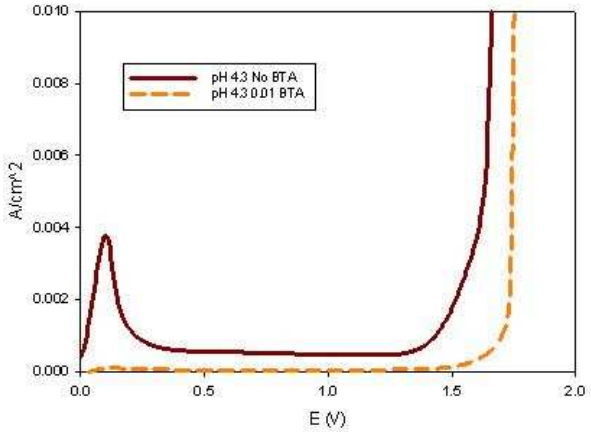

Figure 3. ECMP Device: contact and non- contact
With electrolyte pH 4.85 and 0.01 M BTA

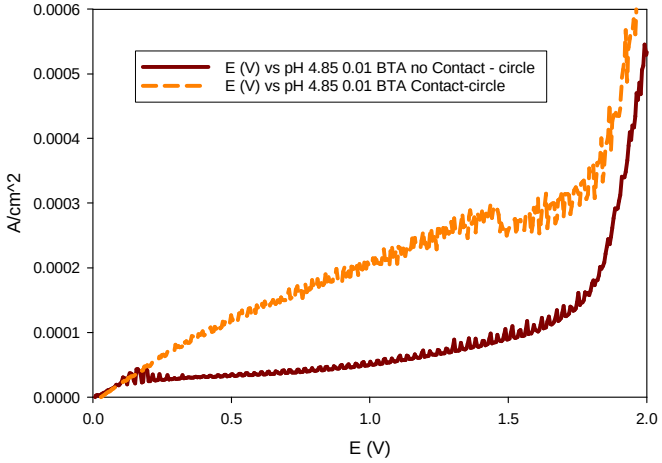

Figure 4. Hypothetical planarization Capability of KPO_3-H_3PO_4 electrolyte as a function of potential for various pH values.

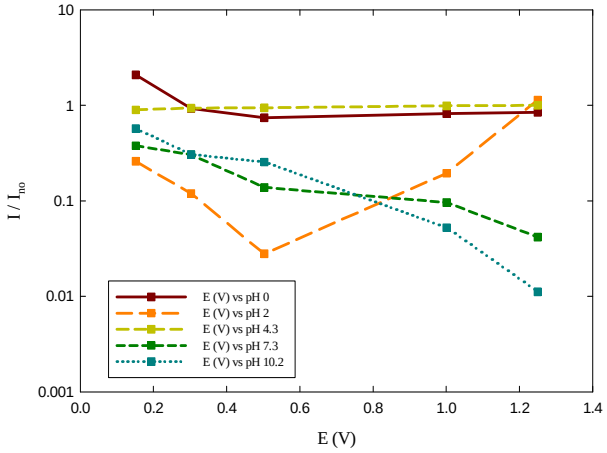

Industrial Interactions and Technology Transfer:

- Feng Liu – Applied Materials – ECMP device collaboration
- Lee Cook – Rohm & Haas – CMP Pads
- Cliff Spiro – Cabot – CMP Pads

ESH Impact:

- Potential elimination of solid particles commonly used in CMP slurries, which would allow for waste to be easily treated.
- The likely removal of harmful oxidizers in electrolyte that would decrease the toxicity of the waste produced.
- Possible reduction in volume of waste produced compared to current waste generated by CMP processing, though it is not know yet whether or not this will be the case.

Conference Presentations:

- West, A.C., "Theoretical Considerations for Cu e-CMP", *11th International Symposium on CMP* (2006), Lake Placid, NY.

Next-Year Plan:

We plan to continue working to characterize the planarization capabilities of various electrolytes using the e-CMP device. We are focusing first on copper, but later will also be looking into the feasibility of polishing barrier materials such as Ru and Ta/TaN. While characterizing these electrolytes, specific attention will be paid to monitoring barrier/Cu selectivity, electrolyte/dielectric compatibility, impact of pad type, and pad/electrolyte interactions.

Low Environmental Impact Processing of sub-50 nm Interconnect Structures

Personnel:
PIs:

- Prof. Karen K. Gleason, Chemical Engineering, MIT
- Prof. Anthony J. Muscat, Chemical and Environmental Engineering, UA

Graduate Students:

- Chia-Hua Lee, Materials Science and Engineering, MIT
- Dr. Kelvin Chan, Chemical Engineering, MIT (current at Applied Materials).
- Rachel Morrish, Chemical and Environmental Engineering, UA

Objectives:

This project will evaluate the performance of gas, liquid, and supercritical fluid processes to clean sub-50 nm structures, fabricate multilevel air gaps, and planarize surfaces without contact. These tasks were chosen because of the potential to reduce resource use and waste production by understanding process limitations. The primary objective of this project is to develop a set of principles to guide the choice of materials and processing fluids to fabricate sub-50 nm structures with the lowest cost of ownership.

Background:

Interconnect technology will require etching, cleaning, and filling high aspect ratio, sub-50 nm structures for the hp45 to 22 nm technology nodes planned for production between 2010 and 2016.[1] These steps will be repeated 3-6 times per wafer with tight tolerances. The processing of low-*k* dual damascene metal structures will be especially challenging because of the near molecular scale dimensions. The fabrication steps to build the structures required to meet the ITRS targets will be developed in the next 5 years.

Modeling predicts that wetting times decrease when contact angles are low for feature widths above 50 nm,[2] but there is an open question whether liquids will wet and penetrate sub-50 nm features, which has been designated a difficult challenge in the ITRS interconnect roadmap.[1] If the resistance to mass transport is augmented by reductions in feature size, then rinsing times could increase significantly, with concomitant increases in cycle times and water, chemical, and energy use.

The challenges for the integration of porous low-*k* materials into future devices are extremely difficult[3] and indeed may be so great that the industry moves instead to air-gap interconnects, since air is the ultimate low-*k*, if stable air cavities can be integrated with copper wires.[4] Sacrificial materials are used in the fabrication of void-containing microstructures.[5] Void, or air in the context of this work, has the lowest possible

[1] ITRS Roadmap, 2004 update, Tables 80 and 81b.
[2] M. T. Spuller and D. W. Hess, J. Electrochem. Soc. 150(8) (2003) G476-G480.
[3] J.P Gueneaa de Mussy, G. Bruynsereade, Zs. Tokek, G.P. Beyer, and K. Maex, "Novel Selective Sidewall Air Gap Process", IITC, 2004.
[4] P. Kohl, *et al.*, "Air-gaps in 0.3 μm interconnections", IEEE Elec. Dev. Lett. 21 (2000) 12.
[5] S. D. Senturia, *Microsystem Design*, Kluwer Academic Publishers, Boston, MA (2003).

dielectric constant of 1.0. In this proposal, all dry methods are proposed for the deposition and removal of the sacrificial layer. The absence of surface tension and water in the processes proposed is well suited for aggressive geometries having high aspect ratios.

Method of Approach:

Air gap structures will be fabricated using sacrificial polymers deposited using initiated CVD (iCVD). The properties and processes required for the integration of the sacrificial layer into interconnect structures will be evaluated. The iCVD method is an all dry technique for depositing polymers that can extend the utility of the process knowledge and tool sets developed for CVD deposition of low k dielectric films. The iCVD method is also an alternative to spin-on deposition. Homogeneity in chemical bonding is crucial for sacrificial polymers because the removal mechanisms for polymer decomposition are highly dependent on the chemical structure and a slight imperfection in structural integrity can lead to undesirable char formation or changes in solubility.

In addition to depositing blanket sacrificial layers followed by etching to form patterns (subtractive processing), the iCVD methodology can be modified to achieve selective growth of patterned layers from regions of the substrates that have been directly initiated. In addition to reducing waste and processing complexity (Fig. 1), the additive patterning approach enabled by selective initiation has the potential to achieve covalent

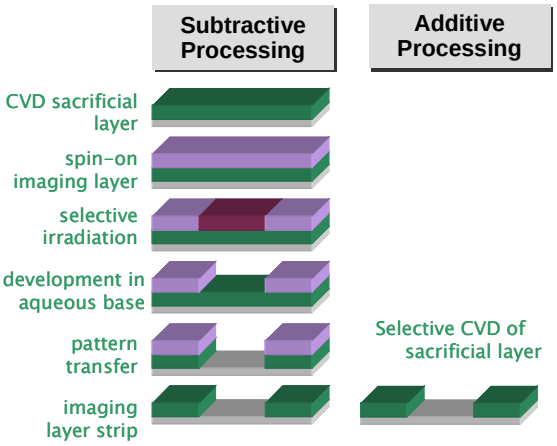

Figure 1. Reduction in number of steps and tools resulting from by additive versus subtractive processing with the potential to streamline process development.

bonds between the substrate and the sacrificial layer which would promote strong adhesion.

The potential for removing iCVD prepared polymer films using supercritical carbon dioxide with cosolvents such as isopropyl alcohol (IPA), acetone, or liquid monomer was tested. Dissolution of the polymer is expected to occur when the solubility parameter of the supercritical solution approaches that of the sacrificial polymer. The solubility parameter depends on dispersion forces, dipole-dipole interactions, and hydrogen bonding. Varying the cosolvents added to the supercritical mixture will provide a knowledge base for how best to change and control polymer solubility.

Supercritical CO_2 is well known for its ability to swell and plasticize polymeric materials which could allow for improved dissolution of the iCVD polymer films with cosolvents. Adding liquid monomer to the supercritical solution provides enhanced solubility of polymers through increasing the fluid density, while also providing

intermolecular forces between the polymer and monomer that favor dissolution. In addition, depressurizing the supercritical solution from approximately 200 atm to ambient may result in a mechanical component for removal of the polymer.

Highlights of Results and Accomplishments:

An existing 200 mm system at MIT was upgraded to allow 300 mm wafers to be accommodated (Fig. 2). A reactor of sufficient size is crucial to being able to send wafers to industrial collaborators for integration testing.

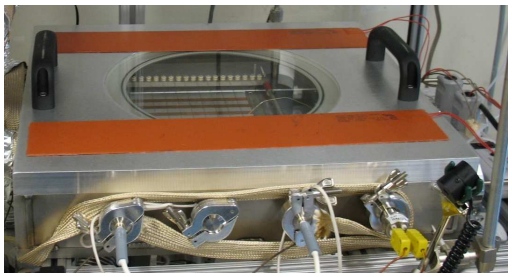

Figure 2. New iCVD chamber capable of accommodating 300 mm wafers.

Thin films of iCVD sacrificial polymers were synthesized using cyclohexyl methacrylate (CHMA) as the monomer and ethylene glycol dimethacrylate (EGDMA) as the cross-linker. The resulting film is composed of only carbon, oxygen, and hydrogen. Although cross-linked, the iCVD sacrificial layer was found to decompose cleanly, leaving behind a maximum of 0.3% of residue by thickness. Cross-linking renders the polymer stable in practically all solvents and results in an onset of thermal decomposition at 270°C, providing compatibility with subsequent microfabrication steps. The high etch rate (0.35 µm/min) in oxygen reactive-ion etching eliminates the need of a hard mask during etching. Fabrication using conventional lithographic, etching, and deposition techniques resulted in single-level void structures.

The concept of additive processing for sacrificial layers was demonstrated using dip-pen nanolithography to define patterns of initiators onto a silicon wafer surface. The dip-pen lithography was done in collaboration with the group of Prof. Angie Belcher (Material Science and Engineering, MIT) and utilizes an atomic force microscope (AFM) for defining the patterned regions (Fig. 3). Once patterned with initiator, the wafers were loaded into a CVD chamber and then exposed to flowing monomer vapors at partial pressures of 0.1 to 1.0 torr. During the monomer flow, UV exposure of the substrate inside the CVD chamber causes the initiator species to produce a free radical site on the surface to which multiple monomer units can add. Using this additive processing scheme permitted growth of directly patterned layers the sacrificial material, poly(cyclohexylmethacyrate).

Preliminary data processing CHMA films with supercritical CO_2 and added cosolvents of IPA, acetone, and hexane are shown in Figure 4. These results were

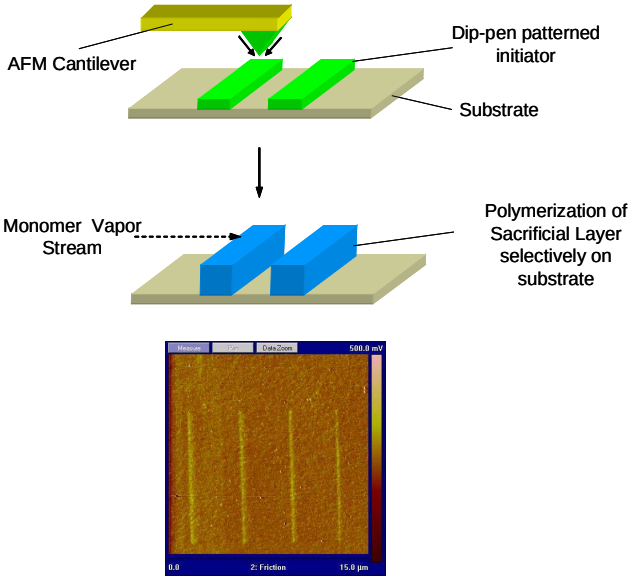

Figure 3. (top) Use of AFM enabled dip-pen nanolithography to apply photoinitiator to a surface. (middle) The polymeric sacrificial layer deposits selectivity from gaseous monomers when the surface patterned with initiator is subjected to UV exposure. (bottom) AFM micrograph of the result of additive processing using dip-pen nanolithography.

compared to the polymer removal by exposure to pure cosolvents under ambient conditions. Ellipsometry was used to measure film thickness. Fourier transform infrared spectroscopy (FTIR) data of the C-H and C=O absorbance intensities at 3000 and 1720 cm-1 verified ellipsometry data. The amount of polymer removed was calculated from an average of two samples reacted under the same conditions with error bars showing ± 1σ.

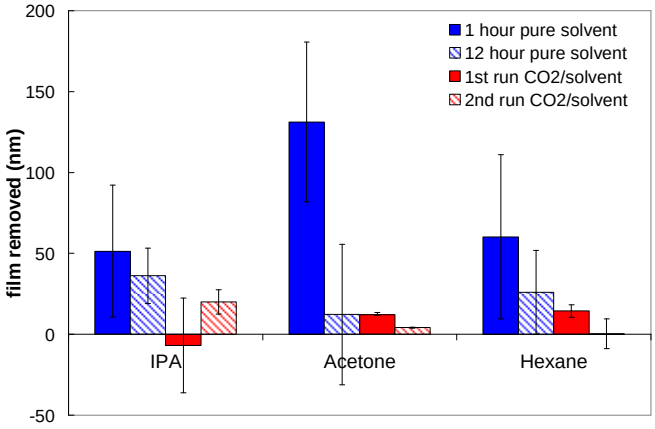

Figure 4. (top) EGDMA polymer film removal by processing in pure solvents of IPA, acetone, and hexane (filled bars) compared to reaction with supercritical CO_2/solvent (striped bars). Error bars show ± 1 σ.

While the polymer removal did vary significantly between samples under the same reaction conditions, trends indicate that processing with a pure cosolvent removed more CHMA than exposure to the CO_2/cosolvent solutions. It should be noted that exposure to pure solvents was done for a total of 13 hours while each CO_2 processing lasted 16 minutes. A second set of reactions in both the pure solvent and CO_2 mixture (striped bars) generally exhibited lower removal, indicating that exposure to the solvents may have only dissolved lower molecular weight components within the film. Within error, none of the cosolvents appear to perform better then the others and in all cases only

partial dissolution was observed. These results demonstrate that the iCVD film was stable in pure liquid solvents as well as when these cosolvents were added to supercritical CO_2 at high pressures, even with rapid depressurization steps.

Industrial Interactions and Technology Transfer:

- Dr. Kelvin Chan, AMAT
- Dr. Thomas Diamond, IBM
- Dr. Iacopi Francesca, IMEC
- Dr. Romano Hoofman, Phillips
- Dr. Dorel Toma, TEL

ESH Impact:

Using air (k=1.0) as a dielectric would allow the highest density of devices per layer and result in the fewest number of metal layers on the chip. This reduced number of steps results in lower materials and energy usage and in less waste production. Reductions in the volume of ESH relevant chemicals that are needed for processing as well as minimization of photolithography and CMP steps, which are among the most expensive, can consequently make a significant impact on lowering the overall cost of device fabrication. Employing dry removal methods such as gas phase and supercritical processing could reduce water and chemical usage while also providing advanced techniques for non-destructive removal of small, high aspect ratio features.

Publications:

- Kelvin Chan and Karen K. Gleason, Air-Gap Fabrication Using a Sacrificial Polymeric Thin Film Synthesized via Initiated Chemical Vapor Deposition, J. Electrochem. Soc., 153(4), C223-C228, 2006.
- Kelvin Chan and Karen K. Gleason, A Mechanistic Study of Initiated Chemical Vapor Deposition of Polymers: Analyses of Deposition Rate and Molecular Weight, Macromolecules, 39 (11), 3890 -3894, 2006.

Conference Presentations:

- KK Gleason, Design of Chemical Vapor Deposition Processes for Low k Dielectrics and Air Gap Formation, IMEC: Leuven, Belgium (invited) 1/23/06
- KK Gleason, Mechanistic Aspects of Initiated Chemical Vapor Deposition (iCVD) of Polymeric Films, 209th Electrochemical Society Meeting: Denver, Colorado (invited) 5/9/06
- KK Gleason, Polymeric Nanocoatings by Chemical Vapor Deposition, Utrecht University, (invited as Debye Lecture) 6/14/06
- KKS Lau and KK Gleason, Initiated Chemical Vapor Deposition: Polymer Chemistry and Practical Applications in Particle Surface Design, 4th Int. Conf. Hot-Wire (Cat-CVD) Process, Takayama, Gifu, Japan (invited as keynote presentation) 10/4/06

Next-Year Plan:

Photoinitiated CVD processes for additive and subtractive processing will be optimized for growth rate, uniformity, absence of surface defects (such as pinholes),

chemical structure, minimization of EHS impact, and compatibility with dry polymeric removal. The chemical structure of the films will be verified by FTIR and x-ray photoelectron spectroscopy (XPS). The electrical and mechanical properties required for the integration of the sacrificial layer into interconnect structures will be measured and optimized.

Air gap test structures will be fabricated using additive processing and several strategies will be tested to for removal of the sacrificial layer. Cross-sectional Scanning Electron Microscopy (SEM) will be used to examine the test structures before and after removal of the iCVD sacrificial layer.

The removal process of sacrificial CHMA polymer films in supercritical CO_2 solution with added polar cosolvents will be tested to conclusively evaluate their mechanism of dissolution. In addition, the potential of a mechanical removal component through rapid fluid depressurization will be explored. The effect of adding liquid monomer as a cosolvent in supercritical CO_2 will be also examined as a potential method for enhanced dissolution of the polymer. Multiple studies report successful dissolution of polymethacrylate films using similar techniques. All removal mechanisms and film characteristics will be further analyzed using XPS and SEM.

Environmentally Benign Vapor Phase and Supercritical CO_2 Processes for Patterned Low k Dielectrics

Personnel:
PIs:

- Christopher K. Ober, Materials Science & Engineering, Cornell University
- Karen K. Gleason, Chemical Engineering, MIT
- James J. Watkins, Polymer Science & Engineering, MIT

Graduate Students:

- Sal Baxamusa, Chemical Engineering, MIT
- Nelson Felix, Chemical and Biomolecular Engineering, Cornell University
- Sivakumar Nagarajan, Chemical Engineering, UMASS Amherst
- Shannan O'Shaughnessy, Chemical Engineering, MIT
- April Ross, Chemical Engineering, MIT (graduated with Ph.D, now at Exxon)
- Yu (Jessie) Mao, Materials Science and Engineering, MIT (graduated with Ph.D, now a professor at Oklahoma State University).

Undergraduate Students:

- Camille Man Yin Luk, Materials Science & Engineering, Cornell University

Objectives:

Selective deposition of patterned low k dielectric layers is an off roadmap, ESH focused approach to process step reduction during integrated circuit fabrication, the successful implementation of which would represent a substantial environmental and economic "win-win". Our long-range objective is to develop new methods to deposit, pattern and process low k materials to meet the roadmap goal of dielectric constants lower than 2.0. We are pursuing several approaches to these goals. Photoinitiated CVD (piCVD), an evolutionary approach to assembly of low k materials, is being investigated for process simplification potential both during initial initiator pattern deposition and then during growth of low k material on those patterns. We are exploring the assembly of molecular glass precursors and porogens, a second approach that is a new concept for engineering the morphology of porous low k materials at scales needed to achieve future roadmap targets. Porogens of selected architectures are being used during CVD deposition to decrease dielectric permittivity. We are comparing porogens with the effectiveness of block copolymer assembly for nanopore formation in ultralow k materials. Finally, the use of $scCO_2$ is being demonstrated as an ESH benign technology capable of driving the self-assembly of both porogens and the low k material itself and for ordered pore formation, pattern development and final removal of the porogen.

Background:

Significant integration challenges and lack of materials that meet process needs have slowed the adoption of very low k dielectrics compared to earlier SIA roadmap projections. Introducing new materials to meet reduced dielectric permittivity requirements and developing new materials that are compatible with current or planned processes represent two of the top three challenges identified for the ITRS Interconnect

Roadmap. Future progress requires fundamental understanding and novel approaches to dielectric deposition, patterning, processing and repair. The rough and permeable sidewalls of traditionally patterned porous low k materials pose new challenges for subsequent barrier and metal deposition steps, providing strong motivation for producing these features by additive rather than subtractive patterning. At the same time, little research has targeted the development of new processes and materials that are directly designed to incorporate new ESH concepts for process simplification or to test ESH focused process improvement. To tackle these issues, we are undertaking a collaborative, multidisciplinary program that combines three innovative approaches to deposition and processing of low k materials to meet ITRS roadmap goal of dielectric constants lower than 2.0. If successful, the resulting low k material will be produced using an all-dry process and patterned using a much simplified process flow.

The three participating research groups bring together expertise in three distinct areas: Gleason is internationally recognized for her work in chemical vapor deposition, Ober is known for his work in high resolution lithography and the investigation of molecular glass photoresists while Watkins is one of the leading innovators in the use of supercritical (sc) CO_2 in the processing of low k materials. Gleason and Ober have established a successful track record of collaboration in the ERC while Watkins and Ober have a successful joint program on the templating and patterning of block copolymers. Each aspect of this program [(i) photoinitiated CVD, (ii) scCO_2 processing, (iii) lithography using molecular glasses] is designed to test new concepts in ESH friendly semiconductor processing. Each research group also provides access to unique facilities (CVD deposition tools [MIT], scCO_2 processing equipment and nanoimprint lithography [UMASS], nanofabrication facility [Cornell CNF]) that is invaluable to this work.

Process simplification and direct pattern formation will be a valuable part of ESH aspects of these studies, because novel processes that avoid costly traditional multistep lithography have enormous potential economic benefit. Use of piCVD will enable the direct formation of small-scale low k structures by additive processes without separate expose and etch steps. Conventional aqueous base development is not appropriate for processing current CVD deposited low k materials, because the non-polar nature of the dielectric material requires non-polar developers such as sc CO_2. High-resolution lithography itself is also currently undergoing dramatic improvements as we continue on the ITRS roadmap to sub-35 nm resolution. It is a goal therefore to incorporate these new lithographic approaches into our studies of candidates for reduced process flow in low k materials. These approaches include the use of shorter wavelength sources (EUV), new molecular architectures (molecular glasses), and unconventional patterning methods (step and flash). We believe that by coupling new lithographic methods and materials with piCVD and processing low k materials with supercritical CO_2 we have the means necessary to make important progress.

The unique physicochemical properties of supercritical fluids (SCF) are ideally suited to materials chemistry and processing within device nanostructures, particularly those related to semiconductors. The density of SCFs, which can approach those of liquid solvents, is sufficient to dissolve small non-polar organic and organometallic compounds to enable solution-based processing while the gas-like transport properties and absence of surface tension provide marked process advantages. Thus the use of solution-based processing (no volatility constraints) in a “dry” media that flows like a gas

is nearly ideal for device fabrication. For example, recent work has demonstrated the utility of SCF processing for conformal metal deposition in high aspect ratio features, the preparation of ultra-low k dielectric films, etching of metals and metal oxides and now the deposition of conformal semiconductor films, including HfO_2. Results to date indicate these approaches can be scaled for utility through the end of the CMOS roadmap. This represents a significant technical driver and while SCF technology implementation is both viable and competitive, SCF processing may also be necessary at 45 and 32 nm given limitations of existing deposition and processing techniques. Moreover, the ESH aspects of sc CO_2 processing extend beyond the use of benign media to include higher conversion of precursors (approaching 100% for metallization and low k applications) and elimination of undesirable chemical constituents such as fluorinated ligands used to promote volatility in vapor phase processing.

Method of Approach:

(i) piCVD: Photoinitiated CVD developed by **Gleason** is an evolutionary approach to plasma enhanced CVD, with the main difference being that UV photons, rather than an electric field, are used to excite the reactive processes. Indeed, the use of light exposure in semiconductor manufacture is well known from rapid thermal processing technology. The photoinitiated CVD is used to grow the low k material by initiating free radical chemistry from the patterned surface (Fig. 1). Selectivity is obtained by first patterning a thin base layer of a material containing abstractable hydrogens onto an aprotic base layer using either (i) DUV lithography or (ii) step and flash imprint lithography. Next a vapor phase initiator in the presence of ultraviolet light is used to generate growth sites for the low k material. Low k matrix precursors are subsequently assembles onto the reactive surface sites. The low k precursors include CVD capable silicate species which form molecular glasses.

An existing 200 mm diameter CVD reactor system in the **Gleason** lab is being used for the photoinitiated CVD. High resolution patterning and reactive site deposition is being carried out at the **Cornell** Nanoscale Facility. Step and flash lithography will be performed on equipment which is newly available at **UMASS**. All instrumentation required to evaluate film chemistry (Fourier Transform IR and X-ray photoelectron spectroscopies), mechanical properties (nanoindentation), dielectric properties, and thermal stability is available at **MIT**.

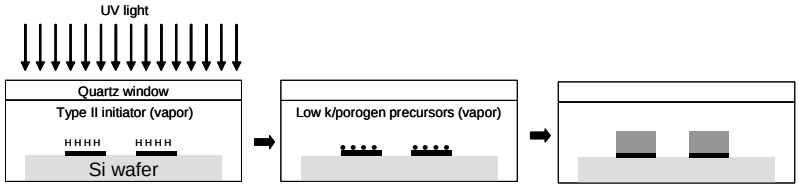

Figure 1. Schematic (not to scale) of piCVD process for selective deposition of patterned low k dielectric lines (dark grey, right) using existing 200 mm diameter chamber at MIT.

(ii) Molecular Glass Precursors and Porogens for Low k: We are investigating molecular glass precursors and porogens for low k materials. Molecular glasses are large molecules (500 to 1000 g/mol) that form non-crystalline bulk and thin film structures. As film formers they have many of the properties of polymers. Molecular glasses formed from non-polar hydrocarbon or inorganic materials make ideal components for a new generation of low k materials. Molecular glass precursors are being synthesized by **Ober** using synthetic schemes developed expressly for these studies. New structural concepts

from organic and inorganic materials that provide low k, high T_g, thermal stability and mechanical robustness will be developed. Low dielectric constant films will be formed from these precursors by selected deposition processes including piCVD in collaboration with **Gleason.**

Porogens and pore formation represent an important strategy for lowering the dielectric constant of low k materials. Porogens are added to a low k matrix to act as spacers and are ultimately removed leaving air as a key part of the dielectric. Porogens, dispersed during deposition into low k materials, will be derived from a number of materials including small molecules and molecular glasses. The strategy of mixing an organosilicon glass (OSG) matrix and porogen precursors grown by CVD will be compared to the strategy of synthesizing a single low k precursor deposited by other means, such as a block copolymer (discussed below) comprised of both matrix and pore forming regions. Porogens will be removed by UV exposure or by $scCO_2$ processing by **Ober** and **Watkins** and the resulting dielectric permittivity of these new materials will be thoroughly investigated.

(iii) $scCO_2$ Processing of Low k Materials: Recently **Watkins** reported a new approach to mesoporous ultralow k (ULK) silicate films that involved 3-D replication of self-assembled block copolymer templates in $scCO_2$. We are investigating this new process as a simplified alternative to CVD methods. The approach, involving the deposition of polymer films and infusion with inorganic precursor, yields families of films with highly ordered spherical pore structures (Fig. 2) and dielectric constants as low as 1.8. A film with a dielectric constant of 2.2 was shown to survive a planar CMP test under conditions typically employed for dense carbon doped oxides. Now, second-generation template systems based on the self-assembly of blends of amphiphilic block copolymer surfactants and homopolymers that exhibit strong interactions with the hydrophilic segment of the template are being explored to yield well ordered films with spherical pores of less than 2 nm.

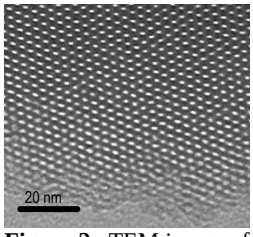

Figure 2 . TEM image of a mesoporous silicate film templated by a blend of a block copolymer and poly(hydroxystyrene).

Nanoscale pores which are significantly smaller than feature dimensions and self assembled to create ordered rather than random pore arrangements hold the promise of not only provided dielectric permittivity lower than possible today but also improving the mechanical properties of the low k materials above the threshold required by subsequent chemical mechanical polishing (CMP) and flip chip bonding steps. An enabling advantage of this approach is the separation of template preparation (via spin coating and self assembly) and silicate network formation into discrete steps. Using this method, structures can be wholly reproduced in the silicate film with high fidelity. We are investigating an extension of the $scCO_2$ replication technique to yield directly patterned ULK films that will eliminate or substantially reduce the need for dielectric etch and will offer good dimensional control in small features. These goals are being accomplished by preparing photo-patternable templates based on block copolymer resist structures and potentially molecular glasses that will be patterned prior to infusion. With **Ober**, new block copolymers and molecular glasses are being synthesized capable of template formation and direct lithographic processing. Recent feasibility experiments have demonstrated that selective infusion of exposed homopolymer resists containing a photoacid generator prior to development yield patterned dielectrics directly. Now, the work is being extended to self-assembled block copolymer resist systems. The technique can be expanded to other means of polymer template patterning including nano-imprint lithography (available at

UMass with the installation of a Molecular Imprints tool in February '06) and substrate-directed block copolymer assembly. The latter has been demonstrated by Nealey and others to yield superior dimensional control at length scales of 20 nm and less. Direct replication of patterned polymer templates to yield patterned dielectrics would represent a significant compression of process steps yielding both economic and technical benefit**.**

Highlights of Results and Accomplishments:
(i)piICVD

Tethered initiators have been prepared in order to grow low-k films directly from a substrate. Both a type I and type II initiators have been synthesized and tethered to a silicon wafer for preliminary experiments (Fig. 3). The optimal strategy for patterning the surface tethered initiators is currently being explored. Ideally, these initiators can be vapor deposited in a patterned way using a shadow mask. They can also be initiated in a patterned way using masked UV exposure. This dual strategy allows for flexibility in patterning in growth techniques.

Fig. 3. Type I and type II tethered radical initiators synthesized and attached to a silicon wafer.

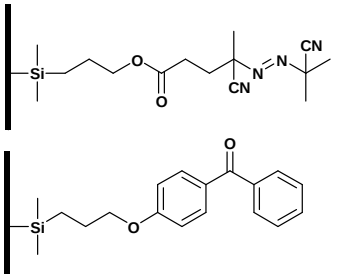

Direct deposition of patterned features by vapor deposition by using prepatterned, yet untethered, initiators was also successfully achieved. These selective piCVD experiments were performed utilizing microcontact printing of patterned type II initiator on silicon wafers. Initial pattern features were 100 μm by 200 μm rectangles and the benzophenone initiator was stamped from an acetone solution. Following stamping, wafer samples were exposed to 254 nm UV irradiation in the presence of vinyl deposition precursors. These conditions did not yield continuous deposition within the feature area but instead left thin (~3 μm) lines of deposition demarking the outside edge of the pattern. However, these lines do not always follow the outline of the stamp (Fig. 4). The high solubility of the initiator in the solvent was the likely cause of this phenomena, allowing for movement and concentration of the initiator during the drying of the solvent on the surface of the microcontact stamp.

Fig. 4. Scanning electron micrographs of 'outline' deposition created by first patterning experiments showing fidelity for one rectangle while the corner of an adjacent rectangle is not faithfully reproduced. Linewidth of the directly deposited feature is ~3 μm.

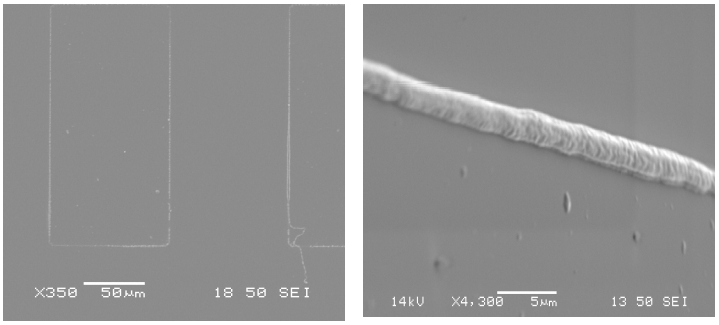

In order to avoid this issue, another type II initiator with significantly reduced solubility

was selected, Michler's Ketone (MK). At first, use of the MK initiator yielded no deposited material. The affinity of the initiating species for the surface of the stamp over the surface of the wafer was determined to be the cause. To overcome this issue, the wafer surface was modified with a monolayer of a hydrophobic silane. This created a favorable change in surface energy of the wafer, allowing the deposition of completely filled in 100 µm scale rectangular features (Fig. 5).

Fig. 5. Optical micrograph of completely filled 100 x 200 µm rectangular features selectively deposited by piCVD.

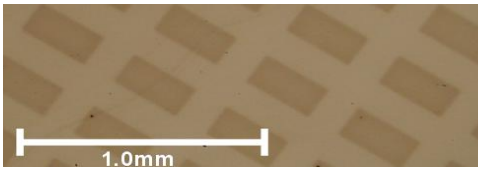

Optimization of process conditions was required in order to create thicker features as initial 100 µm feature deposition only reached a total thickness of 30-50 nm. Deposition pressure and wavelength of UV excitation were both optimized, with a final wavelength of 365 nm irradiation selected. This allowed for higher deposition rates, increasing from 50 nm in 45 min to rates as high as 7.5 nm/min for deposition of 100 µm lines (Fig. 6, left).

Fig. 5. Scanning electron micrograph of lines and spaces at 100 µm (left) and 25 µm (right) resolution created through selective piCVD starting from a patterned of surface initiator. Feature heights are ~300 nm as determined by profilometry.

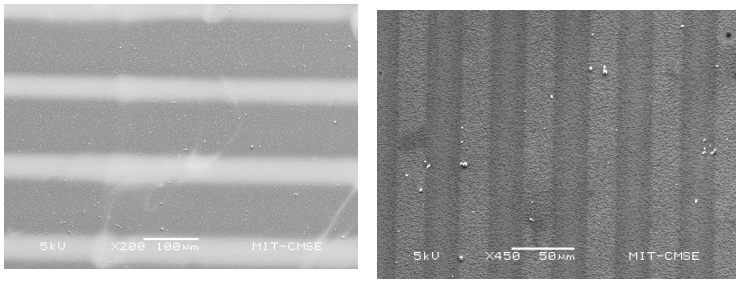

Using these improved conditions, smaller Line features in the 10-25 µm range were deposited with good repeatability (Fig. 6, right). Further optimization of feature size will be sought through modification of the surface patterning method. Other lithographic methods such as photo-bleaching of blanket initiator films will be undertaken.

Fig 6. Dissolution rates of various protection ratios of HHPB in $scCO_2$. Above 70% protected, these molecules are very soluble in $scCO_2$.

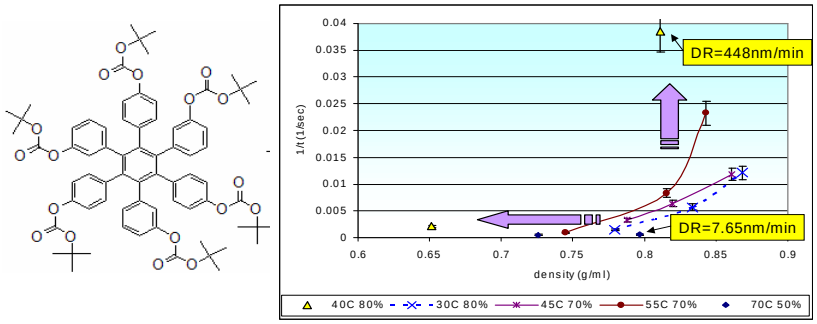

(ii) Molecular Glass Precursors and Porogens:

Past work has demonstrated the solubility of small glass-forming molecules in $scCO_2$. From this, general trends of $scCO_2$-solubility could be inferred. However, more specific solubility properties need to be calculated in order to design appropriate molecular glass precursors and porogens for $scCO_2$ processing. A supercritical CO_2 dissolution rate monitor (DRM) was used in order to study and compare the dissolution rates of molecules with different sizes and functionalities.

Hexa(hydroxyphenyl)benzene (HHPB) derivatives have shown excellent $scCO_2$ solubility while still showing patternability like a photoresist. Using the DRM, dissolution rates of these fully-protected molecules at some conditions were above 400 nm/min. In contrast, HHPB derivatives protected less than 70% dissolved at less than 10 nm/min. This suggests that any small molecule with more than one free hydroxyl group is sparingly soluble in $scCO_2$, while molecules with 0 or 1 free hydroxyl groups can have excellent solubility (Fig. 7). This was also investigated using a trisphenol-based molecular glass.

Molecular glasses of this type have also shown versatility in their method of deposition. Because of their small size, these molecules do have a nonzero vapor pressure at elevated temperatures. Using this fact, one can conceive of vapor depositing these materials onto a cooled substrate. In this way, small molecule photoresist components have been deposited using a vacuum chamber equipped with individually-heated material sources to evaporate the components. Photoresist films created using this physical vapor deposition (PVD) process have been patterned and developed with submicron features shown. These concepts can easily be applied to low-k analogs of these components. As an added ESH benefit, the system shown in Fig. 7 was developed in pure water.

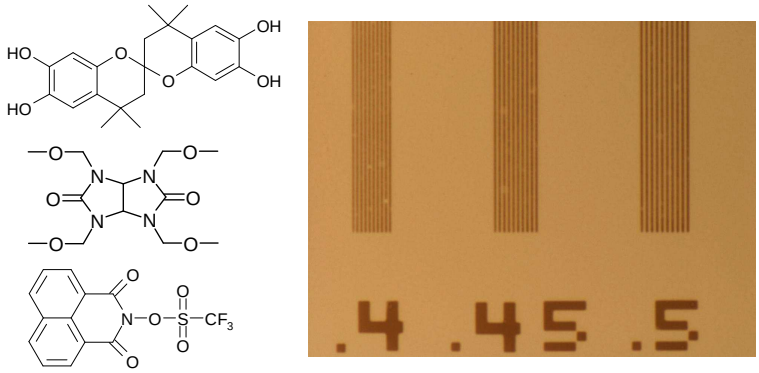

Fig 7. A three-component photoresist system applied using PVD, patterned using an i-line stepper, and developed in water.

Materials based on simple sugars have been synthesized in an effort to make porogens that can be vapor deposited and have a low decomposition temperature. These porogens can be inert in type or have reactive groups to chemically bind it to the surrounding low-k matrix (Fig. 8). The smallest of these compounds have a clean decomposition temperature of <200ºC, meaning that post-deposition processes can occur at much lower temperatures than used currently. Also, all porogens should be independently soluble in $scCO_2$ given their small size and non-polarity.(iii) $scCO_2$ Processing of Low k Materials

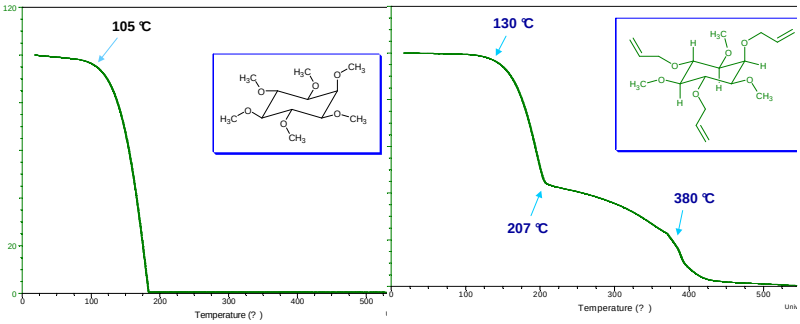

Fig. 8. Decomposition temperatures and weight losses for two porogens synthesized. The porogens on the left decomposes cleanly

Mesoporous silica films with microscopic and nanoscopic features are fabricated by infiltrating silica precursors into patternable block copolymer templates containing photoacid generators. In our scheme the PAG serves two purposes: it deprotects the resist while simultaneously providing the acid catalyst required for silica network formation upon infusion of the precursor. During this period we have demonstrated the feasibility of this approach using a contact mask. Using selective irradiation, the presence of acid in the film can be spatially controlled, yielding in turn selective condensation of silica within the exposed regions. Moreover, because the acid segregates to the hydrophilic block of the deprotected resist, silica condensation is further localized to the hydrophilic domains in the block copolymer template. Since little silica condensation occurs in the hydrophobic domains, which serve as the porogen, mesoporosity is generated in the patterned film upon template removal. The process is shown schematically in Scheme 1.

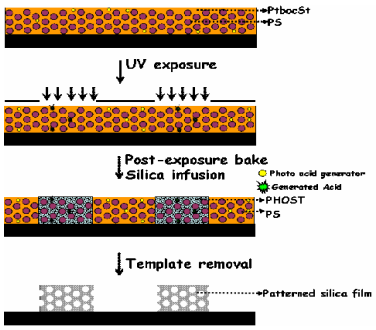

Scheme 1. Using selective irradiation, the presence of acid in the film can be spatially controlled, yielding in turn selective condensation of silica within the exposed regions.

Figure 9 shows an AFM image of a patterned mesoporous silica film having ~ 13 μm holes prepared by exposure of poly(styrene-b-tertiary butyl oxy carbonyloxy styrene) (PS-b-PtbocSt) block copolymer (55% PtbocSt) exposed using a contact mask followed by infusion and condensation of TEOS within the patterned template using CO_2 as the carrier. Triphenyl sulfonium triflate was used as the photo acid generator. AFM section profiles in figure 5b reveal sharp sidewalls within the ~ 200 nm deep features. The chemical amplification process used to deprotect this PS-b-PtbocSt copolymer is essential to limit the diffusion of generated acid from exposed regions to unexposed regions. Now that feasibility has been established, high resolution patterning is currently underway to achieve sub-micron features and ultimately to determine process resolution. The mesoporous structure of the silica films imparted by removal of the block copolymer template is shown in the TEM image shown in Fig. 10. The pores are not well ordered due to weak microphase segregation in the template copolymer used for the feasibility

study. The preparation of well-ordered mesoporous structures using suitable chemically-amplifiable block copolymer systems are now being explored.

Figure 9 (a and b): AFM image of patterned mesoporous silica film templated from P(S-b-tbocSt) and its section profile.

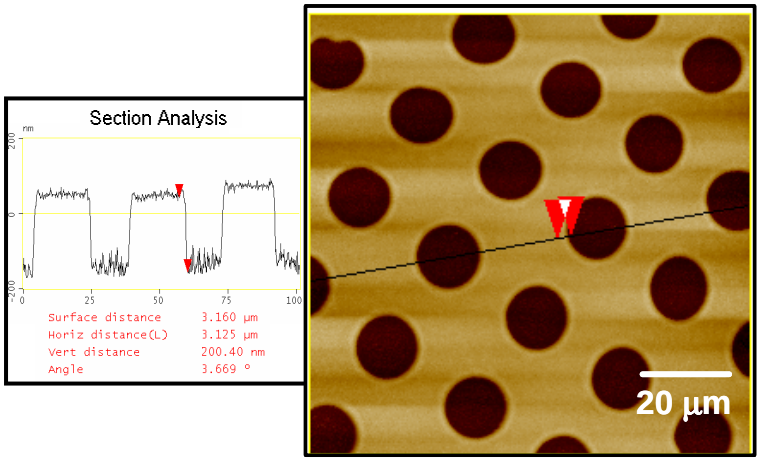

Figure 10: TEM image showing the Mesoporous structures present in the mesoporous silica film templated from P(S-b-tbocSt).

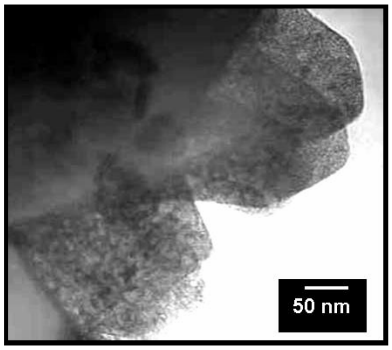

Industrial Interactions and Technology Transfer:

- George Barclay, Rohm & Haas Microelectronics
- Heidi Cao, Intel
- Dr. Kelvin Chan, AMAT
- Ralf Dammel. AZ-Microelectronics
- Dr. Thomas Diamond, IBM
- Li Jia, Rohm & Haas Microelectronics
- Mingqi Li, Rohm & Haas Microelectronics
- Dr. Todd Ryan, AMD
- Richard Schenker, Intel
- Dr. Dorel Toma, TEL
- Dr. Qingguo Wu, Novellus

ESH impact:

	Usage Reduction			Emmision Reduction			
Goals/Possibilities	Energy	Water	Chemicals	PFCs	VOCs	HAPs	Other
Reduce organic solvents used in processing materials	No energy used to purify and treat water	Eliminate need for water usage	Up to 100% reduction of organic solvents used	N/A	Minimal use of organic solvents	Up to 100% reduction of HAPs	N/A
Reduce processing time / temperature	Reduce anneal process costs	N/A	N/A	N/A	N/A	N/A	N/A
Additive processing	N/A	N/A	Eliminate waste of costly material	N/A	Minimal use of organic solvents	N/A	N/A

Publications:

- Dai, Junyan; Chang, Seung Wook; Hamad, Alyssandrea; Yang, Da; Felix, Nelson; Ober, Christopher K. Molecular Glass Resists for High-Resolution Patterning. Chemistry of Materials (2006), 18(15), 3404-3411.
- Mao, Yu; Felix, Nelson M.; Nguyen, Peter T.; Ober, Christopher K.; Gleason, Karen K. Positive- and negative-tone CVD polyacrylic electron-beam resists developable by supercritical CO_2. Chemical Vapor Deposition (2006), 12(5), 259-262.
- Bratton, Daniel; Ayothi, Ramakrishnan; Felix, Nelson; Cao, Heidi; Deng, Hai; Ober, Christopher K. Molecular glass resists for next generation lithography. Proceedings of SPIE-The International Society for Optical Engineering (2006), 6153(Pt. 1, Advances in Resist Technology and Processing XXIII), 61531D/1-61531D/9.
- Felix, Nelson; Tsuchiya, Kousuke; Luk, Camille Man Yin; Ober, Christopher K. Supercritical CO2 for high resolution photoresist development. Proceedings of SPIE-The International Society for Optical Engineering (2006), 6153(Pt. 1, Advances in Resist Technology and Processing XXIII), 61534B.
- Chang, Seung Wook; Ayothi, Ramakrishnan; Bratton, Daniel; Yang, Da; Felix, Nelson; Cao, Heidi B.; Deng, Hai; Ober, Christopher K. Sub-50 nm feature sizes using positive tone molecular glass resists for EUV lithography. Journal of Materials Chemistry (2006), 16(15), 1470-1474.
- Ober, Christopher K.; De Silva, Anuja; Felix, Nelson; Bratton, Daniel; Ayothi, Ramakrishnan. Achieving high resolution patterning using molecular glass photoresists. Abstracts of Papers, 231st ACS National Meeting, Atlanta, GA, United States, March 26-30, 2006 (2006)

- Felix, Nelson M.; Tsuchiya, Kousuke; Ober, Christopher K. High-resolution patterning of molecular glasses using supercritical carbon dioxide. Advanced Materials (Weinheim, Germany) (2006), 18(4), 442-446.
- A. D. Ross, K. K. Gleason, The CVD of Nanocomposites Fabricated via Ultrasonic Atomization Chemical Vapor Deposition, Volume 12, Issue 4, Date: April, 2006, Pages: 225-230
- W. Shannan O'Shaughnessy, Meiling Gao, and Karen K. Gleason, Initiated Chemical Vapor Deposition of Trivinyltrimethylcyclotrisiloxane, Langmuir 2006, 22, 7021-7026
- Yu Mao and Karen K. Gleason,Vapor-Deposited Glycidyl Copolymer Thin Films with Improved Mechanical Properties, Macromolecules, 39 (11), 3895 - 3900, 2006.
- Yu Mao and Karen K. Gleason, Positive-Tone Nanopatterning of Chemical Vapor Deposited Polyacrylic Thin Films, Langmuir, 22 (4), 1795 -1799, 2006.
- Nagarajan, S.; Pai,, R.A.; Russell, T.P.; Watkins, J.J.*; Li, M.; Bosworth, K.S.; Busch,P.; Smilgies, D. M.; Ober, C.K. An Efficient Route to Mesoporous Silica Films with Perpendicular Nanochannels; submitted to Advanced Materials, 2006

Conference Presentations:

- C. K. Ober, American Physics Society, Baltimore, MD, March 11 – 12, 2006. "Short Course Lecture on Lithography", *invited talk.*
- C. K. Ober, 231st American Chemical Society Meeting, Atlanta, GA, March 26 – 30, 2006, "Achieving high resolution patterning using molecular glass photoresists", *invited talk*
- C. K. Ober, 23rd Photopolymer Conference, Chiba, Japan, June 27 to June 30, 2006, "New PFOS-free photoresist systems for EUV lithography"
- C. K. Ober, 2006 IEEE Lithography Workshop, Charlottetown, PEI, Canada, July 31-Aug 4, 2006. "Molecular Glass Resists: Do We Need Polymers Anymore?", *invited talk.*
- Felix, N. M. "Supercritical CO_2 for High-Resolution Photoresist Development", SPIE Microlithography, San Jose, CA, Feb 2006.
- Felix, N. M. "Molecular Glasses for Next-Generation Lithography", INVENT EUV Symposium, Albany, NY, April 2006.
- Felix, N. M. "High-Resolution Photoresist Systems Developable in Supercritical CO_2", SRC Student Symposium, Cary, NC, October 2006.
- KK Gleason, "Design of Chemical Vapor Deposition Processes for Low k Dielectrics and Air Gap Formation", IMEC: Leuven, Belgium (invited), 1/23/06
- KK Gleason, "Fundamentals of Chemically Vapor Deposited Organosilicate Glass (OSG) Low-k Dielectrics", MIRAI workshop on Interconnect Technology for low k Interlayer Insulation", Tsukuba, Japan (invited plenary), 2/17/06

- WS O'Shaughnessy, DJ Edell, and KK Gleason, “Initiated Chemical Vapor Deposition of Organosilicon Coatings”, 2006 Spring Materials Research Society Conference, San Francisco, CA, 4/17/06
- KK Gleason, “Initiated Chemical Vapor Deposition (iCVD) of Polymeric Thin Films”, City College of New York City College NY, Chem. Eng. Departmental Colloquium (invited), 4/24/06
- KK Gleason, “Mechanistic Aspects of Initiated Chemical Vapor Deposition (iCVD) of Polymeric Films”, 209th Electrochemical Society Meeting: Denver, Colorado (invited), 5/9/06
- KK Gleason, “Polymeric Nanocoatings by Chemical Vapor Deposition”, Utrecht University, (invited as Debye Lecture), 6/14/06
- WS O'Shaughnessy, N. Mari-Buye, DJ Edell, and KK Gleason, “Vapor phase polymerization of Organosilicons”, PPST 20th Anniversary Symposium, MIT, Cambridge, MA, 9/8/06
- KKS Lau and KK Gleason, “Initiated Chemical Vapor Deposition, 4th Int. Conf. Hot-Wire” (Cat-CVD) Process, Takayama, Gifu, Japan (invited as keynote presentation), 10/4/06
- KK Gleason, “Density functional theory applied to the Chemical Vapor Deposition of Low Dielectric Constant Materials”, ERC for Environmentally Benign Manufacturing Webcast, 11/30/06
- Watkins, J.J. International Symposium on Supercritical Fluids, Kyoto Japan, Plenary Lecture "Supercritical Fluid Technology for the Fabrication of Functional Nanostructured Films and Devices"(Invited, November 2006)
- Watkins, J. J. American Chemical Society 2006 Fall Meeting, San Francisco, CA, PMSE Division " Preparation of Nanostructured Materials by the 3-D Replication of Block Copolymers in SCFs"(Invited, September 2006)
- Watkins, J. J. American Chemical Society 2006 Polymer Biennial, Key Biscayne, FL "Preparation of Nanostructured Materials by the 3-D Replication of Block Copolymers in SCFs" (Invited, May 2006)
- Nagarajan, Sivakumar; Russell, Thomas; Watkins, James; “Patterned mesoporous media via 3-D replication in supercritical carbon dioxide”, paper R24.00005, 2006 APS Annual Meeting, Baltimore, MD.

Next Year Plan:

- Synthesis, deposition, and lithographic patterning of novel type 2 initiating species to decrease feature size and improve morphology
- Photoinitiated CVD of molecular glass low k materials with optimized morphology.
- Test utility of novel porogen materials in reducing dielectric constant of molecular glass structures
- Uniform organosilicate ULK film containing ~ 2 nm pores with a dielectric constant less than 2.1 and a hardness > 1 GPa. Optimize film composition and chemistry. Begin template development for directly patterned films.
- Development of a photo-patternable template for SCF infusion and feasibility demonstration for a directly patterned ULK film.

- Prepare and assess new porogens for ULK materials compatible with $scCO_2$ processing

Non-PFOS/non-PFAS Photoacid Generators: Environmentally Friendly Candidates for Next Generation Lithography

Personnel:

PIs:

- Reyes Sierra, Chemical and Environmental Engineering, UA
- Christopher K. Ober, Materials Science & Engineering, Cornell University

Other Research Personnel:

- Dr. Ramakrishnan Ayothi, Materials Science & Engineering, Cornell University

Graduate Students:

- Victor M. Gamez, Chemical and Environmental Engineering, UA
- Nelson Felix, Chemical and Biomolecular Engineering, Cornell University

Undergraduate Students:

- Matthew West, Chemical and Environmental Engineering, UA

Objectives:

This project aims to develop new perfluoro-octyl sulfonate (PFOS)-free (and perfluoroalkyl sulfonate (PFAS)-free) PAGs and investigate the environmental behavior of these PFOS-free alternatives. The proposal will continue work on the development of PFOS-free ionic and non-ionic PAGs in the Ober group. This research will be conducted in close collaboration between the Sierra and Ober groups that will evaluate the environmental compatibility of the new chemistries.

Background:

Perfluorooctyl sulfonate and related long-chain perfluorinated compounds (PFOS/PFAS) are under increased scrutiny as priority environmental contaminants due to recent reports of their detection in environmental and biological matrices as well as concerns regarding their persistence and toxicity. PFOS has a significant bioaccumulation potential and this chemical has been detected in part-per-billion levels in animals worldwide, including remote locations such as Siberia and Antarctica and in the international blood bank. In response to the increasing concern about the public health risks associated to PFOS, a major manufacturer of this chemical, 3M, recently ceased production of this chemical and the US Environmental Protection Agency is moving forward with a ban to its manufacture and use.

Nevertheless, PFOS and other long chain perfluorinated materials are vital to many industrial processes, including semiconductor manufacturing where they are utilized in photoacid generators (PAGs), anti-reflective coating (ARCs) and certain surfactants. PAGs are light sensitive compounds that are used to alter the solubility of photoresists in regions exposed to UV or e-beam radiation. Perfluorination increases acidity of the chemical and reduces the volatility of the generated acids. There is some urgency in finding a replacement family of materials, because any commercial use may take as long as 10 years to become fully qualified. [1]

We therefore propose to develop new PFOS-free (and PFAS-free) PAGs and investigate the environmental behavior of these PFOS-free alternatives. Our strategy is to create PAGs that have acidity equivalent to that of PFOS based materials by incorporating short (1, 2 or 3) CF_2 units next to the sulfonic acid. Our hypothesis is that these materials are environmentally friendly because the additional functions on the PAG lack fluorination. The performance characteristics of such materials have been demonstrated [2], but the ESH attributes are virtually unknown. We therefore propose to couple work on the development of non-PFOS/non-PFAS PAGS (Ober group) to environmental studies of these new materials (Sierra group).

Method of Approach:

Ober and his group have synthesized new PFOS- and PFAS-free photoacid generators following a design strategy involving use of short CF_2 segments linked to sulfonic acid groups. Both iodonium and sulfonium cation groups will be used for the chromophore. The remainder of the PAG is built from specially synthesized non-PFOS/non-PFAS sulfonium anions and consist of functions that are chosen for their ability to improve resist compatibility, reduce PAG volatility and improve line edge roughness performance. To date we have examined alkyl, phenyl ether and alkyl halide groups. PAGs with such structures are being synthesized for resist performance evaluation and environmental assessment. We plan to explore other chemical units such as lactones, ketones and other groups that have been used in photoresists to enhance PAG miscibility and other performance factors. A schematic of PAG structures is shown in the Figure 1.

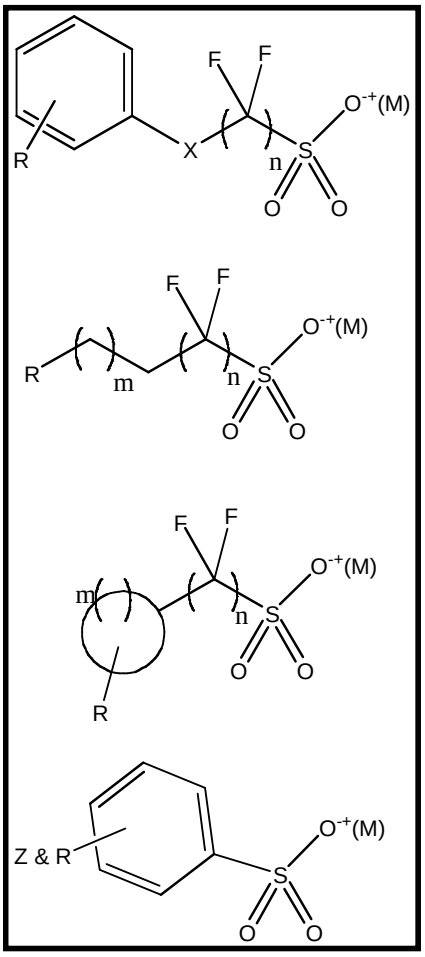

Figure 1 *Non-PFOS/non-PFAS PAGs that will be synthesized and studied in this proposal. SF1 and SF2 have the structure of the uppermost acid.*

We are assessing PAG lithographic performance at both 193 nm and EUV wavelengths in a series of resists selected from commercial, commercially inspired and experimental resists for 193 nm patterning (both dry and immersion) [3] and experimental EUV resists [4]. As we test PAG performance, it will be important to examine photoresists with demonstrated high performance for valid comparison with existing commercial and experimental resists. We expect to work closely with the experts at International Sematech for resist selection. We plan to make use of the excellent facilities provided by the Cornell Nanofabrication Facility and those of International Sematech as needed. The activities of SRC supported graduate students will be leveraged in this work, as they will supply the experimental host resists.

Dr. Sierra's research group is evaluating key environmental properties of the novel PAGs, *i.e., 1)* their

bioaccumulation potential; *2)* susceptibility to biodegradation by microorganisms commonly found in wastewater treatment systems; and *3)* toxic effects. The tendency of PAGs to accumulate in biosolids is being assayed using standard techniques. The biotransformation of PAGs by cometabolism and their utilization as sole carbon source will be evaluated in laboratory assays. Cooxidation potential will be evaluated under aerobic heterotrophic- and nitrifying conditions. Assays will be designed to simulate typical conditions in biological wastewater treatment plants. The new PAGs considered in this study are only partially fluorinated. Lower halogenated hydrocarbons are generally susceptible to attack by monooxygenases [5]. An interesting approach for the biodegradation of the non-perfluorinated PAGs is to take advantage of ammonia monooxygenases (AMO) of nitrifying microorganisms. Since a nitrification stage is typically part of the wastewater treatment train in most publicly owned treatment works (POTWs), cooxidation with AMO would imply no modification of existing wastewater treatment processes to attain biodegradation goals. Toxicity testing will employ common indicator organisms (e.g., Microtox assay, toxicity to aerobic and anaerobic bacteria). Cytotoxicity will be monitored using the MTT assay (mitochondrial activity) [6]. In addition to PAGs, the toxicity of metabolites from their microbial conversion will be also profiled. Compounds passing the initial technical and environmental compatibility screening will be tested for their treatability by conventional methods. Treatment of PAGs is not only a prerequisite for discharge but will also be required for the reuse of water. Techniques to be evaluated will include physico-chemical and biological methods such as activated carbon adsorption, ion exchange, advanced oxidation methods and activated sludge treatment. This research will benefit from state-of-the-art pilot-scale effluent treatment facilities available at the NSF/SRC Engineering Research Center for Environmentally Benign Semiconductor Manufacturing (ERC).

Highlights of Results and Accomplishments:
Cornell University:

The new PAGs are readily soluble in common organic solvents (dichloromethane, ethyl acetate, acetone and acetonitrile) and polar solvents (PGMEA, DPGM, PGME, EL, GBL and 2-butanone). In addition to solvents we also tested PAG miscibility in resist formulations. We prepared both P(hydroxystyrene-*co*-styrene-*co*-t-butyl acrylate) and P(γ-butyrolactone methacrylate-*co*-methyl adamantly methacrylate) photoresist formulations in PGMEA. The PAGs were incorporated at 10 weight percent with respect to polymer. High solubility of these PAGs in all the preferred solvents as well as in a resist is expected to provide more compositional flexibility and limit the risk of aggregation during storage. The size of the photogenerated acid (PGA) was estimated in terms of the molar volume using ACD software. The molar volume of the PGA follows the molecular weight trends within estimated error (± 3 cm^3) [7]. The acid strength was also estimated by using Taft additive constants [8]. The acid strength and size of both $C_6H_5OCF_2CF_2SO_3H$ (pKa = -4.86; Size = 170 ± 3 cm^3) and $CF_3CF_2CF_2CF_2SO_3H$ (pKa = -4.99; Size = 162 ± 3 cm^3) acids are comparable and the difference is within estimated error.

Photoacid generation and photosensitivity. The most important property of a PAG is its ability to generate acid upon irradiation. This property was confirmed by both IR and

UV-VIS spectroscopy. The photoacid generation in solution was detected by employing Rhodamine B (Rb), a xanthene dye whose optical properties change upon protonation. This property was used to detect acid generation by a PAG in non-aqueous media using a UV-VIS spectrophotometer Solutions dye with PAGs (1 and 2) absorb strongly at 555 nm due to protonation of the dye. Photoacid generation in a film was confirmed using IR spectroscopy by the formation of PHS from poly(4-*tert*-butoxycarbonyloxystyrene). The appearance of a hydroxyl absorbance at 3500 cm^{-1} after irradiation of the polymer with PAGs followed by a mild post exposure bake step at 60 °C results in a decrease in the characteristic *tert*-butoxycarbonyl ester band centered at 1756 cm^{-1} and confirms photoacid generation in the film. The experiments show the effectiveness of the PAG but the results are qualitative in nature. In microlithography studies, the energy to clear (E_0) and energy to size (Es) is commonly used as a measure of photosensitivity of a particular CAR system. The smaller the required dose, the more sensitive the resist formulation. Photosensitivity measurements were carried out using a positive tone high activation energy resist [P(HS-*co*-S-*co*-tBA); 10 % tBA] with ~ 2 wt % PAG with respect to resist (same molar concentration of PAG). The E_0 was found to be 1.36 mJ/cm^2 for both iodonium PAGs (SF1 Iodonium and DPI PFBS) and 1.53 and 1.70 mJ/cm^2 for SF2 sulfonium and TPS PFBS indicating that PAG 1 and 2 behave similar to the standard PAG. In order to determine the Es, DUV experiments were performed with standard P(HS-*co*-S-*co*-tBA), photoresist (25 % tBA). The resist film containing all the PAGs and a standard ESCAP polymer (25 % tBA) resolved 1μm to 500 nm feature size upon exposure to 254 nm. The Es for all the PAGs were in the range of 8 – 10 mJ/cm^2. The experiment above confirms that the performance of the new PAGs in chemically amplified resists is comparable to or better than conventional, less environmentally friendly PFOS and PFAS-based PAGs.

E-beam and EUV lithography imaging. The role of PFOS free PAGs as an effective tool to catalyze the deprotection of high activation type acid labile groups (~ 35 kcal/mol) in a positive tone chemically amplified resist is best demonstrated through E-beam and EUV lithography. E-beam experiments were performed to understand the basic lithographic response (sensitivity and resolution) of these PAGs since e-beam patterning is considered to be a close analogue of EUV lithography. The same resist compositions were then evaluated in EUVL experiments. High activation type P(HS-*co*-S-*co*-tBA) and P(GBLMA-*co*-MAdMA) photoresists were selected for imaging experiments as both are used extensively as photoresist materials for 248 nm and 193 nm lithography with potential for EUVL application.

The lithographic experiments were conducted using standard processing conditions including commonly used solvents and developer. The best and most reproducible results in terms of sensitivity and resolution were achieved by optimizing the processing conditions used for DUV lithography. As discussed above, initial imaging characteristics of PFOS free PAGs as well as PFBS PAGs in P(GBLMA-*co*-MAdMA) and P(HS-*co*-S-*co*-tBA) photoresist were evaluated using e-beam radiation. As an example, Figures 4 and 5 show top-down SEM micrographs obtained for a resist film containing P(GBLMA-*co*-MAdMA)-iodonium PAG and P(HS-*co*-S-*co*-tBA)-sulfonium PAG after development with 0.26 N TMAH. P(GBLMA-*co*-MAdMA)-sulfonium PAG

and P(HS-*co*-S-*co*-tBA)-iodonium PAG resist performance under e-beam radiation and their high resolution SEM images are shown in the supporting information.

Subsequently, EUVL experiments were performed with films containing P(GBLMA-*co*-MAdMA) photoresist and PFOS free as well as PFBS onium PAGs. We selected the P(GBLMA-*co*-MAdMA) photoresist because it shows better overall imaging performance with e-beam radiation under simple processing conditions. Line and space patterns down to 30 nm were resolved. The dose required to resolve sub 40 nm L/S for the all the resists were lower than 8.6 mJ/cm^2. Figure 2 shows high resolution SEM micrographs of the P(GBLMA-*co*-MAdMA)-sulfonium PAG resist that was exposed to EUV radiation and developed using aqueous 0.26 N TMAH.

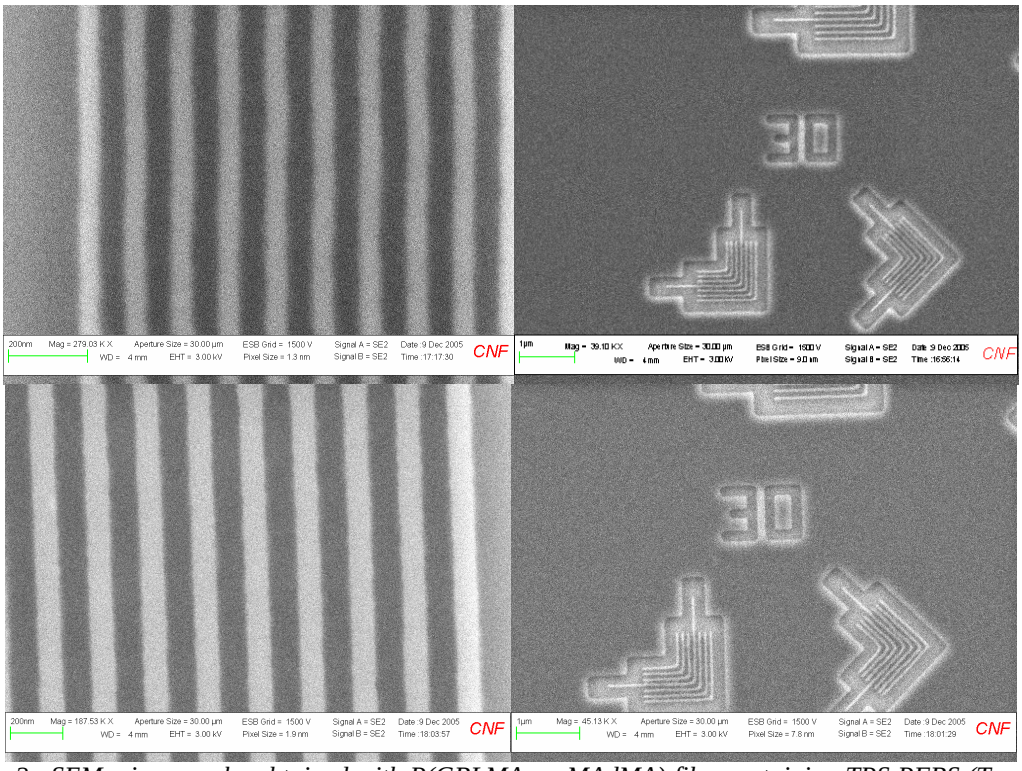

Figure 2. SEM micrographs obtained with P(GBLMA-co-MAdMA) film containing TPS PFBS (Top; Es = 8.6 mJ/cm^2) and SF1 sulfonium (bottom; Es = 7.5 mJ/cm^2) exposed to EUV radiation and developed using 0.26 N TMAH.

University of Arizona:

- Analytical methods have been developed to detect and quantify the ionic PAG compounds supplied by Dr. Ober's group. Compound analysis is performed using an ion chromatograph fitted with an Acclaim Polar Advantage II, C18 column (Dionex), and a suppressed conductivity detector. A mixture of 20 mM boric acid (pH 9.0) and 95% acetonitrile was used as the mobile phase at a flow rate of 1 ml/min. Different gradient programs were developed for the separation of the various PAGs. Non-polar compounds recently received will be determined by high performance liquid chromatography (HPLC) with ultra-violet (UV) detection. Compound degradation is monitored by

chromatographic methods and by analysis of fluoride release (using an ion selective electrode).

- Microbial toxicity experiments with several PAG compounds (sodium salts) and with the PAG counterions, diphenyliodonium and triphenylsulfonium, are currently ongoing. Perfluorobutane sulfonate (PFBS), a commercial compound that has been proposed as a more environmentally benign alternative to perfluorooctane sulfonate (PFOS), has also been included as a reference compound in these assays. The toxicity of these compounds to methanogenic microorganisms has been tested in assays utilizing acetate and hydrogen as substrate. Methanogens are important microorganisms in anaerobic wastewater treatment systems and their activity is required to ensure effective removal of organic matter exerting biological oxygen demand (BOD).

  PFBS and the tested PAGs (sodium salts) were not inhibitory to hydrogen-utilizing methanogens at the highest concentration tested, 500 mg/l (Fig 3). Acetate-utilizing methanogens were more sensitive and some of the compounds tested caused significant inhibition when present at relatively high concentrations (500 mg/l). The PAG counterions, diphenyliodonium and triphenylsulfonium (Fig. 4), were also found to be moderately inhibitory. A concentration of 400 mg/l of either counterion resulted in 50% inhibition of the activity of H_2-utilizing methanogens, and approximately 32% inhibition of acetoclastic methanogens.

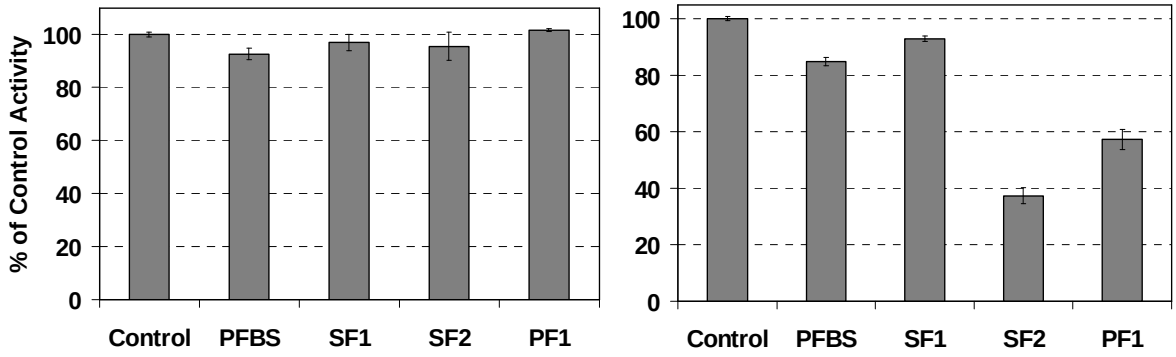

Figure 3. Effect of different PAG compounds (500 mg/l) on the methanogenic activity of: (Left panel): hydrogenotrophic methanogens; (Right panel) acetoclastic methanogens.

Additional assays will be performed to evaluate the impact of PAG chemicals to other key microbial populations in wastewater treatment systems.

Figure 4. Chemical structure of the PAG counterions diphenyliodonium and triphenylsulfonium

Diphenyliodonium Triphenylsulfonium

Figure 5. Toxic response of different PAGs in the MTT assay.

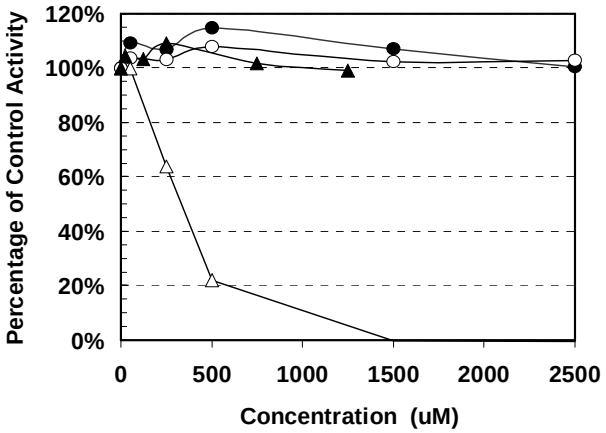

- Preliminary assessment of the cytotoxicity of several PAG compounds (sodium salts), PFBS and the PAG counterions, diphenyliodonium and triphenylsulfonium, has been performed using a colorimetric method, the MTT cell proliferation (cell growth) assay. The MTT assay is widely used in the testing of drug action, cytotoxic agents and screening other biologically active compounds. The assay is based on the cleavage of the yellow tetrazolium salt MTT (3-(4,5-dimethylthiazol-2-yl)-2,5-diphenyltetrazolium bromide) to purple formazan crystal by a mitochondrial dehydrogenase enzyme of metabolic active cells. The number of surviving cells is directly proportional to the level of the formazan product formed, which can be quantified using a simple colorimetric assay.

  The toxic response of PFBS and different PAGs in the MTT assay is illustrated in Fig. 5. Only one of the PAG compounds (PF1) displayed toxicity in this assay with a 50% inhibitory concentration of 90.9 mg/l. The rest of the PAGs did not cause any inhibition even when present at concentrations of 500 mg/l or higher. In contrast, the counterions, diphenyliodonium and triphenylsulfonium, were highly inhibitory and displayed 50% inhibition at concentrations of only 3.6 and 15.6 mg/l, respectively. Additional experiments will be performed to confirm the high toxicity of the PAG counterions.

- Biodegradation assays have been initiated with several PAG compounds and are currently ongoing. Biodegradation assays with PFBS are also run in parallel. Current experiments aim at evaluating the susceptibility of the compounds to degradation under conditions that promote degradation of highly halogenated compounds including aerobic methylotrophic - and anaerobic reductive dehalogenation mechanisms. Activated sludge and anaerobically digested sludge, both obtained from a local municipal wastewater treatment plant, are used as inoculum in the aerobic and anaerobic degradation experiments, respectively. Both inocula are characterized by a high microbial diversity. No significant fluoride release has been detected in the aerobic degradation experiments after 8 weeks of incubation, nor in the anaerobic assays after only 1 week of incubation. Extended periods of adaptation are often required to attain initial biodegradation of complex aromatic compounds. Therefore, monitoring of these assays will be continued over the coming weeks/months.

References:

[1] Jewett, J., S. Harper, B. Leet, R. Meagley, "Perspectives on PFOS". *Teleseminars of the NSF/SRC Engineering Center for Environmentally Benign Semiconductor Manufacturing*. Jan. 27, (2005).

[2] Ayothi, R., C.K. Ober, "A Perspective on perfluorooctyl sulfonate (PFOS) and an overview of non-PFOS based photoacid generators (PAGs): Design, synthesis and performance", *Proc. 12th Annual Int. Semiconductor ESH Conf.*, June 18 - 24, 2005, Portland, OR.

[3] Opitz, J., R.D. Allen, G. Breyta, D.C. Hofer, N. Sundararajan, C.K. Ober, "Polymer-platform-dependent characteristics of 193-nm photoresists." *Proc. SPIE - Int. Soc. Optical Eng.* (1999), 3678(Pt. 2, Advances in Resist Technology and Processing XVI), 1096-1105.

Sundararajan, N., S. Yang, J. Wang, K. Ogino, S. Valiyaveettil, C.K. Ober, S.K. Obendorf, R.D. Allen, "Supercritical CO_2 processing for sub-micron imaging of fluoropolymers", *Chem. Mater.*, 2000, **12**, 41-48.

[4] Chang, S.W., D. Yang, J. Dai, N. Felix, D. Bratton, K. Tsuchiya, Y.-J. Kwark, J.-P. Bravo, C.K. Ober, H.B. Cao and H. Deng, "Materials for future lithography", *Proc. SPIE - Int. Soc. Optical Eng.*, 1 (2005), **5753**.

J. Dai, C.K. Ober, "Novel resists with non-traditional compositions for EUV lithography", *Proc. SPIE - Int. Soc. Optical Eng. (*2004), 5376(Pt. 1, Advances in Resist Technology and Processing XXI), 508-516.

D. Junyan; C.K. Ober, L. Kemper; L. Wang, Cerrina; P.F. Nealey. "Organoelement resists for EUV lithography"**.** *Proc. SPIE – Int. Soc. Optical Eng*. (2002), 4690 1193-1202.

[5] Field J.A., R. Sierra-Alvarez, Biodegradability of chlorinated solvents and related chlorinated aliphatic compounds". *Reviews Environ. Sci. Biotechnol.*. (2004) 3, 185–254.

[6] Mosmann, T., Rapid Colorimetric Assay for Cellular Growth and Survival: Application to Proliferation and Cytotoxicity Assays. *J. Immunol. Meth.* (1983), 65, 55-63.

[7] Ablaza, S. L.; Cameron, J. F.; Xu, G.; Yueh, W. *J. Vac. Sci. Technol., B* **2000**, *18*, 2543.
[8] Perrin, D. D.; Dempsey, B.; Serjeant, E. P. *pKa Prediction for Organic Acids and Bases*, Chapman and Hall, London, 1981.

Industrial Interactions and Technology Transfer:

- Jim Jewett (jim.jewett@intel.com), Intel Corporation
- Ralph Dammel (ralph.dammel@az-em.com), AZ-Microelectronic Materials, Inc.
- George Barclay (GBarclay@rohmhaas.com), Rohm and Haas Microelectronics

ESH Impact:

The creation of new, high performance photoacid generators is needed in view of the EPA ban on the use of PFOS/PFAS chemicals. Such needs also provide an opportunity to optimize PAG design for next generation lithographies. However, little is known if simple chemical changes are sufficient to make new PAGs environmentally acceptable. These studies will thus be of critical importance in assessing synthetic strategies for environmental acceptability and will be used to guide the design of new PFOS-free photoacid generators.

Publications:

- Daniel Bratton, Ramakrishnan Ayothi, Hai Deng, Heidi B. Cao and Christopher K. Ober, "Diazonaphthoquinone Molecular Glass Photoresists: Patterning without Chemical Amplification ", *Chem. Mater*., submitted.
- R. Ayothi, Y. Yi, H. Cao, Y. Wang, S. Putna, C. K. Ober, "Photoacid Generators Containing Arylonium and Aryloxyperfluoroalkylsulfonate Groups for Chemically Amplified Resists", *Chem. Mater*., under revision.
- Ramakrishnan Ayothi, Seung Wook Chang, Nelson Felix, Heidi B. Cao, Hai Deng, Wang Yueh, Christopher K. Ober, "New PFOS Free Photoresist Systems for EUV Lithography"**,** *Journal of Photopolymer Science & Technology*, 19(4): 515-520 2006.
- Ramakrishnan Ayothi, Yi Yi, Christopher K Ober, Steve Putna, Wang Yueh and Heidi Cao, "All-organic Non-PFOS Nonionic Photoacid Generating Compounds with Functionalized Fluoroorganic Sulfonate Motif for Chemically Amplified Resists", *Proceedings of SPIE-The International Society for Optical Engineering* (2006), 6153 -61530J.
- Daniel Bratton, Ramakrishnan Ayothi, Nelson Felix, Heidi Cao, Hai Deng, Christopher K. Ober, "Molecular Glass Resists for Next Generation Lithography", *Proceedings of SPIE-The International Society for Optical Engineering* (2006), 6153 61531D.
- Ramakrishnan Ayothi, Yi Yi, Nelson Felix, Christopher K. Ober, Heidi Cao and Wang Yueh, "Non-PFOS photoacid generating compounds for chemically amplified resists", *Polymer Preprints*, (2006), 47(1), 528-529.
- Seung Wook Chang, Ramakrishnan Ayothi, Daniel Bratton, Da Yang, Nelson Felix, Heidi B. Cao, Hai Deng and Christopher K. Ober, "Sub 50 nm Feature

Sizes using Positive Tone Molecular Glass Resists for EUV Lithography", *J. Mater. Chem*., 2006, **16**, 1470.

Conference Presentations:

- C. K. Ober, 23rd Photopolymer Conference, Chiba, Japan, June 27 to June 30, 2006, "New PFOS-free photoresist systems for EUV lithography"
- C. K. Ober, 2006 IEEE Lithography Workshop, Charlottetown, PEI, Canada, July 31-Aug 4, 2006. "Molecular Glass Resists: Do We Need Polymers Anymore?", invited talk.
- C. K. Ober, Advanced Metallization Conference (AMC) 2006, San Diego, CA, October 17-19, 2006. "Molecular Glass Photoresists: Do We Need Polymers Anymore?", *invited talk.*
- C. K. Ober, University of North Carolina at Chapel Hill, Chapel Hill, NC, Nov. 10, 2006. "Rethinking Photoresists: New Approaches to Making Very Small Structures", *invited talk*

Disclosures and Patents:

A patent application has been filed on ionic non-PFOS/non-PFAS PAGs following the general design strategy described in the proposal. Details of this patent application can be obtained at the Cornell Center for Technology, Enterprise and Commercialization.

Next-Year Plan:

Cornell University: Research will focus on new PFOS free photoacid generators, especially lactone containing PAGs. These materials show excellent performance characteristics for both EUV and also 193 nm lithography. We plan:

1) *Synthetic studies of the new PAGs.*
2) *Lithographic characterization of the PAGs*
3) *Sample preparation of bioassay studies.*

University of Arizona: Research to be conducted in the second year of the project will complete ongoing work aimed at evaluating key environmental properties of the novel PAGs developed by the Cornell University, in particular:

1) Susceptibility to biodegradation by microorganisms commonly found in wastewater treatment systems;
2) Toxic effects;
3) Tendency of PAGs to accumulate in biosolids.

Compounds passing the initial technical and environmental compatibility screening will be selected for further study. In the last year of the project, the most promising PAGs will be assessed for their amenability to treatment by conventional methods.

CMOS Biochip for Rapid Assessment of New Chemicals

Personnel:

PIs:

- David Mathine, Optical Sciences Center, UA
- Raymond Runyan, Cell Biology and Anatomy, UA

Objectives:

The production of a CMOS-based device comprising an array of electro-optical detectors housed within a control reactor amenable to cell culturing and microscale biochemical studies. The device will be used for rapid assessment of the toxicity of new chemicals at the molecular, cellular and tissue levels. Aims include:

1. Fabricate CMOS circuitry to orchestrate electrochemical and photometric measurements of chemical reporters.
2. Construct a microscale reaction chamber that provides adequate control of experimental conditions, including maintenance of a sterile environment suitable for long-term hosting cells and tissues.
3. Genetically engineer cells and tissues for use as harbingers of toxicity.
4. Demonstrate on-device assessment of the toxicity of TCE (known toxin) then move on to new chemicals.

Background:

Traditional means of determining chemical toxicity typically involve expensive and laborious animal studies. These methods cannot keep pace with the rapid pace of development of new chemicals introduced by industry. The advent of biosensing technology promises to yield a high-throughput means of screening even complex mixtures of chemicals for toxicity. By monitoring the physiological activity of cells and tissues, investigators can identify signature responses that indicate toxic insult. Monitoring levels of specific gene or protein expression, cell death and proliferation, and cellular action potentials are some of the ways in which researchers can assay whether a treated model exhibits stress response.

Our approach develops a multi-functional biosensor for the measurement and analysis of cellular responses to experimental interventions or environmental stimuli. The goal of this work is the fabrication and demonstration of a flexible and inexpensive electro-optical platform that can be adapted to assay a wide variety of toxicological endpoints. As one example of the device's application, human cells can be genetically engineered such that certain proteins they produce in reaction to toxic insult are coupled to fluorescent reporters detectable by on-device photodetectors. Exquisitely sensitive, optical measurements of this fluorescence can be used to monitor cell health in real time. Our multisensor fusion approach will permit us to monitor numerous physiological processes simultaneously (gene and protein expression, cellular electrical activity, cell proliferation, etc.) and thus provide a multiform assay of cell health. This will in turn permit online toxicity testing of individual chemicals and complex mixtures.

Method of Approach:

Three main aims must be accomplished before realizing the proposed technology:

1. Next-generation fabrication of a CMOS platform with multi-channel optical and electrochemical detectors integrated into a sterile control reactor.
2. Demonstrate toxic assessment of cells.
3. Development of cell lines that generate molecules that will "report" cell health to the electro-optical detectors.

Aim 1: Device Fabrication

While a prototype device with a CMOS detector chip housed within a biochamber has already been constructed, work continues in this area. Specifically, fabrication already-designed optical filters that capture two-channel fluorescent emissions while filtering excitation wavelengths requires completion. Next multisensor fusion will proceed, in which these optical detectors will be merged with electrochemical sensors on single pads. A pump system has been devised for the sterile, low-flow introduction of analytes (DNA, cells, etc.) into the biochamber but has yet to be purchased and installed. Finally, as the final product is meant to be a self-contained unit, on-board power and information storage equipment will need to be designed and fabricated as well.

Aim 2: Toxic Assessment of Chemicals

Initial work concentrated on calcium studies of cells with exposure to TCE. TCE was chosen because it is a known toxin and can be used to verify the sensor approach. Calcium was chosen since it is a common intracellular messenger used in cells. Initial results were successful in showing toxic response of heart cells. Future work will concentrate on new chemicals.

Aim 3: Development of in vitro *Models*

Based on previous results collected by other labs as well as our own *in vivo* studies, exposure to different chemicals leads to distinct patterns of altered gene and protein expression in specific tissues. Cellular and molecular techniques will be employed to produce a cell line that reproducibly and quantitatively expresses fluorescent reporters in response to the introduction of chemical stimuli. The response will manifest itself as an up-regulation of the expression of the one of the reporter transcripts while leaving the other unchanged. This will lead to the production of proteins that can be measured in ratio to one another via their intrinsic and distinct fluorescence.

Initially, two constructs will be developed. The first will clone the promoter region of CYP 1A1 into a vector encoding for green fluorescent protein (GFP). CYP 1A1 is a metabolic enzyme whose expression is induced in estrogen receptor positive MCF-7 cells in response to exposure to aromatic hydrocarbons such as benzo[a]pyrene. The second construct will result after cloning the promoter of a housekeeping gene coding for the ribosomal 18s protein into a vector encoding yellow fluorescent protein (YFP).

In vitro experiments using fluorescent confocal microscopy will confirm the specificity and linearity of reporter response to benzo[a]pyrene and set benchmarks against which biosensor performance will be compared. Later we intend to expand the set of chemicals tested and organs/systems targeted. Industry input will guide the classes of chemicals explored in this later research.

Highlights of Results and Accomplishments:

I. CMOS Integration

A first generation biochamber has been constructed for maintaining and monitoring cell health. Cells and analytes can be injected into a PDMS inlet port. They are then transported through a microfluidic channel to the PDMS growth chamber. This growth chamber puts the cells and analytes in contact with a silicon smart chip for electrical and optical monitoring of the cells' health and environment.

Figure 1. CMOS chip packaging for integration of fluidic substances with a CMOS chip.

A new packaging approach has also been developed for rapid integration of fluids with the CMOS chip (Fig. 1). This package allows the fluid to make an intimate contact with the CMOS chip without shorting the electrical bond wires and is compatible with existing wire bonding approaches.

II. Calcium Studies

While toxins may act via a variety of mechanisms, we have an interest in using assays that can be optimized for utilization in the CMOS biosensor. Calcium is a common intracellular messenger used in cells. Recent studies in the Runyan lab showed that the solvent, TCE, altered expression of several calcium channel genes in developing hearts. This lead to the prediction that calcium handling would be altered in cells exposed to low levels of TCE. While TCE is not a solvent of major concern for current manufacturing, it provides a useful toxin for laboratory studies as it is commonly found at Superfund cleanup sites, Figure 2 shows differences in calcium handling within TCE exposed cells using the fluorescent dye, Fura 2. P19 cells were exposed in culture to low levels of TCE for 24 hours and then treated with vassopression (VP) to produce an intracellular flux of calcium that could be measured by changes in fluorescence. The data show that intracellular calcium is delayed in both release and uptake from intracellular stores but that the total calcium flux is much greater in TCE treated cells. This may indicate the involvement of cell surface calcium channels as well. The images shown in this figure were produced with a conventional microscope and CCD camera, but we expect that the greater sensitivity of the CMOS chip will be able to provide efficient measurement of calcium changes and a more accurate measurement of calcium release from the intracellular store.

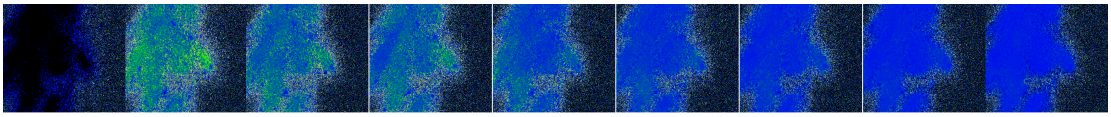

Control for 10ppb/100ppb TCE cells @ 10nM VP

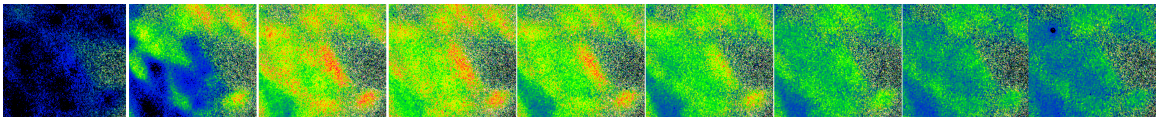

Treated: 10ppb TCE cells @ 10nM VP

Low Calcium flow

High Calcium flow

Figure 2. Panel of images captured at equivalent intervals after treatment with vasopressin to induce a calcium flux. Calcium intensity was measured by fluorescence and the scale was concerted to false color as indicated. The data show that calcium can be developed as a sensitive indicator of exposure.

III. Ascorbic Acid Characterization

The electrochemical characterization of the cell culture media contains a wealth of information about cellular metabolism. Ascorbic acid concentration is an indicator of cellular metabolism and therefore provides information about cells exposed to a toxic chemical.

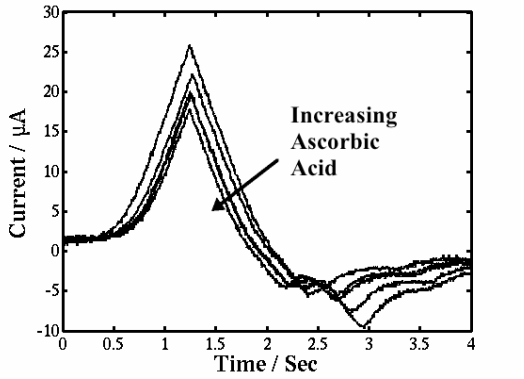

Figure 3. Studies show a definite dependence on ascorbic acid concentration.

We have simplified the problem by starting with ascorbic acid in PBS, next more complex mixtures will be evaluated. Cyclic voltammetry was performed using a Au-Pt-Pt set of working electrodes to monitor the chemical change. Fig. 3 presents a chronological display of the resulting current amplitude for each cyclic voltammetry scan. This display superimposed five runs from a single series. Each run showed the detected response to a unique ascorbic acid molarity as the as the ascorbic acid was increased from 0 to 532 µ*M* in 133 µ*M* increments. This figure was generated to realize the effect of the time course on the current waveforms resulting from the CV input signal.

Table C-1. ESH Metrics

I) Basis of Comparison - Current best technology involves animal studies to determine toxicity of new chemicals. Approaches to solve this problem center around reduced usage of toxic materials.

II) Manufacturing Metrics - The new approach aims to increase the through put of chemical toxicity testing so that new chemicals will not be introduced into the manufacturing line before the toxicity effects of these chemicals is known.

III) ESH Metrics

The goals of this work are to determine the toxicity of new chemicals. This work hopes to define the standards for toxicity.

Interactions with Other ERC Projects:

This is a module in the overall plan to develop an environmentally benign recycle process (Task C-4).

Next-Year Plan:

- Test optical and electrochemical sensors on prototype CMOS biochip
- Expand Ca testing to chemicals other than TCE
- Optimize CMOS circuitry based on preliminary results

Long-Term Plan:

- Demonstrate the assessment of the toxicity of new chemicals
- Develop and demonstrate an automated, self-contained biochip capable of easy online integration and operation.
- Work with manufactures to assess chemical toxicity of new chemicals in the early stages of development.

Environmentally-Friendly Cleaning of New Materials and Structures for Future Micro-and Nano-Electronics

Personnel:

PIs:

- Prof. Yoshio Nishi, Electrical Engineering, Stanford University
- Srini Raghavan, Materials Science and Engineering, UA
- Farhang Shadman, Chemical and Environmental Engineering, UA

Other Research Personnel:

- James P. McVittie, Electrical Engineering, Stanford University

Graduate Students:

- Jungyup Kim, Materials Science and Engineering, Stanford University
- Nandini Venkataraman, Materials Science and Engineering, UA
- Asad Iqbal, Chemical and Environmental Engineering, UA
- Junpin Yao, Chemical and Environmental Engineering, UA
- Harpreet Juneja, Chemical and Environmental Engineering, UA

Objectives:

- Develop a fundamental understanding of the performance of semi-aqueous and all-aqueous chemical systems in cleaning copper oxide residues
- Evaluation of metal removal efficiencies of aqueous solutions from Ge surfaces.
- Evaluation and modeling of the halide passivated Ge surfaces.
- Proposal of a baseline aqueous cleaning method for Ge.
- Determine the fundamentals of moisture interactions with blanket, and patterned porous low-*k* films: Loading, outgassing dynamics, transport, incorporation and removal of moisture in all forms in the matrix.
- Develop a process model that could be used to design a more efficient purging and drying process for contaminated low-*k* films.

Background:

Cu Cleaning

Removal of post-etch residues (PER) from copper damascene structures requires chemical formulations that can penetrate narrow, high aspect ratio features. Additionally, these formulations must exhibit a high degree of selectivity in removing copper oxide over the underlying copper without attacking the low k dielectric sidewalls.

Several semi-aqueous fluoride based chemistries (SAC) have been developed commercially to meet this end, where the fluoride component functions as the active ingredient in removing copper oxide [1]. Because of the general desire to decrease the use of solvents in fabrication plants, much attention is paid to the development of all-aqueous formulations. Of these formulations, those based on ammonium phosphate and a mixture

of organic acids have gained the most attention. Due to the proprietary nature of many of these formulations, their mechanism of action is not known in the open literature.

Ge Cleaning

Germanium is an important material for applications in the next generation high mobility devices. Metal contamination causes detrimental effects including premature dielectric breakdown and V_{th} shift. Therefore effective surface cleaning and preparation of Ge substrates are becoming important and are crucial for successful integration and realization of the high mobility substrate. Effective surface cleaning involves removing metal contaminants with minimal consumption and roughness of the Ge with sturdy surface passivation characteristics. Bulk contamination of the wafer evaluated. Metal removal efficiencies of various aqueous solutions were evaluated and the fundamental mechanisms were developed with oxidation reduction potential and Pourbaix diagrams. Passivated Ge surface layers were studied and modeled with synchrotron XPS. The differences in passivation properties among the tested aqueous solutions were explained by an oxidation model initiated by water molecules. Finally, a baseline aqueous solution cleaning method was proposed for efficacious cleaning of the Ge surface.

Drying of Porous low-k

Ultra-low-*k* materials, are highly susceptible to atmospheric molecular contamination (AMC), especially moisture and organics[5-6]. The porous nature of the low-*k* dielectric films also results in retention and incorporation of moisture which might lead to outgassing in further processing steps[7-8]. Moisture, even in very small concentrations, can deteriorate the effective dielectric constant value significantly, given that the dielectric constant value of water is as high as 80. Previous studies have shown that certain fabrication steps, such as, plasma etching and/or ashing, can dramatically affect the physical properties of porous Methysilsesquioxane (p-MSQ) low-dielectric films[9-10], which in turn may affect moisture uptake of the film. Moisture uptake and clean up has a complex dependence on the solubility and diffusivity values of the cap layers. In order to design a process which can minimize the impact of moisture, it is critical to understand the fundamental interaction mechanism between moisture and low-k materials. In this study, a methodology is developed to study molecular interactions with low-*k* dielectric materials and is used to compare the effect on as-received and processed films. The proposed model fits well with the experimental data.

Method of Approach:

Cu Cleaning:

In this study, semi aqueous fluoride chemistries based on Dimethyl Sulfoxide (DMSO) and all -aqueous chemistries based on ammonium hydrogen phosphate ($(NH_4)_2HPO_4$), have been investigated for their ability to selectively remove copper. Cleaning experiments were carried out on copper oxide films formed on polished copper blanket wafers by thermal oxidation at 300^oC. The thickness of copper oxide was determined by an electrochemical reduction technique[2]. Films of thickness 55 nm, formed by oxidation for five minutes at 300^0C, were used for most experiments. The removal rate of copper oxide and copper was determined by immersing samples in various chemical systems and measuring the concentration of copper in the solution. DC

electrochemical investigations were conducted using a Potentiostat/Galvanostat (PAR 263A). A Gain Phase Analyzer (Solartron SI 1260) was interfaced with the Potentiostat to facilitate EIS studies performed to investigate the transition from copper oxide to copper.

Ge Cleaning:

Ge doped p-Ge(100) single crystal CZ wafers were used for the analysis. Small piece of the wafer was completely dissolved in a mixture of nitric and hydrochloric acid and the effluent was measured using Inductively Coupled Plasma-Mass Spectrometry (ICP-MS). The metal cleaning efficiency of aqueous solutions were evaluated by utilizing wafer scanning analysis (WSA) method (shown in Figure 1a)

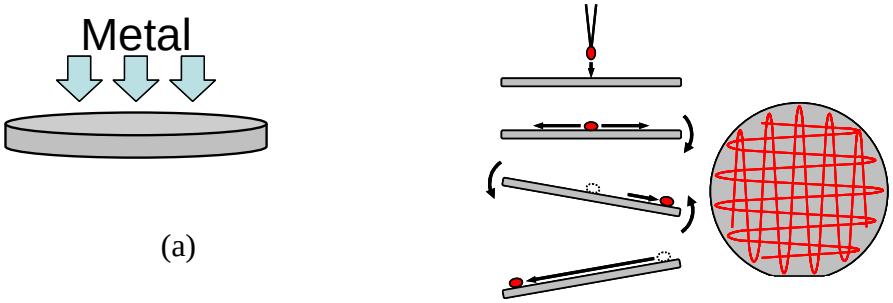

Figure 1 (a) Ge wafer is intentionally contaminated with metal and (b) wafer scanning analysis (WSA) method employed for evaluating the metal cleaning efficiency of a particular solution.

The relative stability of the passivated Ge surface against atmospheric oxidation is evaluated by exposing the Ge surfaces treated by concentrated HF, HCl, HBr and HI solutions and looking at the time to oxidation initiation as indicated by the increase in the oxygen 1s signal in the high resolution XPS. Halogen passivated Ge surfaces were probed with synchrotron XPS to determine the surface bond structure. The surface bond structure, electronegativity and size effects of the passivating species allows one to develop an explanation for the trend of better passivation for heavier halogen species.

Drying of Porous Low-k:

The experimental procedure consisted of the following steps: initial purge and bake, isothermal sorption, isothermal desorption, followed by a baking cycle. Before each experiment, the reactor was purged and baked under zero-gas nitrogen up to 380^{o}C to desorb any residual molecular contaminants from the wafer surface. Moisture concentration in the outlet-gas from the reactor was the primary variable monitored during each experimental run. Experiments were carried out at different temperatures from 25 to 380^{o}C and for concentrations from sub ppb levels to ppm levels.

Highlights of Results and Accomplishments:

Cu Cleaning

Figures 1(a) and 1(b) show the removal rate of copper oxide and selectivity between copper oxide and copper in various SAC formulations containing different volume percent of DMSO and HF. The removal rate increases with concentration of HF for a given solvent concentration. Formulations with lower solvent concentrations

(correspondingly, higher amount of H_2O and higher electrical conductivity) are observed to have higher etch rates and selectivity. The formulation with 49 vol% DMSO, 2 vol% HF and 49 vol% H_2O (pH 4.2) has the highest copper oxide removal rate of 170 Å/min and also the highest selectivity between copper oxide and copper of 42:1.

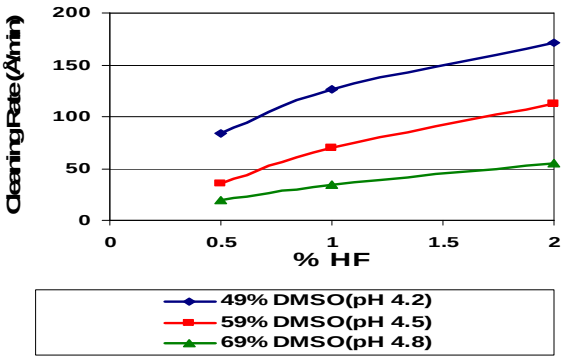

Figure 1(a): Removal rate of Copper Oxide as a function of %HF in SAC chemistry

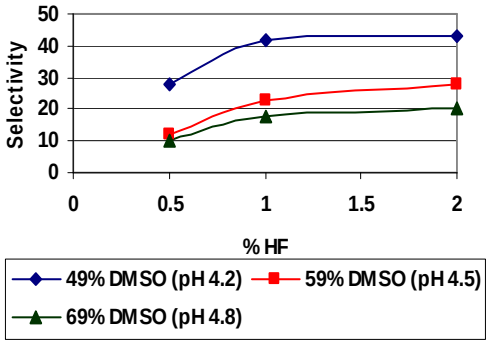

Figure 1(b): Selectivity of Copper Oxide over Copper as a function of %HF in SAC chemistry

Ammonium Hydrogen Phosphate ($(NH_4)_2HPO_4$) based all-aqueous chemical systems have also been evaluated as candidates for removing copper oxide. The removal rates and selectivity have been investigated as a function of concentration of $(NH_4)_2HPO_4$ and pH as shown in Figures 2(a) and 2(b) respectively. Both removal rates and selectivity increase as the pH is made more alkaline. Formulation with 15 wt% of $(NH_4)_2HPO_4$ is shown to have the highest removal rate of 115 Å/min with a selectivity of 8:1 between copper oxide and copper. The highest selectivity of 10:1 has been observed in the chemistry with 5 wt% $(NH_4)_2HPO_4$, with a corresponding removal rate of 80 Å/min.

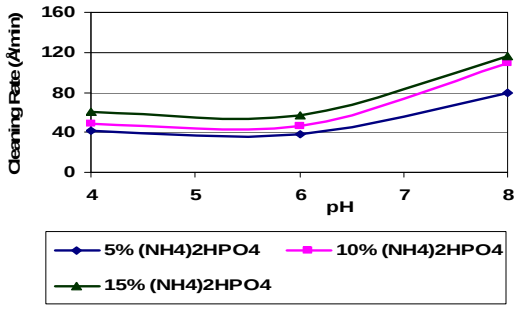

Figure 2(a): Removal rate of Copper Oxide as a function of pH in $(NH_4)_2HPO_4$ based chemistry

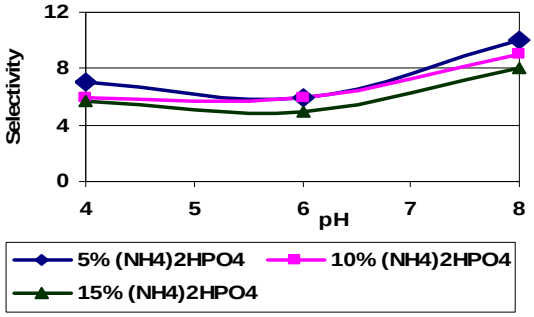

Figure 2(b): Selectivity of Copper oxide over Copper as a function of pH in $(NH_4)_2HPO_4$ based chemistry

The semi aqueous formulation containing 49% DMSO, 1% HF and 50% H_2O (pH 4.2) was chosen for the EIS investigations. The impedance spectra collected in the frequency range of 100 kHz to 0.1 Hz with an AC perturbation potential of 5 mV is shown in Figure 3 as a function of time.

Ge Cleaning:

Bulk contamination levels of the Ge wafers are shown in Figure 3(a). Ga concentration was measured at 1.9E14cm^{-3}. Using the resistivity vs. impurity concentration graph in Figure 3(b) with the resistivity of 1.5 Ωcm for the sample gives us a corresponding impurity concentration of 2E14cm^{-3} which corresponds well with the measured value. Therefore this bulk contamination measurement method is reliable. Al, Ca and Fe show the highest levels of contamination in the bulk whereas Cr, Co, Li, Ti and W have levels below the detection limit.

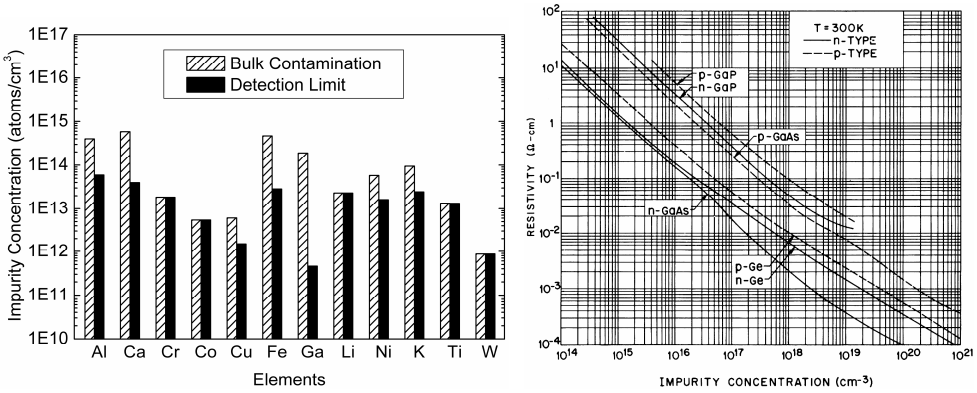

(a) (b)

Figure 3:(a) Bulk contamination level of the p-Ge(100) wafer by complete dissolution of a small piece of wafer and measurement using ICP-MS showing Ga concentration of 1.9E14cm^{-3}. (b) Resistivity vs. impurity concentration graph that gives an impurity concentration of 2E14cm^{-3} that corresponds to resistivity of 1.5 Ωcm for the sample wafer (S. M. Sze, Physics of Semiconductor Devices, 2nd Edition).

Figure 4 shows the cumulative metal removal efficiency of Cu, W, Ti, Cr, Co and Ni in concentrated HF(49%), HCl(36%) and HBr(48%) aqueous solutions. W shows limited metal removal efficiencies for all three solutions. Cu shows limited metal removal efficiency for HF but is efficiently removed in HCl and HBr. Concentrated HCl and HBr solutions have enough oxidation potential to remove Cu. These differences between the different solutions can be explained using the standard electrode potential and Pourbaix diagrams. Cumulative removal efficiencies of over 100% are due to the metal contaminants already present before the intentional contamination. Al, Ca, Fe, K, Ti,Cr, Co, Ni can be removed efficiently from the Ge surface using HF, HCl and HBr.

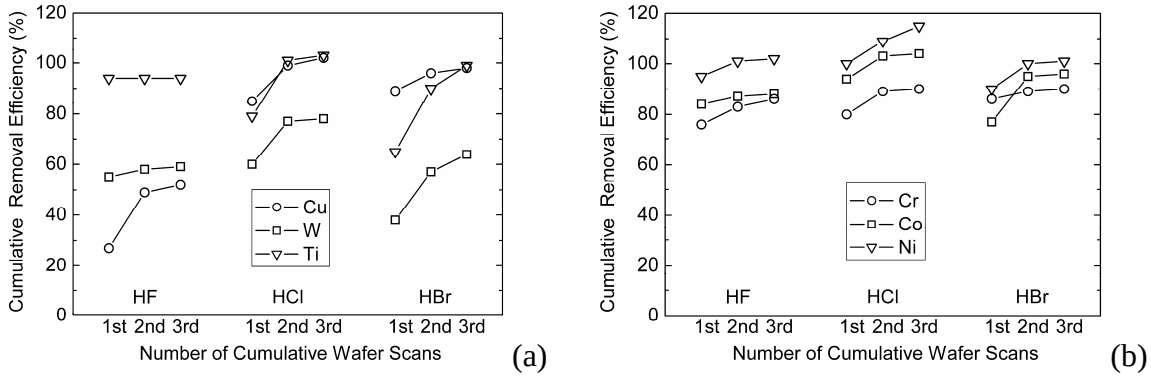

(a) (b)

Figure 4. Cumulative metal removal efficiencies of (a)Cu, W, Ti, (b)Cr, Co and Ni in HF(49%), HCl(36%) and HBr(48%) aqueous solutions.

Therefore by looking at results for optimizing (1) minimal etch rate (2) minimal surface roughness (3) minimal native oxide (4) minimal organic contamination and (5) maximum metal removal rate one can propose the following integrated process:

(1) UV-O_3 treatment & minimal exposure to environment (minimize organic contamination).
(2) DI-O_3 treatment (minimize surface roughness).
(3) Cyclic concentrated HCl & HBr treatment (metal & native oxide removal).
(4) HBr Passivation (passivation).
(5) Heat treatment (de-passivation of Br passivation + organic removal).

Drying of Porous Low-k*:*

As schematically shown in Figure 5, the process of transport in porous low-*k* film is assumed to consist of several simultaneous steps. Solving the governing equations for transport of moisture in pores and bulk matrix along with the overall mass balance equation, will allow determining various physical parameters such as solubility and diffusivity of moisture in pores and bulk matrix.

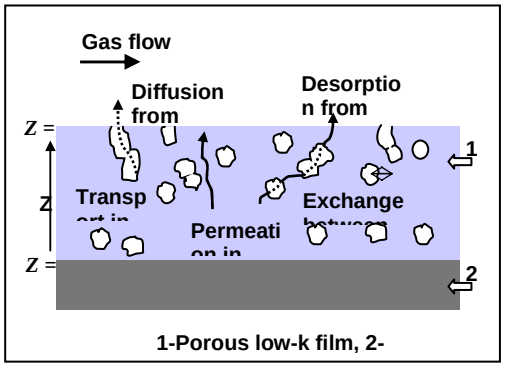

Figure 5. Moisture Transport Pathways in a porous low-k film

Figure 6 shows the percentage of moisture removed during isothermal desorption at 380^{o}C for 153 ppm moisture challenge concentration for all three p-MSQ A, B and C films. Figure 7 shows typical experimental results for interaction of moisture with Black Diamond II as-received and processed films with k value of 2.3.

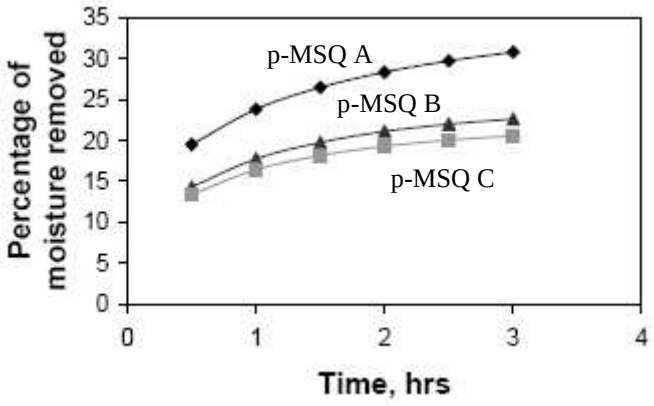

Figure 6. Dynamics of purge at 380^{o}C

It is observed from the figure that the moisture interaction behavior for the processed film is different than the as-received film, suggesting that the properties of processed film have been significantly altered. The etching and ashing processes may significantly change physical properties of low-k film, such as diffusivity, porosity, and moisture solubility.

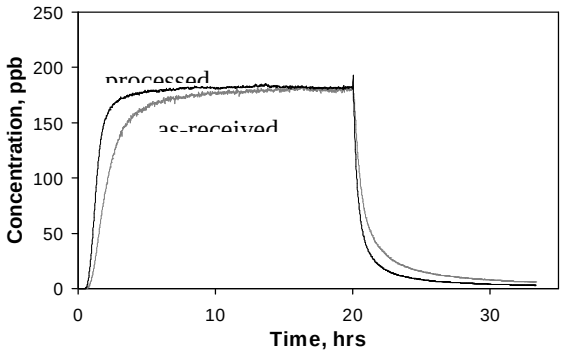

Figure 7. Comparison of temporal profile of sorption (challenge 181 ppb moisture), followed by isothermal desorption for as-received and processed Black Diamond II films.

Figure 8 also indicates a delay in response. This delay is much greater than the residence time of the reactor and therefore not due to reactor break through. The delay is caused by rapid and complete removal of moisture from the challenge gas early in the process while the dielectric surfaces are totally dry and fast sorbing.

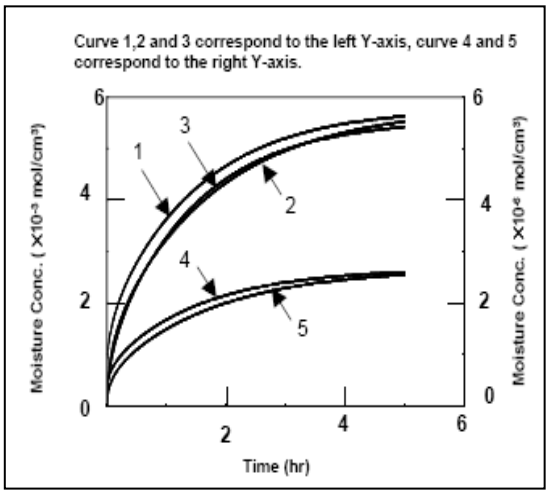

Figure 8. Temporal profile of moisture absorption in capped and uncapped films. Challenge Concentration = 1500 ppm; temperature=25ºC.

ESH Impact:

The Cu and Ge cleaning research will lead to the development of FEOL and BEOL cleaning formulations with reduced amount of cleaning solutions and organic solvents. The low-k cleaning and drying results will have significant impact on reducing the purge-gas use and the thermal energy needed for drying and outgassing of thin films.

Next-Year Plan:

- Investigate the effect of contamination on electrical properties of Ge

- Investigate the effect of organic and metal contaminations on Ge MOS capacitor characteristics
- Model the Ge passivation/re-oxidation; confirm with methods such as ab-initio modeling.
- Determine the applicability of the EIS technique to evaluate cleaning performance of these formulations in patterned test structures with high aspect ratio features
- Use sensor developed by Shadman's group to follow rinsing of structures after cleaning
- Experimentally study the effect of different capping materials on outgassing dynamics.
- Study the effect of porosity, pore size distribution and thickness on moisture intrusion and uptake of porous low-k drying; extend this study to investigate behavior of impurities other than moisture.
- Develop FTIR-based methodology to study dynamics of outgassing of low-k films.

References:

1. M. A. Lester. "Semi-Aqueous Cleaning Approaches the Forefront," Semiconductor International, (March 2001) p. 48
2. Y. Y. Suk, M. Marek, "Cathodic Reduction of Oxides formed on Copper at Elevated Temperatures," Journal of the Electrochemical Society, (April 1994) p. 940
3. Mosig K, Jacobs T, Brennan K, Rasco M, Wolf J, Augur R. *Microelectron Eng.* 2002;64:11-24.
4. A. Humbert, L. Mage, C. Goldberg, K. Junker, L. Proenca, and J. B. Lhuillier, *Microelectronic Engineering*, **82,** 399 (2005).
5. F. Iacopi, S. H. Brongersma, B. Vandevelde, M. O'Toole, D. Degryse, Y. Travaly and K. Maex, *Microelectron Eng*, **75,** 54 (2004).
6. A. Iqbal, H. Juneja, J. Yao, and F. Shadman, *AIChE Jounal*, **52,** 1586 (2006).
7. Lu D, Kumar R, Chang CK, Du AY, Wong TKS. *MicroelectronEng.* 2005;77:63-70.
8. Clarke ME. www.mykrolis.com/publications.nsf/ docs/MAL123. 11/2005.
9. D. Eon, V. Raballanda, G. Cartry, M.-C. Peignon-Fernandez, and Ch. Cardinaud, Eur. Phys. *J. Appl. Phys.*, **28**, 336 (2004).
10. K. Yonekura, S. Sakamori, K. Goto, M. Matsuura, N. Fujiwara, and M. Yoneda, *J. Vac. Sci. Technol.* **B 22,** 553 (2004).

Industrial Interactions and Technology Transfer:

- Joint study on the metal removal efficiencies of Ge surfaces : Samantha Tan and Shi Liu of Chemtrace Corporation.
- Joint work with Sematech and TI on preparation of low-k film samples and patterned wafers.

Publications:

1. J. Kim, J. McVittie, K. Saraswat and Y. Nishi, "*Passivation Studies of*

Germanium Surface", 8th International Symposium on Ultra Clean Processing of Silicon Surfaces, Sep. 18th-20th 2006, Antwerp, Belgium.

2. J. Kim, J. McVittie, K. Saraswat and Y. Nishi, *"Germanium Surface Cleaning with Hydrochloric Acid"*, ECS Transactions; v.3, no.7, p.1191-1196 (2006).
3. H. Jagannathan, J. Kim, M. Deal, M. Kelly, Y. Nishi, *"Halide Passivation of Germanium Nanowires"*, ECS Transactions; v.3, no.7, p.1175-1180 (2006).
4. Juneja, H. S.; Iqbal, A.; Yao, J.; Shadman, F., "Mechanism and Kinetics of Non equilibrium and Multilayer Adsorption and Desorption of Gases on Solids," Ind. Eng. Chem. Res.; (Article); 2006; 45(19); 6585-6593
5. Asad Iqbal, Harpreet Juneja, Junpin Yao, Farhang Shadman, "Removal of moisture contamination from porous polymeric low-k dielectric films," AIChE, Volume 52, Issue 4, Date: April 2006, Pages: 1586-1593

Conference Presentations:

1. *"Passivation Studies of Germanium Surface"*, 8th International Symposium on Ultra Clean Processing of Silicon Surfaces, Antwerp, Belgium.
2. *"Effective Surface Preparation Study of Germanium"*, SRC Student Symposium, Cary, North Carolina.
3. *"Germanium Surface Cleaning with Hydrochloric Acid"*, 2nd International SiGe & Ge: Materials, Processing, and Device Symposium, Cancun, Mexico.
4. Iqbal, A., Juneja, H., Yao, J., Shadman, F. ?Fundamentals of Outgassing and Drying of Porous Low-k Dielectrics Films" SRC Symposium, October, 2006.
5. Iqbal, A., Juneja, H., Yao, J., Shadman, F., "Moisture Retention and Outgassing in Porous Low-k Dielectric Films' presented at 7th International Conference on Microelectronic and Interfaces, March, 2006.
6. Nandini Venkataraman, Ashok Muthukumaran and Srini Raghavan, "Evaluation of Copper Oxide to Copper Selectivity of Chemical Systems for BEOL Cleaning Through Electrochemical Investigations", MRS, MRS Spring Meeting, 2007.

Low-Water and Low-Energy Rinsing and Drying of Patterned Wafers and Nano-Structures

Personnel:

PIs:

- Farhang Shadman, Chemical and Environmental Engineering, UA
- Bert Vermeire, Electrical and Computer Engineering, ASU

Graduate Students:

- Jun Yan, Chemical and Environmental Engineering, UA
- Kedar Dhane, Chemical and Environmental Engineering, UA

Objectives:

The primary objective of this work is to determine ways in which DI water usage in rinse processes can be reduced without sacrificing overall wafer cleanliness. In order to meet that objective, a study of the fundamental mechanisms involved in contaminant removal during rinse is being undertaken. The goals of this study are:

- Investigate the fundamental mechanisms governing the removal of chemical contaminants from the surface of both smooth and patterned wafers.
- Conduct experiments, which measure the temporal and spatial variations of the contaminant concentrations in the water near the wafer surface as the rinse process proceeds.
- Conduct experiments, which measure the temporal variations of the contaminant concentrations within a trench as the rinse process proceeds.
- Using the in-situ trench device as a prototype, develop robust industrial device that could become a benchmark for standard rinse evaluations.

Background:

Increasing environmental and economic concerns have brought attention to the need for efficient and effective rinse processes to clean residue from wafer surfaces. In particular, optimized rinsing processes can yield better device performance, reduced water consumption, shorter cycle times, higher tool utilization, and higher throughputs, which can lead to reduced cost of ownership [Helms (1994), Rosato et al. (1994), Kempka et al. (1994), Hall et al., (1995), Tonti (1995), Chiarello et al. (1997,2000)]. Cost of ownership models indicates that the relative cost of DI water will nearly triple compared to other cost. Unfortunately, process optimization is limited by the lack of suitable diagnostic techniques to non-intrusively monitor the chemical carryover removal during wafer rinse.

There is a desire for reliable methods to measure the temporal variation of the concentration of acid in high purity water in the vicinity of the silicon wafer surface. Two approaches are taken: an ion-selective probe, used successfully to study various biological systems (Kuhtreiber and Jaffe, 1987; Schiefelbein et al, 1992; Marcus and Shipley, 1994) with a spatial resolution of 2 to 5 microns; and second, a method for measuring contaminant concentration in the water trapped within the structure of a patterned wafer.

On rinsing of high aspect ratio surface features such as trenches and vias, relatively little published work exists. Most of the limited previous work focuses on the dominating effect of diffusion over fluid velocity (Nakao et al., 1990). Under normal post-HF rinse conditions the bottom of a typical DRAM trench (4 x 0.5 x 0.5 μm) decreases in concentration by seven orders of magnitude in roughly 10 seconds. Recent modeling and experimental work on post-piranha

rinse (Aoki et al. 1999) found much longer rinse times, >1000 sec, due to the strong adsorption of SOx species on the SiO_2 sidewalls. All previous experimental techniques relied upon ex-situ measurements (Nakao et al. 1990, Aoki et al. 1999). This project incorporates in-situ, real-time measurements.

Method of Approach:

A novel Electrochemical Residue Sensor (ECRS) is designed, fabricated, and utilized to monitor the process of cleaning and rinsing in patterned wafers and well-characterized micro- and nano-structures. ECRS is capable of sensing the cleanliness of the small structures by monitoring the changes in the impedance of the fluid between two electrodes embedded in the microstructure. The unique features of this sensor include:

- Sensitivity of about 5 ppb (measured for sulfate ion contamination in water) during rinse; this cannot be achieved with conventional metrology methods, such as conductivity probes, used in rinse tanks
- Fast response time needed for rinse that is typically a highly transient process
- Real-time, and in-situ capability; currently no other metrology method is available to provide this for cleaning and rinsing tools.

Last year's work focused on a new ECRS design for improving the signal to noise ratio as well as methods for packaging and integration of the sensor into a full wafer that can be used in conventional rinse tanks. To replicate industrial rinse conditions, a full flow experimental setup was designed. Tests were also conducted at Freescale Semiconductor Inc as a part of joint effort with the Freescale team of co-investigators. A part of the work also focused on fabricating a version of the sensor, which is compatible with the chemical environment actually present in processing patterned wafers. In addition to rinsing experiments for various chemicals, a process model was developed to interpret the experimental results for better understanding of the cleaning mechanisms and revealing the bottlenecks of rinse.

Highlights of Results and Accomplishments:

A version of the ECRS was fabricated on a monitoring wafer and exposed to the chemicals environment present during the cleaning and rinsing processes. This allowed monitoring the actual concentration in the sensor trench representing the features of a patterned wafer. The results show that the concentration in the trench is quite different from that read by the resistivity probe which is typically located at the outlet of the tank. Figure 1 shows the difference in reading of a resistivity probe and that of the ECRS for a single wafer application. ECRS also shows that there is a delay for chemicals to move out from the wafer gap in the case of multi-wafer cassette rinse. This is due the laminar flow between the wafers, leading to a lack of adequate mixing. The results clearly indicate that using resistivity probe to monitor the rinse is ineffective and unreliable.

As shown in Figure 2, the ECRS monitoring results revealed the significant difference in the rinse dynamics among various chemicals. This indicates significant differences in the fundamental chemistry of transport processes and contaminants interactions with the fluid and the walls of the small structures. For example, the results show that the cleaning of HCl is much faster than that of H_2SO_4 and NH_4OH. Results also show the ECRS measuring the effect of wafer spacing on the surface cleanup during rinse in situ and in real time. A wafer exposed to the full turbulence of the rinse tank, such as the wafer in the front of a carrier, is more rapidly rinsed than one where water flow is forced into a narrow spacing. The ECRS shows a dramatic difference in reading on the two wafers, while the standard resistivity probe in the tank only gives a single average weighted measurement. Clearly the ECRS is more useful in developing rinse recipes.

Figure 1: Comparison of resistivity probe reading vs the Electrochemical Residue Sensor reading.

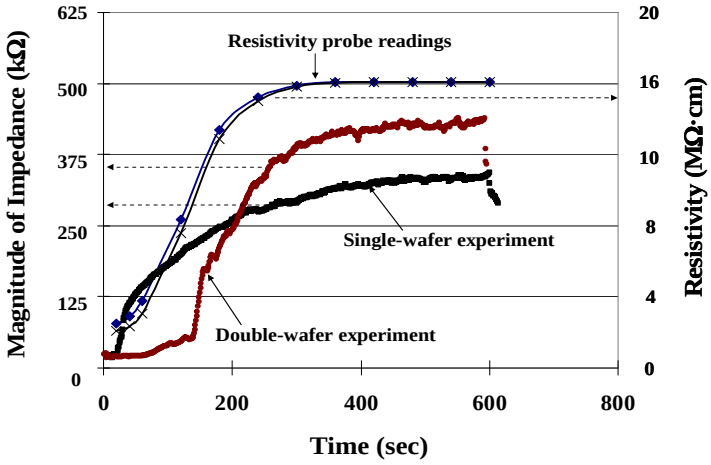

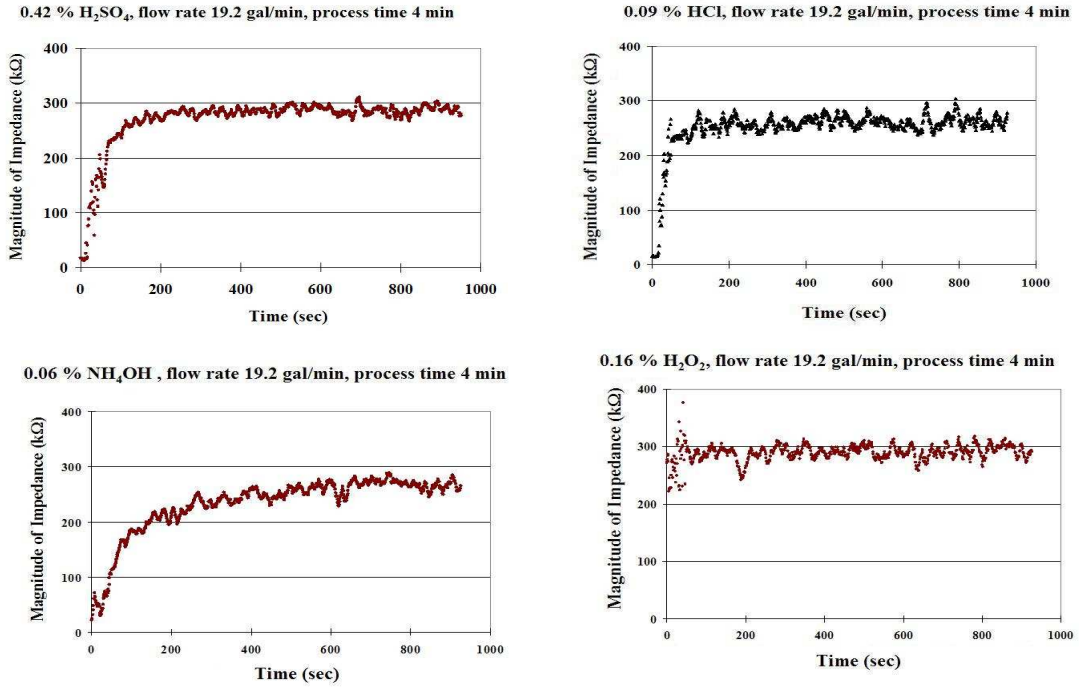

Figure 2: Response of the Electrochemical Residue Sensor to various chemicals.

A comprehensive model was developed to determine the fundamentals of rinsing procedure for the purpose of data analysis and process parametric studies. The model consists of equations describing diffusion and migration for all the ionic species present during a typical rinse. In addition to the transport in the fluid phase, residual surface contaminants undergo adsorption and desorption. Moreover, the ionic species in a high aspect ratio feature experience electrostatic interaction with the surface. At low ionic strength, the potential resulting from the surface charge penetrates a few tenths of a micron into the liquid and significantly impacts the ion motion. In narrow pores, this can impact the rinsing time. Electrostatics are described by

Poisson equation and included in the model. Lastly, concentration is related to the impedance measured by the ECRS, following Ohm's law. Following is a list of the key model equations:

$$\frac{\partial C_i}{\partial t} = \nabla \cdot (D_i \nabla C_i + z_i \mu_i F C_i \nabla \varphi) \qquad \text{- - - (1)}$$

$$\frac{\partial C_{s2}}{\partial t} = k_{a2} C_2 \left(S_{02} - C_{s2}\right) - k_{d2} C_{s2} \qquad \text{- - - (2)}$$

$$\nabla^2 \varphi = -\frac{\rho}{\varepsilon} \qquad \text{- - - (3)}$$

$$\rho = F \sum_i z_i C_i \qquad \text{- - - (4)}$$

$$\sigma \cdot \nabla V = J \qquad \text{- - - (5)}$$

$$\sigma = \sum_i \lambda_i C_i \qquad \text{- - - (6)}$$

Figure 3 shows typical model prediction and agreement with the experimental results. Using the parameters obtained by the process simulation, parametric studies were conducted. Sample results are shown in Figure 4, which shows the significant effect of feature size on the cleaning time. This indicated the potential challenges in cleaning and the increase in resource utilization as we move form micro to nano-scale processing. The cleaning time is also strongly dependent on the charge of the species. This may explain why NH_4OH is difficult to rinse.

Figure 3: Simulation vs experimental data for sulfuric acid.

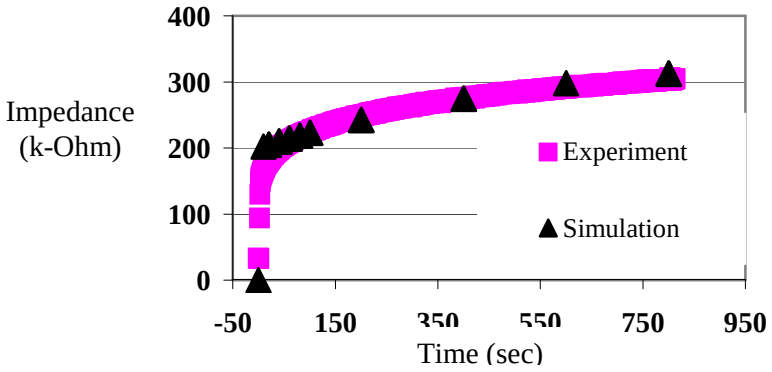

Figure 4: Effect of width of the trench on 99.99% cleanup of NH_4^+ for aspect ratio of 10.

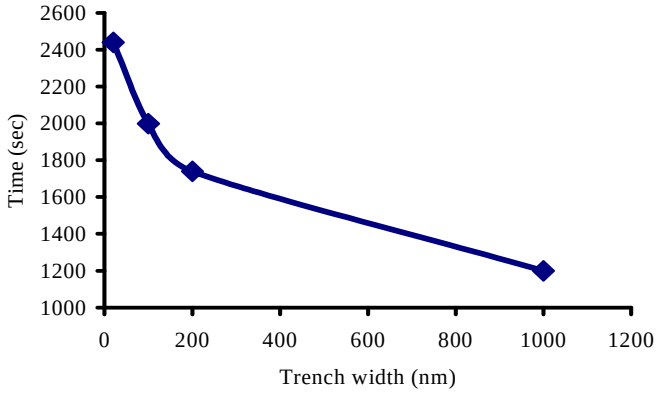

Long-Term Plan:

- Application of sensor to cleaning and drying processes involving other fluids such as supercritical carbon dioxide.
- Application of this sensor to monitor the rinsing and cleaning of porous layers such as porous low-k films.
- Develop efficient low-water rinse processes by applying this sensor to monitor the kinetics of rinse under realistic operating conditions.
- Relate bulk resistivity to the sensor measurements using rinse models developed earlier in this project to fully describe the rinse process.
- Determine if desorption is dependent on the electric field and model this effect
- Develop robust measurement technology for rapid, feature scale analysis of important wafer surface properties.

Industrial Interaction:

- The Fab tests were performed at Freescale. The joint effort and contributions by Tom Roche, Hsi-An Kwong, Jack Shively, and Marie Burnham (Freescale team) and efforts of Doug Goodman (Environmental Metrology Corp) are acknowledged.

References:

1. Helms, C. R. et al., "Strategies for Reduced Water Use in Semiconductor Manufacturing," Draft Report for Period through 12/31/95, work at Stanford supported by SEMATECH and the Semiconductor Research Corporation.
2. Rosato, J. J., et al., in *Cleaning Technology in Semiconductor Device Manufacturing/1994*, J. Ruzyllo and R.E. Novak, Editors, 94-7, p.140, The Electrochemical Society Proceedings Series, Pennington, NJ (1994).
3. Kempka, S.N. et. al., "Evaluating the efficiency of overflow wet rinsing," *Micro*, 41, (1994).
4. Hall, R. M. et. al., "Improving Rinse Efficiency with Automated Cleaning Tools", *Semiconductor International*, Nov 96
5. Tonti, A. in *Cleaning Technology in Semiconductor Device Manufacturing/1992*, J. Ruzyllo and R.E. Novak, Editors, PV 92-12, p.41-47, The Electrochemical Society Proceedings Series, Pennington, NJ (1992).
6. Chiarello, R. P., et al. *Proceedings of the Materials Research Society*, 477, (1997).
7. Chiarello, R. P., et. al. " Optimizing Wafer Rinsing Processes to Conserve DI Water", *MICRO: Surface Chemistries*, June 2000.
8. Kuhtreiber, W. M. et al., "Direct microinjection of substances in penetration sensitive embryos" *Differentiation; research in biological diversity (1987), 34(2), 156-9*
9. Schiefelbein et al, "Calcium influx at the tip of growing root-hair cells of Arabidopsis thaliana", *Planta, Biomedical and life sciences*, 187(4), 455-9, (1992)
10. Marcus, D C and Shipley, A M, "Potassium secretion by vestibular dark cell epithelium demonstrated by vibrating probe", *Biophys J*. 1994; 66(6): 1939-1942.
11. Nakao, I. et al., "A Simulation Model for Wet Cleaning of Deep Trenches" *J. Electrochem. Soc.*, 137, 2303 (1990).
12. Aoki, H., Yamasaki, S., and Aoto N. "Cleaning for Deep-Submicron Structures." *Proceedings of the 6th International Symposium on Cleaning Technology in Semiconductor Device Manufacturing* – pp. 1-12, (1999)

Notation:

- C_i- Concentration of H^+, OH^-, NH_4^+ and $SO4^{-2}$ [mole/m^3]
- D_i- Diffusion coefficient of H^+, OH^-, NH_4^+ and $SO4^{-2}$[m^2/sec]
- z_i- valence of ion of interest
- μi-Mobility of ion
- F- Faraday's constant
- φ- Potential [Volt]
- C_{s2}- Concentration of NH_4^+ or $SO4^{-2}$ on the boundary of the trench [mole/m^2]
- k_{a2}- Adsorption constant of NH_4^+ or $SO4^{-2}$ on the boundary of the trench[m^3/mole/sec]
- C_2- Concentration of NH_4^+ or $SO4^{-2}$ near the boundary.[mole/m^3]
- S_{o2}- Maximum number of active sites available for SiO_2[mole/ m^2]
- k_d- Desorption constant of NH_4^+ or $SO4^{-2}$ on the boundary of the trench[1/sec]
- ε - Permitivity of space
- σ - Electrical conductivity[S/m]
- V- Applied voltage[Volt]
- J- Current density

Reductive Dehalogenation of Perfluoroalkyl Surfactants in Semiconductor Effluents

Personnel:
PIs:

- Reyes Sierra, Chemical and Environmental Engineering, UA
- Neil Jacobsen, Chemistry Department, UA
- Vicki Wysocki, Chemistry Department, UA

Other Research Personnel:

- Jim A. Field, Chemical and Environmental Engineering, UA

Graduate Students:

- Valeria L. Ochoa, Chemical and Environmental Engineering, UA

Undergraduate Students:

- Beshoy Latif, Chemical and Environmental Engineering, UA

Objectives:

The main objective of this research is to investigate the feasibility of reductive dehalogenation of perfluorooctane sulfonate (PFOS) and related long chain perfluoroalkyl surfactants (PFAS) using two different approaches, chemical biomimetic treatment and anaerobic microbial degradation. The degradation of perfluoroalkyl sulfonates by microbial- and chemical-catalyzed reductive dehalogenation processes will be evaluated and optimized, and the kinetics of compound degradation will be quantified.

Background:

PFOS and other PFAS are critical components in a variety of IC manufacture process steps, including photolithography, wet etch and wafer cleaning. Perfluorinated surfactants are under increased scrutiny as global environmental pollutants due to recent reports of their detection in human blood and in wildlife tissues collected worldwide, including biota from pristine areas (5). The ubiquity of these fluoro surfactants has been attributed to their wide use, persistence and high bioaccumulation potential. In response to these concerns, regulatory agencies in numerous industrialized countries have initiated studies to quantify the use of perfluorinated chemicals, assess their potential risks, and consider regulations restricting or banning their use.

There is an urgent need for feasible methods to remove PFOS/PFAS from semiconductor effluents in order to minimize environmental release of these emerging pollutants. Although more environmentally benign chemistries are under development, commercial alternatives to PFOS for critical photolithography uses are still lacking. PFOS is poorly removed by conventional biological treatment methods applied in publicly-owned water treatment works (POTWs). Physico-chemical treatment methods such as advanced oxidation processes and ion exchange are ineffective due to the highly stable nature of the carbon–fluoride bonds and the hydrophobic–oleophobic properties of the alkyl tail in fluorosurfactants. Work conducted at our laboratory has shown that the affinity of PFOS for granular activated carbon is poor to moderate when compared to that

of chemical compounds traditionally considered as suitable for activated carbon treatment (13). Recent studies indicate that considerable volume reduction of PFOS-containing waters can be achieved by reverse osmosis, but the process is costly and generates concentrated brines that require disposal (14).

Reductive dehalogenation is a well-known microbial catalysed process occurring with a wide variety of chlorinated compounds (4). Certain microorganisms can rapidly utilize the organohalogens as electron acceptors in an energy yielding reaction known as halorespiration. Bioreactor technology with halorespiring biofilms can convert perchlorinated solvents such as perchloroethylene at high volumetric rates. Cometabolic reductive dehalogenation is also known to occur due to the chemical reactivity of common occurring organo-metallic enzyme cofactors present in anaerobes. One such cofactor, vitamin B_{12} (cobalamin) is known to directly catalyze reductive dehalogenation reactions when supplied with an appropriate reducing agent such as Ti(III)-citrate (8). Vitamin B_{12} is also a component of all known reductive dehalogenases. The direct catalysis of dehalogenation by enzyme cofactors is known as *biomimetic dehalogenation*, because it mimics reactions expected in microorganisms.

Although microbial degradation of various organofluorines compounds is well documented (12), reductive defluorination has not yet been considered. Two previous studies have demonstrated defluorination of simple chlorofluorocarbons with vitamin B_{12}/Ti(III) (8) or in anaerobic groundwater (10). Recent research conducted in our lab has unequivocally demonstrated that vitamin B_{12}/Ti(III) can catalyze the reductive defluorination of PFOS. Fig. 1 illustrates the proposed mechanism of biomimetic reductive dehalogenation of PFOS with vitamin B_{12} / Ti(III).

Method of Approach:

This research investigates the feasibility of reductive dehalogenation for the degradation of PFOS and related long chain perfluorinated compounds. Two different approaches are considered, chemical biomimetic treatment and anaerobic microbial degradation. The aim is to attain complete degradation of PFOS through sequential steps of reductive defluorination followed by biological oxidation. Partially hydrogenated PFOS derivatives, comparable to degradation products expected from reductive defluorination are known to be susceptible to biodegradation by aerobic bacteria (7). Cooxidation of halogenated solvents by monooxygenase enzymes is well documented (4). Ammonia monooxygenase is an enzyme that occurs naturally in most POTWs due to the occurrence of nitrification. Therefore, our hypothesis is that a reductive defluorination pre-treatment followed by conventional biological treatment will result in extensive biodegradation of PFOS to safe end products.

Anaerobic microbial degradation of PFOS and selected fluorinated compounds (e.g. perfluorobutane-sulfonate derivatives) that are under development to replace PFOS will be evaluated in shaken batch bioassays inoculated with sediments or sludge samples previously exposed to perfluorinated compounds. The microorganisms responsible for defluorination will require primary electron-donating substrates for the reduction. In the laboratory study, compounds such as lactate or ethanol will serve this purpose. In practice, these substrates will most likely be other organic co-contaminants present in semiconductor effluents. Control assays (e.g. abiotic treatments) will be run in parallel to account for the loss of PFOS by mechanisms other than reductive dehalogenation.

The susceptibility of PFOS and other PFAS to *chemical reductive dehalogenation* with vitamin B_{12}/Ti(III) will be examined in laboratory assays. The impact of vitamin B_{12} and Ti(III) dosage, pH and temperature will be assessed to determine the optimal treatment conditions. Immobilization of vitamin B_{12} on solid supports (e.g. activated carbon) will be investigated to facilitate continuous treatment. Assessment of reductive dehalogenation will rely on the monitoring of fluoride release and the removal of PFOS. Analysis and identification of PFOS degradation products will be attempted.

Biotransformation of the products formed by reductive dehalogenation of PFOS *by microorganisms in aerobic activated sludg*e will be investigated. Co-oxidation may be a requirement for aerobic oxidation, in which case co-oxidation by ammonia monooxygenase-producing nitrifying bacteria (occurring in activated sludge plants) will be examined. Simple, partly defluorinated compounds will be utilized to test the hypothesis that dehalogenated products of PFOS are susceptible to cooxidation by nitrifying cultures. Inocula will be obtained from various wastewater treatment plants receiving perfluorinated contaminants.

In the final phase of this research, *continuous flow studies* will be conducted to assess the impact of the integrated reductive dehalogenation-biological process on the removal of PFOS and PFOS degradation products. A flow-through laboratory-scale system combining a reductive dehalogenation step followed by biological aerobic treatment will be operated with a synthetic influent containing PFOS to study the effectiveness of the system. The final phase of this study will evaluate the effectiveness of the proposed sequential process for treating PFOS-containing wastewaters from an industrial semiconductor facility.

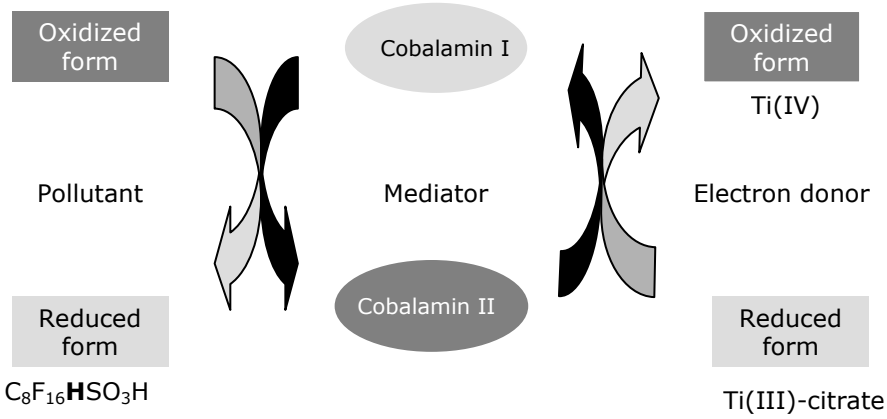

Fig. 1. *Proposed mechanism of biomimetic reductive dehalogenation of PFOS with vitamin B_{12} / Ti(III).*

Highlights of Results and Accomplishments:

Analytical Methods: Techniques set up during the initial phase of this study for the detection and quantification of PFOS, PFOS degradation products and fluoride ions were expanded and improved during the first year of the project. These methods included quantification of perfluorinated organics by ^{19}F-NMR and analysis of fluoride release by

ion-selective electrode. An analytical method utilizing a newly acquired suppressed conductivity ion chromatography system was developed for the routine analysis of perfluorinated acids and sulfonates. Compound analysis is performed using an ion chromatograph fitted with an Acclaim Polar Advantage II, C18 column (Dionex), and a suppressed conductivity detector. A mixture of 20 mM boric acid (pH 9.0) and 95% acetonitrile was used as the mobile phase at a set linear gradient. As an example, a chromatogram is shown in Figure 2. In addition, a method utilizing the advanced liquid chromatography tandem mass spectroscopy (HPLC/MS/MS) equipment available at the Chemistry Department was developed for the identification of PFOS and its degradation products. Chromatographic separation was performed on a Discovery1 HS C18 column (Supelco). The mobile phase consisted of a buffer (5mM ammonium formate, 0.1% formic acid, in ddH2O) and acetonitrile at a set linear gradient.

Solid phase extraction (SPE) procedures were also set up to facilitate the analysis of perfluorinated compounds present in solid matrices or aqueous samples at low concentrations (< 0.5 mg/l). Sample clean up and concentration was performed using SPE cartridges (3 ml, 500 mg ODS-C18, Agilent Technologies, DE).

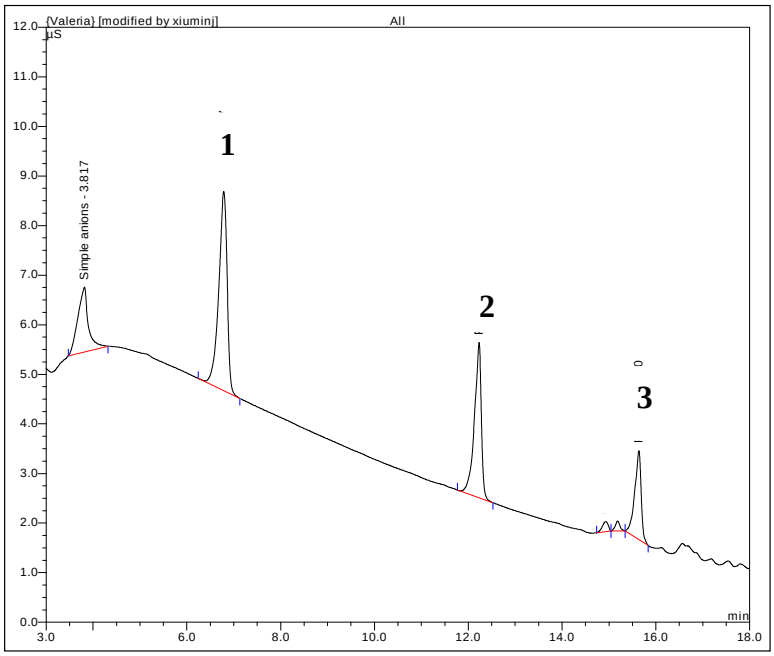

Fig. 2. HPLC-suppressed conductivity ion chromatograph of a solution containing PFBS (1), PFOA (2) and PFOS (3).

Microbial Toxicity: The inhibitory effects of PFOS, TH-PFOS (1*H*,1*H*,2*H*,2*H*-perfluorooctane sulfonic acid, a partially defluorinated surfactant closely related to PFOS), perfluorobutane sulfonate (PFBS) and tetramethyl ammonium hydroxide (TMAH) towards methanogenic microorganisms in anaerobic wastewater treatment sludge were tested at concentrations ranging from 5 to 500 mg/l as described elsewhere (6). The highest concentration tested is close to the solubility limit for PFOS. Assays utilized either acetate or H_2 as substrate. PFOS lead to only a minor decrease in the methanogenic activity (20% compared to the control) when present at very high

concentrations (500 mg/l). None of the other compounds tested were found to cause significant microbial inhibition in these assays.

Anaerobic Biodegradation: Microbial reductive dehalogenation experiments were set up to determine the ability of six different microbial inocula to degrade PFOS and PFBS. Bioassays were initiated with six different microbial consortia obtained from various municipal and industrial treatment works, including biomass from various installations receiving PFOS-containing wastewaters. The latter were obtained from publicly-owned treatment works in Austin, TX, and from industrial wastewater treatment plants operated by the companies IBM and 3M, respectively. To promote reductive dehalogenation, hydrogen gas (H_2) was supplied as the electron donor. Fluoride concentrations in the liquid medium were monitored periodically using an ion-selective electrode to determine if the surfactants are susceptible to microbial defluorination. Non-inoculated controls were run in parallel to correct for the possible release of fluoride by abiotic reaction. Sludge controls (no PFOS added) and killed-sludge controls (by autoclaving) were also set up to determine background fluoride concentrations and to quantify surfactant removal by sorption to the biomass, respectively. No evidence has been obtained after 1 year that the perfluorinated compounds are degraded. Our assays included wastewater treatment sludges previously exposed to PFOS, however, liquid and sludge retention times in wastewater treatment systems are relatively short. Future efforts will attempt to obtain anaerobic sediments that have been exposed to high concentrations PFOS for long periods of time (years).

Biomimetic Dehalogenation: Recent research conducted in our lab has unequivocally demonstrated that vitamin B_{12} (260 µM) and Ti(III)-citrate (36 mM) at ambient conditions (30°C, pH 7) can catalyze the reductive defluorination of PFOS. Reduction of PFOS was confirmed by measurement of the release of fluoride (Fig. 3), which accounted for 17.6% of the initial fluorine content after 7 days. No significant reduction of PFOS was observed in the absence of either vitamin B_{12} or Ti(III) citrate, nor in controls in which vitamin B_{12} was replaced with cobalt (II) or in controls with Ti(IV)- in lieu of Ti(III)-citrate. Monitoring of PFOS degradation by suppressed conductivity ion chromatography revealed that PFOS isomers differed in their susceptibility to reductive degradation by vitamin B_{12}/Ti(III) citrate. Chromatographic peaks corresponding to branched PFOS isomers disappeared whereas the peak corresponding to linear PFOS was stable.

Technical PFOS is a mixture of linear and branched structural isomers, with the latter making 20 to 30% of the total mass (2,3) (Fig. 4). ^{19}F-NMR and HPLC-MS/MS studies revealed that the PFOS material used in our study contained 24.6% branched isomers, consisting chiefly of the following perfluoromonomethyl and perfluoroisopropyl isomers: 3-CF_3-PFOS, 4-CF_3-PFOS (**I**), 5-CF_3-PFOS, 6-CF_3-PFOS (**II**) and 1-CF_3-PFOS (**III**) by LC-MS/MS. The branched isomers were separated from the linear PFOS and assessed for reductive dehalogenation by vitamin B_{12} at 70°C, pH 9.0. The susceptibility of the branched PFOS isomers to attack by vitamin B_{12} was confirmed by fluoride release measurements (70.6% initial fluorine released after 5 days) as well as suppressed conductivity ion chromatography, HPLC-MS/MS and ^{19}F-NMR studies. The HPLC-MS/MS chromatograms indicate complete removal of the isomers, 3-, 4-, 5- and 6-CF_3-

PFOS, after 5 days, while traces of 1-CF_3-PFOS were still present. Isomer degradation was confirmed by the nearly complete disappearance of the signal corresponding to the branched CF_3 group and other organic fluorine signatures characteristic of the branched PFOS structures in ^{19}F-NMR spectra. Defluorination was also observed at ambient conditions (30°C, pH 7.0) albeit at lower rates.

Extensive work has been dedicated to the identification of the products formed by reductive dehalogenation of PFOS. Degradation products could not be detected in the gas phase using GC/MS. Likewise, HPLC-MS/MS (electrospray ionization, negative and positive mode) and direct injection MS/MS analysis have failed to confirm the presence of PFOS derivatives in the liquid phase. Current efforts are directed at the analysis of relatively polar compounds not detected by the previous methods in the liquid phase and at the fractionation and analysis of insoluble/colloidal materials present in the reaction mixture.

The enhanced susceptibility of branched PFOS isomers to reductive dehalogenation may be related to the stabilizing effect of branched structures on radical intermediates resulting from the reductive attack. The reaction mechanism of vitamin B_{12}-catalyzed reductive dechlorination is poorly understood. The most commonly accepted models hypothesize that attack involves radical intermediates (1).

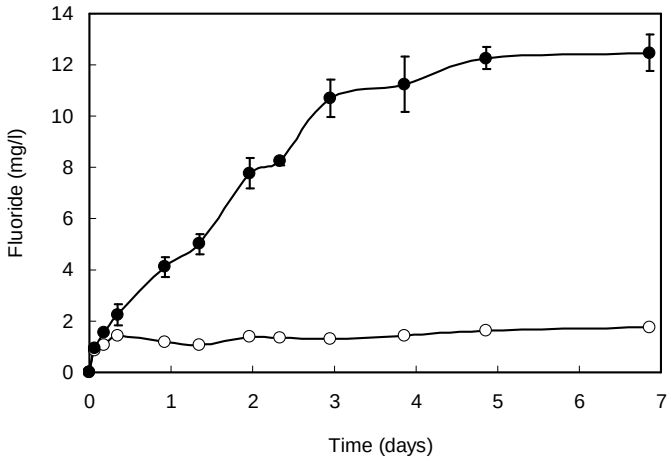

Fig 3. Biomimetic reductive dehalogenation of branched PFOS isomes with vitamin B12 (260 µM) and Ti(III) citrate (36 mM) in control samples (PFOS + Ti(III) citrate) and treatment samples (PFOS + Ti(III) citrate + Vitamin B_{12}). Samples were incubated at 70ºC and pH 9.0. Time course of fluoride release in control samples (○) and treatment samples (●). Error bars (shown if larger that the symbols) represent standard deviations of triplicate assays.

To our knowledge this is the first report of *in vitro* reductive dehalogenation of PFOS catalyzed by a biomolecule. These results have important implications for biodegradation since partially defluorinated PFOS derivatives, comparable to the products expected from reductive defluorination are known to be susceptible to biodegradation by aerobic bacteria (7). The findings also suggest that microbial reductive defluorination of PFOS might be possible. Furthermore, the observation that branched PFOS isomers are more susceptible to attack than linear PFOS provide clues for the design of perfluorinated chemicals more prone to degradation in the environment.

Industrial Interactions and Technology Transfer:

- Tim Yeakley**,** Texas Instruments; E-mail: t-yeakley@ti.com
- Walter Worth, Sematech, E-mail: Walter.Worth@sematech.org

ESH Impact:

This research proposes the development of an abatement option to reduce environmental releases of PFOS and related perfluorinated compounds. There is a great need for feasible methods for the treatment of PFAS compounds in wastewaters from semiconductor manufacturing, particularly in the light of the critical importance of these components in photolithography and other semiconductor operations, the current lack of feasible alternatives, the important limitations of existing treatment technologies, and the increasing concern of regulatory agencies about the ecological and public health risks associated with these perfluorinated compounds. Evidence that PFOS is biodegradable in the environment can be used in compound risk assessment.

The applicability of the approach proposed in this research is not limited to the treatment of PFOS. A wide variety of perfluoroalkyl chemicals, including perfluorobutane sulfonate (PFBS), can be target of reductive dehalogenation processes. PFBS is currently being considered as an alternative to PFOS for a wide variety of applications.

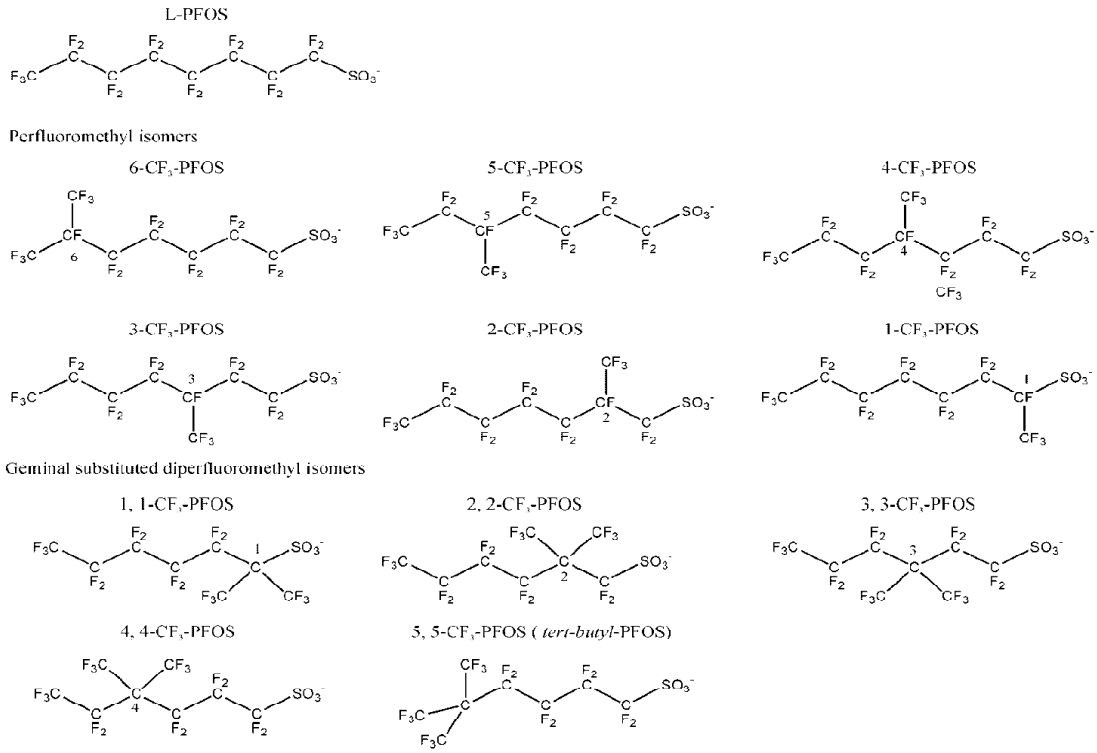

Fig. 4. Chemical structures of linera PFOS (L-PFOS), perfluoroisopropyl (6-CF_3-PFOS), 5-perfluoromethyl (5-CF_3-PFOS),4- perfluoromethyl (4-CF_3-PFOS), 3-perfluoromethyl (3-CF_3-PFOS), 2-perfluoromethyl (2-CF_3-PFOS), 1-perfluoromethyl (1-CF_3-PFOS), tert-perfluorobutyl-PFOS and of the geminal substituted diperfluoromethyl-PFOS isomers (Source: Langlois and Oehme, 2006 [9]).

Publications:

- Ochoa, V. L. 2006. Removal of perfluorooctane sulfonate (PFOS) by sorption onto activated carbon and onto wastewater treatment sludge. August 2006. MS report. Environmental Engineering MS report. University of Arizona.

Conference Presentations:

- Sierra-Alvarez R, Farrell J. 2006. Treatment of PFOS in semiconductor effluents. Annual Meeting NSF/SRC Engineering Research Center for Environmentally Benign Semiconductor Manufacturing, Feb 23-24, Tucson, AZ. [Invited presentation].
- Ochoa V, Sierra-Alvarez, R. 2006. Processes for the removal of PFOS from semiconductor effluents. Teleseminars of the SRC Engineering Research Center for Environmentally Benign Semiconductor Manufacturing. November 2, 2006. [Oral presentation].

Disclosures and Patents:

- Biomimetic degradation of perfluorinated and highly-fluorinated organic compounds.
  R. Sierra-Alvarez.

Next-Year Plan:

- Complete the optimization of the biomimetic reductive dehalogenation of PFOS and related perfluorinated compounds.
- Identification of degradation products from the biomimetic reductive dehalogenation of PFOS.
- Evaluation of the susceptibility of PFOS and related perfluoroalkyl surfactants to microbial reductive dehalogenation using inoculum sources exposed.
- Assessment of the susceptibility of partially dehalogenated perfluoroalkyl-sulfonate compounds to biodegradation by aerobic microorganisms in municipal wastewater treatment systems, including co-oxidation by ammonia monooxygenase-producing nitrifying bacteria (occurring in activated sludge plants).

References:

1. **Banerjee, R., S.W. Ragsdale.** 2003. The many faces of vitamin B12: Catalysis by cobalamin-dependent enzymes. *Annu. Rev. Biochem.*, **72:**209-247.
2. **Company, 3M.** 1997. Fluorochemical Isomer Distribution by 19F-NMR Spectroscopy. US EPA Public Docket AR226-0564.
3. **De Silva, A.O., S.A. Mabury.** 2006. Isomer distribution of perfluorocarboxylates in human blood: Potential correlation to source. *Environ. Sci. Technol.* **40**(9): 2903-2909.
4. **Field, J.A., R. Sierra-Alvarez.** 2004. Biodegradability of chlorinated solvents and related chlorinated aliphatic compounds. *Rev. Environ. Sci. Biotechnol*. **3:**185-254.
5. **Giesy, J.P., K. Kannan.** 2002. Perfluorochemical surfactants in the environment. *Environ. Sci. Technol.* **36:**146A-152A.

6. **Hollingsworth, J. et al.** 2005. Anaerobic biodegradability and methanogenic toxicity of key constituents in copper chemical mechanical planarization effluents of the semiconductor industry. *Chemosphere*, **59**(9): 1219-1228.
7. **Key, B.D. et al.** 1998. Defluorination of organofluorine sulfur compounds by *Pseudomonas* sp. strain D2. *Environ. Sci. Technol*. **32:**2283-2287.
8. **Krone, U.E. et al.** 1991. Reductive formation of carbon-monoxide from CCl_4 and freon-11, freon-12, and freon-13 catalyzed by corrinoids. *Biochem.* **30:**2713–2719.
9. **Langlois, I., M. Oehme.** 2006. Structural identification of isomers present in technical perfluorooctane sulfonate by tandem mass spectrometry. *Rapid Comm. Mass Spectrom.*, **20**(5):844-850.
10. **Lesage, S. et al.** 1990. Occurrence and fate of organic-solvent residues in anoxic groundwater at the Gloucester landfill, Canada. *Environ. Sci. Technol*. **24:**559-566.
11. **Martin, J.W. et al.** 2004. Analytical challenges hamper perfluoroalky research. *Environ. Sci. Technol.* **38:**248A-255A.
12. **Natarajan, R. et al.** 2005. Microbial cleavage of C-F bond. *J. Fluorine Chem*. **126:**425-436.
13. **Ochoa, V. L.** 2006. Removal of perfluorooctane sulfonate (PFOS) by sorption onto activated carbon and onto wastewater treatment sludge. August 2006. MS report. Environmental Engineering MS report. University of Arizona.
14. **Tang, C.Y. et al.** 2006. Use of reverse osmosis membranes to remove perfluorooctane sulfonate (PFOS) from semiconductor wastewater. *Environ. Sci. Technol.* 40(23):7343 -7349.

Destruction of Perfluoroalkyl Surfactants in Semiconductor Process Waters using Boron Doped Diamond Film Electrodes

Personnel:

PIs:

- James Farrell, Chemical and Environmental Engineering, UA
- Reyes Sierra, Chemical and Environmental Engineering, UA
- Srini Raghavan, Materials Science & Engineering, UA

Other Research Personnel:

- Fiona L Jordan, Chemical and Environmental Engineering, UA

Graduate Students:

- Kim Carter, Chemical and Environmental Engineering, UA
- Valeria Ochoa, Chemical and Environmental Engineering, UA

Undergraduate Students:

- Beshoy Latif, Chemical and Environmental Engineering, UA

Objectives:

The objectives of this research are to: 1) determine the feasibility of electrochemical destruction of perfluorooctyl sulfonate (PFOS) and related perfluoroalkyl surfactants (PFAS) using boron doped diamond (BDD) film electrodes; 2) determine the degree of electrolysis required to generate products that are readily biodegraded in municipal wastewater treatment plants; and 3) develop an adsorptive method using hydrophobic zeolites and/or anion exchange resins for concentrating PFAS compounds from dilute aqueous solutions.

Background:

PFOS and other perfluorinated alkyl surfactants (PFAS) are widely used in semiconductor manufacturing. Recent studies have detected PFOS in human blood and wildlife tissue samples collected from around the globe. Regulatory agencies in the United States and Europe have initiated studies to quantify the use of PFAS, assess their potential risks, and consider regulations banning or restricting their use.

Much of the PFOS used in semiconductor fabrication is disposed of in solvent-based wastes by incineration. However, there is no effective treatment for the removal of PFOS or any other PFAS compounds from wastewater streams. Adsorption on activated carbon is believed to be ineffective, while membrane methods and ion exchange are expensive and merely concentrate the aqueous compounds which then require disposal. Destructive treatment via advanced oxidation processes (AOPs) using UV light with TiO_2 photocatalysts or peroxide, or ozone/peroxide systems, are ineffective for PFAS oxidation. The carbon-fluorine bonds in fluorinated organics are very stable and have slow reaction rates with the hydroxyl radicals ($HO^{\bullet}$) produced in conventional AOPs. Additionally, perfluorinated surfactants are not biodegradable in municipal wastewater treatment plants. This research will investigate an electrochemical treatment method for removing PFOS from dilute aqueous streams.

Method of Approach:

The first task of the research will determine the optimal conditions for oxidative and reductive destruction of PFOS and related PFAS compounds (*e.g.*, perfluorobutane sulfonate derivatives) in semiconductor wastewaters. This task will involve determining the effect of electrode potential, solution pH value, reactant concentration, temperature, and electrolysis time on the reaction rates and oxidation and reduction products for the target compounds at BDD anodes and cathodes. The current efficiency, defined as the fraction of the cell current going towards electrolysis of the target compound and its daughter products, will be determined for all operating conditions. This will enable the cost-effectiveness of the process to be evaluated. These studies will be performed in both parallel plate, flow-through reactors and in batch reactors using a rotating disk electrode (RDE). Comparisons between the RDE and flow-through experiments will allow identification of any mass transfer limitations in the flow cells.

The second task of the research will determine the most effective method for concentrating the PFAS compounds from dilute aqueous solutions. Adsorption isotherms for PFAS compounds on several anion exchange resins and hydrophobic zeolites will be determined as a function of the solution pH value and ionic strength. Column breakthrough experiments will also be performed to determine the mass transfer characteristics for the best performing adsorbents or ion exchange resins. Regeneration of the adsorbents or anion exchange resins by heating will also be investigated. The equilibrium and kinetics of target compound release from the adsorbents/ion exchange resins will be determined as a function of temperature.

The third task of the research will characterize the fate of the incomplete destruction products from electrochemical treatment in conventional aerobic and anaerobic wastewater treatment systems. Biotransformation of electrolysis products by cometabolism and their utilization as sole carbon source will be evaluated in batch laboratory experiments designed to simulate typical conditions in municipal wastewater treatment plants.

The fourth task will be to build the 4-step prototype treatment system shown in Figure 1 and test it on real PFAS containing wastewaters generated during semiconductor manufacturing.

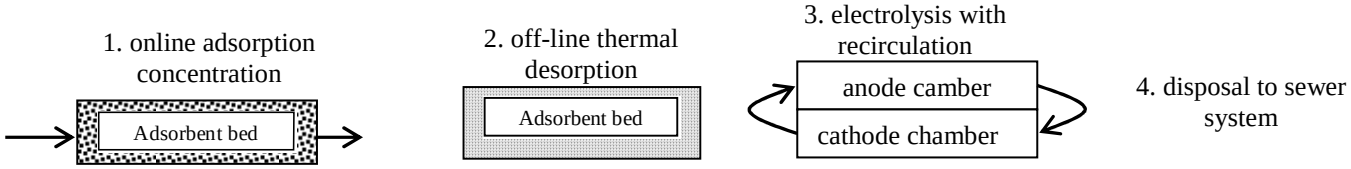

Figure 1. Schematic diagram of proposed treatment scheme.

Highlights of Results and Accomplishments:

Electrolysis experiments were performed in both flow-through and batch reactors. The flow-through reactor had an anode surface area of 25 cm^2 and a bed volume of 15 mL, yielding a surface area to solution volume ratio of 1.67 cm^2/mL. The batch reactor had an anode surface area of 1 cm^2 and a solution volume of 600 mL, yielding a surface

area to solution volume ratio of 2.86 x 10^{-3} cm^2/mL. Reaction rates in the flow-through reactor are representative of those attainable in a real water treatment unit operation.

Electrolysis experiments using the flow through BDD reactor indicate that PFOS can be rapidly removed from water. Figure 2 shows the PFOS and total organic carbon (TOC) concentrations as a function of treatment time. Reaction rates for PFOS and TOC were first order with respect to concentration, with a treatment half-life of less than 10 minutes. The near identical declines in PFOS and TOC concentrations in Figure 2 indicate that PFOS oxidation at a current density of 15 mA/cm^2 does not produce reaction products that build-up in the solution. However, at lower current densities, TOC removal rates were slower than those for PFOS. Figure 3 compares PFOS and TOC removal in a batch reactor and shows that the removal half-life for TOC removal of 16 hours is approximately twice the 8 minute removal half-life for PFOS.

Figure 2. PFOS and TOC concentrations as a function of treatment time in the flow through reactor operated at a current density of 15 mA/cm^2.

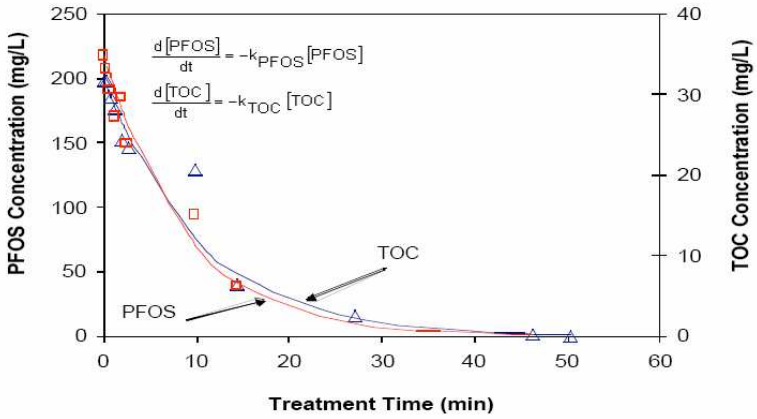

Figure 3. PFOS and TOC concentrations in the batch reactor operated at a current density of 10 mA/cm^2.

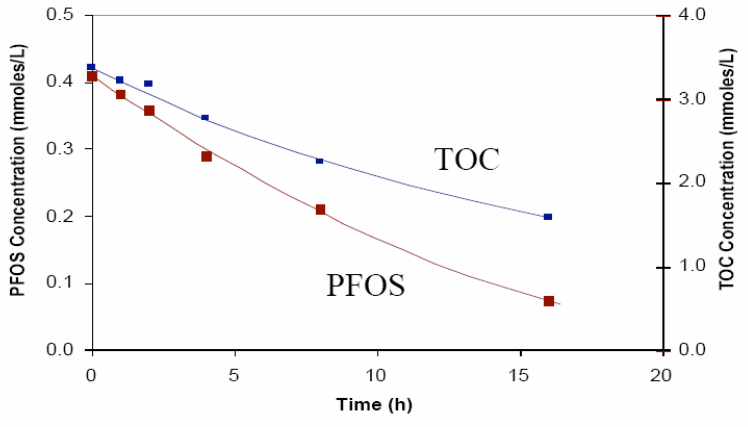

The reaction products for PFOS oxidation were determined by liquid chromatography/tandem mass spectrometry. Additionally, ion chromatography was used to monitor the buildup of fluoride and sulfate ions in the solutions. The first reaction product of PFOS oxidation is perfluorooctanoic acid (PFOA). The overall reaction for PFOA formation can be expressed as:

$$C_8F_{17}SO_3H + 3H_20 \rightarrow C_7F_{15}CO_2H + SO_4^{2-} + 4H^+ + 2F^- + 2H_2 \quad (1)$$

PFOA undergoes further oxidation to produce perfluoroheptanoic (PFHtA) acid by the reaction:

$$C_7F_{15}CO_2H + 2\,H_2O \rightarrow C_6F_{13}CO_2H + CO_2 + 2H^+ + 2F^- + H_2 \quad (2)$$

PFHtA undergoes further oxidation to produce perfluorohexanoic (PFHxA) acid by the reaction:

$$C_6F_{13}CO_2H + 2\,H_20 \rightarrow C_5F_{11}CO_2H + CO_2 + 2H^+ + 2F^- + H_2 \quad (3)$$

No other organic reaction products were detected. Fluoride analyses indicated that an average of 4.5 fluoride ions were released per PFOS molecule degraded. This indicates that TOC in the form of PFOA, PFHtA and PFHxA was removed from the solution via volatilization. The fluoride mass balance indicates that volatilization of PFHxA was the primary factor removing TOC from the solution.

PFOS removal rates were independent of the applied potential for current densities of 5 mA/cm^2 or greater. Figure 4 shows that PFOS removal at 2.5 mA/cm^2 was slightly slower than removal rates at 5 & 15 mA/cm^2, which were identical. This suggests that the reaction mechanism involves indirect PFOS oxidation by hydroxyl radicals produced from water oxidation, rather that direct oxidation of PFOS at the electrode surface. This conclusion is consistent with other investigations of organic compound oxidation at BDD electrodes.

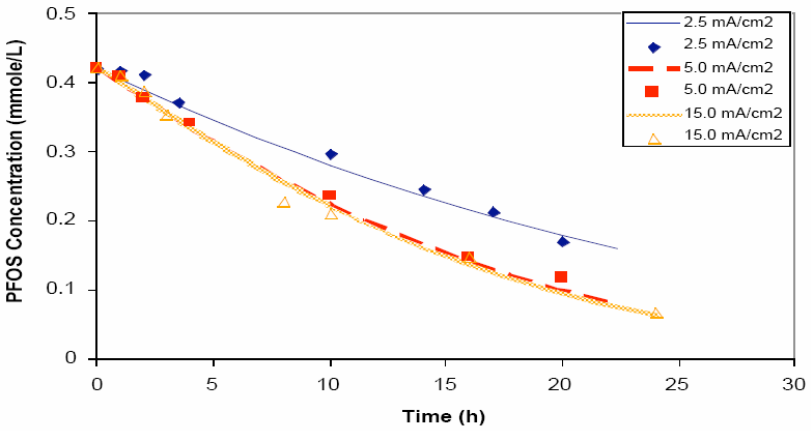

Figure 4. PFOS concentration versus time in the batch reactor for current densities of 2.5, 5 and 15 mA/cm^2. Lines are fits of the kinetic model.

TOC removal rates were dependent on the electrode potential and increased with increasing current density, as shown in Figure 5. In contrast to the identical PFOS removal rates at 5 & 15 mA/cm^2, Figure 5 shows that the shows that TOC removal half-life at 15 mA/cm^2 was ~25% greater than that at 5 mA/cm^2.

Figure 5. TOC concentration versus time in the batch reactor for current densities of 2.5, 5 and 15 mA/cm^2. Lines are fits of the kinetic model.

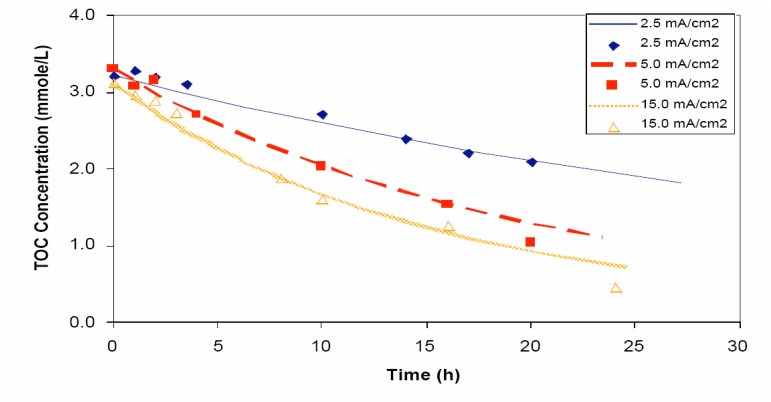

Work on task 2 is ongoing. The effectiveness of different types of granular activated carbon (GAC) and hydrophobic zeolites to remove PFOS and related PFAS from aqueous solutions was evaluated. Adsorption isotherms for PFOS, perfluorobutane sulfonate (PFBS, a compound proposed as possible alternative to PFOS) and PFOA on GAC were determined in a phosphate buffer (3 mM, pH 7.2) at 30ºC. Removal of the perfluorinated compounds from solution was determined by ion chromatography with suppressed conductivity detection and/or TOC analysis. The activated carbon utilized in the experiments was washed thoroughly with deionized water to minimize interferences by soluble organic residues in the material. GAC showed a higher affinity for PFOS than for the other two perfluoroalkyl compounds tested. The adsorptive capacity of GAC decreased in the following order: PFOS > PFOA ≈ PFBS, as shown in Figure 6. Performance of GAC at PFOS concentrations in the high ppm range was moderate to poor. However, our results indicate that GAC could be an attractive sorbent for the removal of PFOS from dilute solutions (low ppm and ppb range). Initial experiments with various hydrophobic zeolites suggest that these sorbents are inferior to activated carbon.

Figure 6. Adsorption isotherms on activated carbon (Calgon F-400) for PFOS, PFOA and PFBS. (Solid line) experimental data fit to Langmuir model; (Dashed line) experimental data fit to Freundlich model.

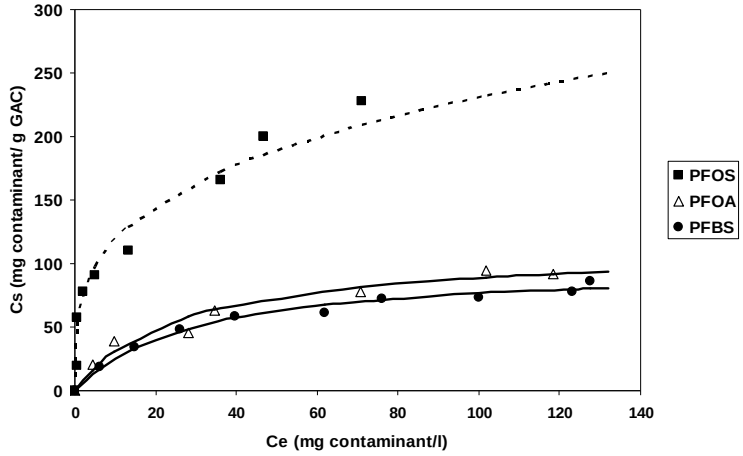

Industrial Interactions and Technology Transfer:

- Walter Worth Sematech
- Tim Yeakley Texas Instruments,
- Thomas P. Diamond IBM
- Jim Jewett Intel
- Laura Mendicino Freescale Semiconductor

ESH Impact:

Proposals are presently being evaluated for banning PFOS and related compounds in both the United States and the European Union. At this time, the semiconductor industry has secured a limited use exemption for PFOS in photoresists and antireflective coatings. The development of effective treatment methods will be essential for securing the critical use exemption status for PFAS and related compounds.

The immediate value of this research will be to address the ESH concerns associated with the use of PFOS and other fluorinated organic compounds by developing a method to destroy these compounds in wastewater streams generated during semiconductor manufacturing. Additionally, the wastewater treatment technology developed here will be useful in the future for destruction of a wide range of hazardous organic compounds. The development of a novel wastewater treatment technology that can completely destroy a wide range of compounds and/or degrade them into products amenable to municipal wastewater treatment systems will eliminate many of the ESH concerns associated with the development of new process technologies.

Next-Year Plan:

- During the next year electrolysis experiments will be performed on other PFAS compounds, such as PFBS. Also, the effects of pH on the rates and products of PFAS oxidation will be determined.
- Work on activated carbon will be continued and experiments will be performed to determine the best zeolite or ion exchange resin on which to concentrate the PFAS compounds before electrolysis.
- The fate of products from electrochemical treatment of PFOS will be evaluated in assays simulating biological wastewater treatment systems. Degradation products generated under different treatment conditions (*e.g.* current density, electrolysis time, pH) will be assessed. Experiments will also be performed to evaluate the susceptibility of perfluorohexanoic acid (PFHxA) acid to biodegradation under aerobic and anaerobic conditions.

ESH Assessments of Materials, Structures and Processes for Nanoscale MOSFETs with High-Mobility Channels

Personnel:
PIs:

- Krishna C. Saraswat, Electrical Engineering, Stanford University
- Paul C. McIntyre, Materials Science and Engineering, Stanford University

Graduate Students:

- Eunji Kim, Materials Science and Engineering, Stanford University

Objectives:

This research is aimed at assessing the ESH impacts of future front materials and processes, with particular focus on achieving a high-quality interface between III-V compound semiconductors and high-k dielectrics. A native oxide-free semiconductor surface prior to deposition of high-k dielectrics is desirable for fabrication of high-performance III-V-based MOSFETs. HCl-etched III-V semiconductor surfaces, however, tend to oxidize readily when they are exposed in air. Therefore, passivation of the oxide-free surface is essential to integrate MOS devices based on III-V semiconductors. Furthermore, achieving a chemically-stable passivation of the III-V substrate surface allows wafers to be queued during manufacturing and reduces the need for subsequent surface cleans. As the cleaning solutions used on (for example) GaAs or InGaAs substrates produce a potentially toxic, As-containing effluent, stable chemical passivation of the surface can provide a substantial ESH benefit.

Background:

As device dimensions are scaled down aggressively, interface properties between dielectrics and channel materials become more critical in order to achieve stable switching of MOS transistors. Unlike SiO_2, an excellent passivation layer for Si, the native oxide of GaAs and InGaAs exhibits poor passivating properties and a large density of defect states exists at the interface between the native oxide and GaAs. Therefore, it is desirable to remove the native oxide on III-V surfaces for fabrication of high-performance MOS devices based on high-mobility channel materials.

Conventional methods to remove native oxide from III-V compound semiconductors such as HCl etching, however, do not produce surfaces that are stable in room air for long periods. Once the HCl-etched surface is exposed to air, it readily forms a new native oxide layer. In order to avoid unwanted oxidation of the surface, it is required to passivate the oxide-free surface. In addition to the practical benefits related to more robust device process flows and improved electrical characteristics, a chemically-passivated oxide-free III-V surface has substantial ESH benefits because repeated wet cleaning of the wafers prior to gate dielectric deposition can be minimized. Among many passivation techniques, S-treatment using $(NH_4)_2S$ solution has been reported to be an effective way to form a monolayer of S bonded to surface of GaAs (100) substrates. By optimizing S-passivation conditions using aqueous $(NH_4)_2S$, we have demonstrated W/ALD-HfO_2/p-GaAs MOS capacitors with promising capacitance and leakage current characteristics.

Method of Approach:

Epitaxial p-type Si-doped GaAs (100) samples with a doping concentration of 1.5×10^{17} cm^{-3} are degreased by sonication in acetone for 5 minutes. After a short DI water rinse, samples are dipped in diluted hydrochloric acid (18%) for 3 minutes to remove native oxide layers. (Same sets of samples are also dipped in diluted hydrofluoric acid (2%) for 3 minutes to compare the effectiveness of the cleaning methods.) After another short DI water rinse, samples are dipped in 10% $(NH_4)_2S$ solution for 15 minutes to form an S-layer to prevent the GaAs surface from oxidizing. After a short DI water rinse, the samples are dried by N_2.

Samples are then placed into the load-lock of the ALD chamber within a very short time. After about 15 minutes' for pumping, samples are transferred into the ALD chamber. After another 30 minute wait for temperature stabilization of the sample stage, HfO_2 is deposited by alternating pulses of H_2O vapor and Tetrakis Diethylamino Hafnium ($((CH_3)_2N)_4Hf$) precursors at 150°C. W gate metal is deposited by e-beam evaporation through a shadow mask. Ti/Au is deposited for back side wafer contact. Chemical states of the GaAs surface with and without S-passivation were investigated by shallow angle x-ray photoelectron spectroscopy. Electrical properties of HfO_2/GaAs MOS capacitors were studied by C-V and I-V measurements.

Highlights of Results and A Highlights of Results and Accomplishments:

We have investigated the electrical and physical properties of W/HfO_2/p-GaAs MOS capacitors with and without sulfur passivation prior to HfO_2 deposition and have studied the chemical stability of the S-passivation. The non-treated epitaxial p-GaAs surface shows various oxide states of GaAs such as Ga_2O_3, As_2O_3, As_2O_5 as shown in Figure 1. Among various surface treatments (HF-etching, HCl-etching, S-passivation followed by HF-etching, S-passivation followed by HCl-etching), S-passivation followed by HCl-etching shows the most effective cleaning results in terms of native oxide removal as a function of exposure time to atmospheric pressure after surface treatment (Table I). Overall, HCl-etching shows better performance on removing native oxide of GaAs than HF-etching, and S-passivation followed by native oxide removal process produces more stable oxide-free surface than non-passivated. S-passivation GaAs surface followed by native oxide removal using HCl etching shows oxide-free and Ga-S bonding (Ga_2S_3) is observed by XPS (Figure 2). The physical thickness of ALD-HfO_2 is estimated to be 18.3 nm for non-treated p-GaAs and 19.8 nm for S-passivated GaAs by x-ray reflectivity. C-V characteristics of W/ALD-HfO_2/p-GaAs with and without S-passivatoin are shown in Fig.'s 3 and 4. The S-passivated sample shows improved electrical properties such as a decrease in CV hysteresis (although it is still significant), recovery of a near-ideal flat band voltage, and complete elimination of frequency dispersion relative to non-treated GaAs, without sacrificing gate capacitance.

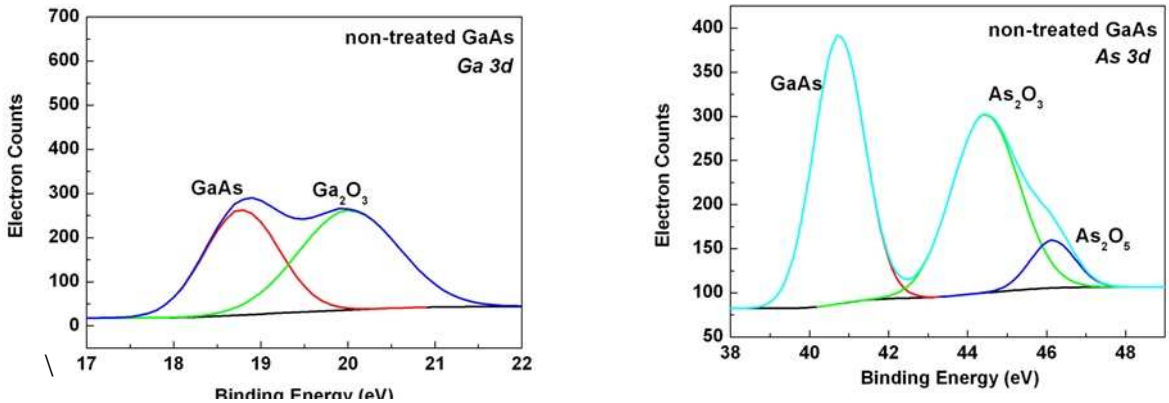

Figure 1. Ga 3d & As 3d peaks of non-treated GaAs (Ga_2O_3/total Ga = 0.56, As_2O_3/total As = 0.43, As_2O_5/total As = 0.08)

Table I. Comparison of cleaning effectiveness & stability measured by shallow angle XPS

	Non-treated GaAs	**HF-etched GaAs**	**HCl-etched GaAs**	**HF-etched & S-passivated GaAS**	**HCl-etched & S-passivated GaAs**
Ga_2O_3/total Ga After surface treatment	56% (reference, no surface treatment)	17%	14%	11%	~0%
Ga_2O_3/total Ga After 6 hour exposure to lab atmosphere	56% (reference, no surface treatment)	25%	19%	13%	11%

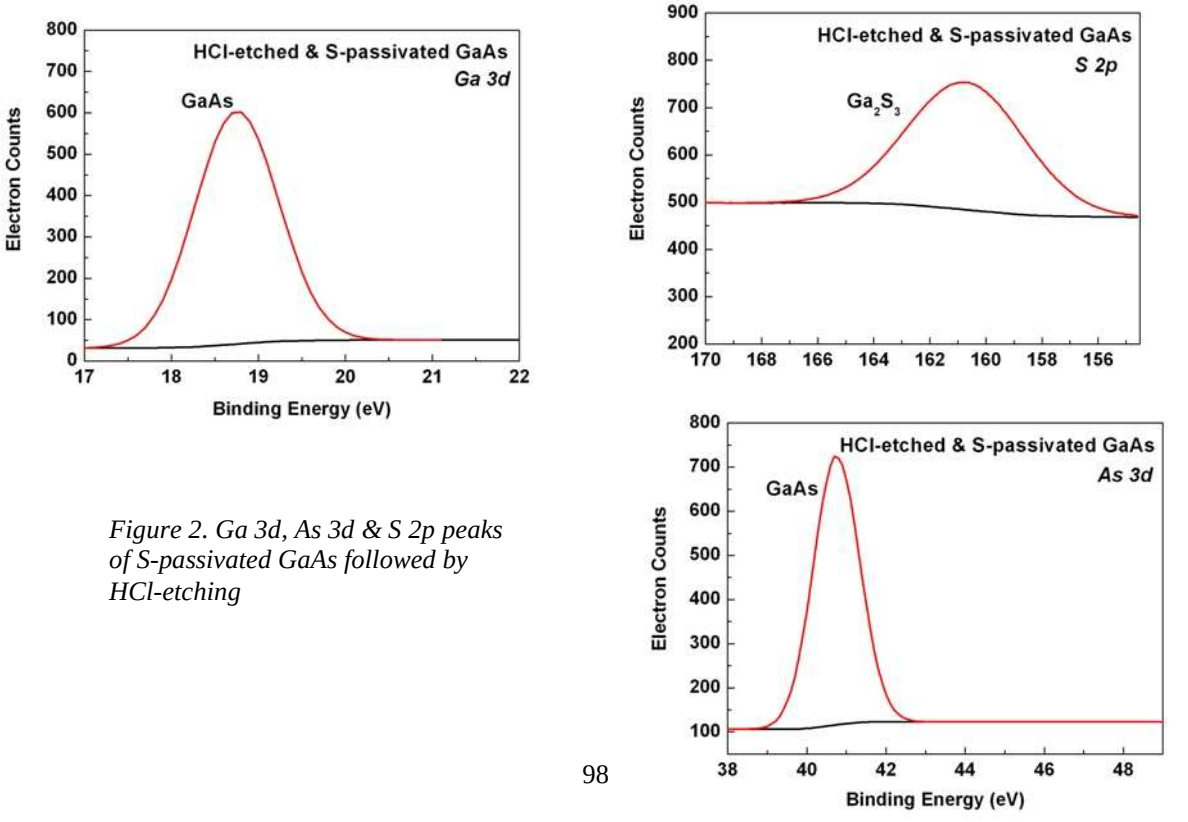

Figure 2. Ga 3d, As 3d & S 2p peaks of S-passivated GaAs followed by HCl-etching

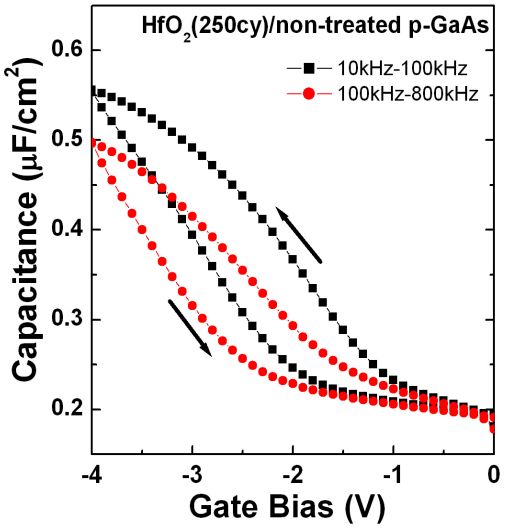

Figure 3. C-V characteristics of as-deposited W/HfO_2/non-treated epi p-GaAs (calculated EOT (100-800kHz) =6.94nm)

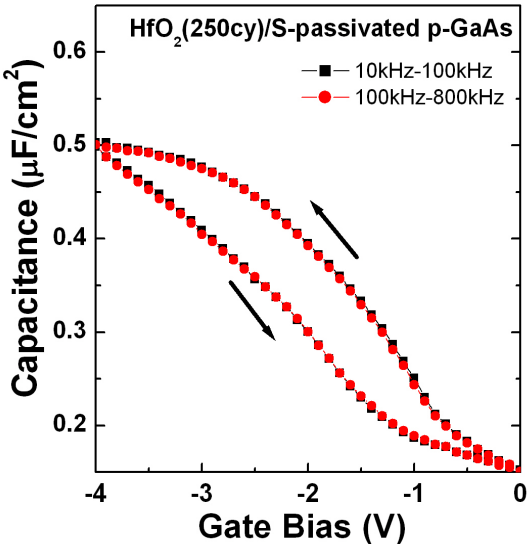

Figure 4. C-V characteristics of as-deposited W/HfO_2/S-passivated p-GaAs (calculated EOT = 6.9nm)

Industrial Interactions and Technology Transfer:

This research involves active collaboration with researchers at Intel Corporation: Dr. Niti Goel and Dr. Wilman Tsai

Next-Year Plan:

We plan to improve properties of HfO_2/GaAs (and InGaAs) further by subsequent post-deposition anneals under various conditions and also plan to investigate *in-situ* hydrogen plasma treatments to remove the S-layer adsorbed on GaAs surface prior to HfO_2 deposition. In addition to providing a barrier to native oxide formation during storage of GaAs and InGaAs substrates prior to gate insulator deposition, it has been reported that S may dope the surface of such crystals, which may have negative consequences in terms of electrical control of MOS devices. Molecular hydrogen and hydrogen plasma exposure in-situ, prior to ALD, will be studied as a means of controlling the S concentration in the surface region of the substrate.

In collaboration with the Nishi and Shadman groups, we plan to perform a systematic assessment of ESH benefits stemming from a stable chemical passivation of III-V surfaces in a realistic device fabrication flow. We will also jointly investigate possible issues associated with removal of residual passivating agent (e.g. S) either before or after gate dielectric deposition.

ESH Impact:

Possible reactions of GaAs with the chemicals used in the research are listed in the table below.

	GaAs	Reactivity
air	Ga_2O_3, As_2O_3	mild
HCl	$GaCl_3$, GaCl, Ga_2Cl_6, GaH_3, $AsCl_3$, H_2, AsH_3, $AsCl_5$ $As_2O_3 + 6HCl \rightarrow 2AsCl_3 + 3H_2O$ $Ga_2O_3 + 6HCl \rightarrow 2GaCl_3 + 3H_2O$	mild

Reactivity and health effects are listed below.

GaAs	
Reactivity	Stable under ordinary conditions Conditions to avoid : water/moisture Incompatibility : Steam, heat, acid, acid fumes Hazardous decomposition products : Highly toxic fumes of Arsenic
Health Effects	May be irritating skin, eyes and mucous membranes

HCl	
Reactivity	Stable under ordinary conditions Conditions to avoid : Heat, direct sunlight Incompatibility : strong bases, metals, metal oxides, hydroxides, amines, carbonates, alkaline, cyanides, sulfides, sulfites, formaldehyde Hazardous decomposition products: toxic hydrogen chloride fumes (when heated), toxic chlorine fumes and explosive hydrogen gas (thermal oxidative decomposition).
Health Effects	Corrosive, any kind of physical contact including inhalation, ingestion, skin contact, eye contact is extremely dangerous.

$(NH_4)_2S$	
Reactivity	Stable under ordinary conditions Conditions to avoid : Heat, flames, ignition sources Incompatibility : Acids Hazardous decomposition products : toxic fumes of sulfur oxides, nitrogen oxides, hydrogen sulfide, ammonium bisulfite, and ammonia (when heated to decomposition)
Health Effects	Corrosive, may cause irritation

$AsCl_3$	May be fatal if inhaled, absorbed through the skin or swallowed.

*Alternative sulfur-passivation methods and their ESH impact are described in the table below.

Cl_2S_2	
Reactivity	Stable under ordinary conditions Conditions to avoid : Heat, water Incompatibilty : Reducing agents, organics, titanium Hazardous decomposition products : chlorine, hydrogen disulfide, sulfur dioxide, sulfur (when heated)
Health Effects	Corrosive, can cause burns

Na_2S	
Reactivity	Darkens on exposure to air or light Conditions to avoid : Heat, flames Incompatibility : Acids, oxidants, aluminum, zinc, carbon, diazonium salts Hazardous decomposition products : Burning may produce sulfur oxides
Health Effects	May be fatal if swallowed, corrosive, causes burns to any area of contact

Section 2

Other Customized Projects

Post-Planarization Waste Minimization

Personnel:
PI:

- Ara Philipossian: Chemical and Environmental Engineering (UA)

Other Research Personnel:

- Yun Zhuang: Chemical and Environmental Engineering (UA)
- Leonard Borucki: (Araca Incorporated)

Graduate Student:

- Ting Sun: Chemical and Environmental Engineering (UA)

Objectives:

The objectives are to: (1) investigate the effect of brush physical properties on tribological behavior during post-CMP cleaning, and (2) design, construct and qualify an incremental loading tool to investigate brush asperity deformation as a function of applied load and extended use.

Background and Method of Approach:

PVA brush life and cleaning effectiveness depends strongly on the magnitude of the frictional forces between the wafer and brush relative to the magnitude of adhesion forces between the particle and the wafer, as well as the particle and the brush. Precise quantification of the extent of frictional forces between the wafer and the brush is critical since low amounts of force will fail to remove particles and high amounts may cause scratching of the wafer surface.

A novel single-sided PVA brush scrubber is used to develop fundamental understanding of the tribology of the process. A fully automated robotics assembly capable of rotation and application of precise amount of brush pressure is secured above the rotating platform such that, during operation, the only points of contact between the robotics assembly and the rotating platform are those between the wafer and the PVA brush. The rotating platform is placed on top of a novel friction table comprised of two parallel steel plates. The plates are allowed to move relative to one another in only one direction. A highly sensitive strain gauge is mounted between the two plates in order to measure the lateral force (through calibration between voltage output and shear force) exerted by the top plate onto the bottom plate during scrubbing. For a given run, coefficient of friction is determined by dividing the magnitude of the shear force (as determined experimentally from the calibrated voltage output of the strain gauge) to the normal force applied to the wafer (i.e. applied normal brush pressure multiplied by the contact area). Both the contact area and the brush pressure are experimentally determined using a thin-film electronic pressure sensor.

PVA brushes type A and type B with different hardness properties (see Table 1) were employed in this study. Ultra pure-water mixed with oxalic acid (pH ~ 3.0) was used as the cleaning solution at a flow rate of 120 ml/min. A blanket copper wafer was used as substrate rotating at 120 RPM. Prior to data acquisition, all brushes were soaked in DI water for 12 hours to ensure absence of chemical residues. Angular brush velocities

and brush pressures were 20, 40 and 60 RPM, and 0.3, 0.5 and 0.7 PSI, respectively. After initial tribological tests at multiple *pV* combinations, a two-hour marathon test was performed with the brush rotating at 60 RPM at 0.5 PSI. Shear force data were collected during the entire two-hour scrubbing.

Highlights of Results and Accomplishments:

Table 1 summarizes the marathon test results. During the two-hour scrubbing period, shear force (both mean and standard deviation), contact area and COF associated with both brush types change. Changes associated with the harder brush are more pronounced.

Table 1. Results Summary

Brush Type	Shear Force (lb_f)		COF		COF Standard Deviation		Contact Area (in^2)		30 % Compressive Stress (kPa)
	0 hr	2 hr	0 hr	2 hr	0 hr	2 hr	0 hr	2 hr	
A	0.113	0.104	0.091	0.084	0.039	0.042	2.48	2.62	8.5
B	0.062	0.051	0.100	0.076	0.054	0.061	1.24	1.34	17.0

These two brushes were selected intentionally so as to yield the same COF regardless of their physical properties. Results indicate that the harder brush was not as stable as its softer counterpart and that it exhibited a greater degree of hydrodynamic chatter (as evidenced by the larger standard deviation in force) compared to the softer brush.

Figure 1 shows the effect of pseudo-Sommerfeld number (i.e. *V/p*) on COF for both brush types at a combination of velocities and pressures. For Brush A, at all pressures, COF has a power dependence on *V*, while increasing brush pressure has no effect on COF. A similar effect of *V* on COF is seen for Brush B, however the power dependence of COF on *V* is not uniform at different pressures. This is likely due to the fact that Brush B has a higher standard deviation of shear force and tends to have greater stick-slip. In order to understand the mechanism of brush wear, we have constructed and in the midst of qualifying a brush deformation measurement tool as shown in Fig. 2. The tool employs a capacitance probe to measure the gap between a reference surface in contact with the brush sample and the probe. The cylindrical nodules are cut from a PVA brush roller using a specially designed device to ensure flat sample surface and identical sample thicknesses. As one nodule has a small surface area, multiple nodules from the PVA brush roller are placed between the sample holder and the optic flat. As the brush samples are loaded, the gap between the brush samples surface and the optical flat surface decreases due to brush deformation and the distance change is measured by the capacitance probe. After hours of scrubbing, the mechanical properties of the brush nodules (specifically their asperities) will change, which can be quantitatively measured by this novel tool.

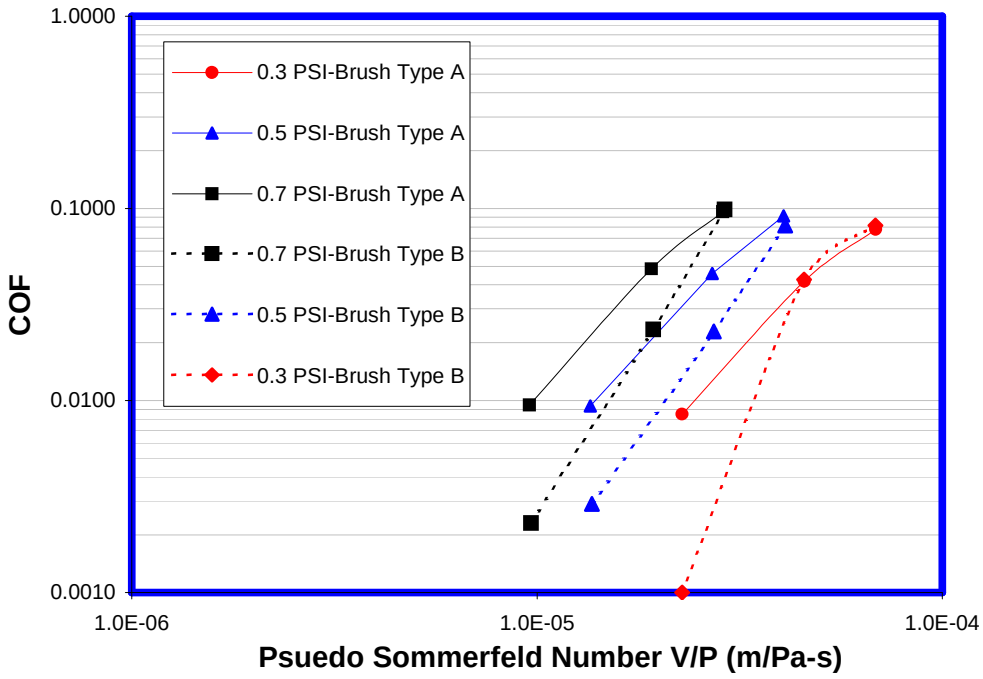

Figure 1. Stribeck Curve of Type A and Type B brushes.

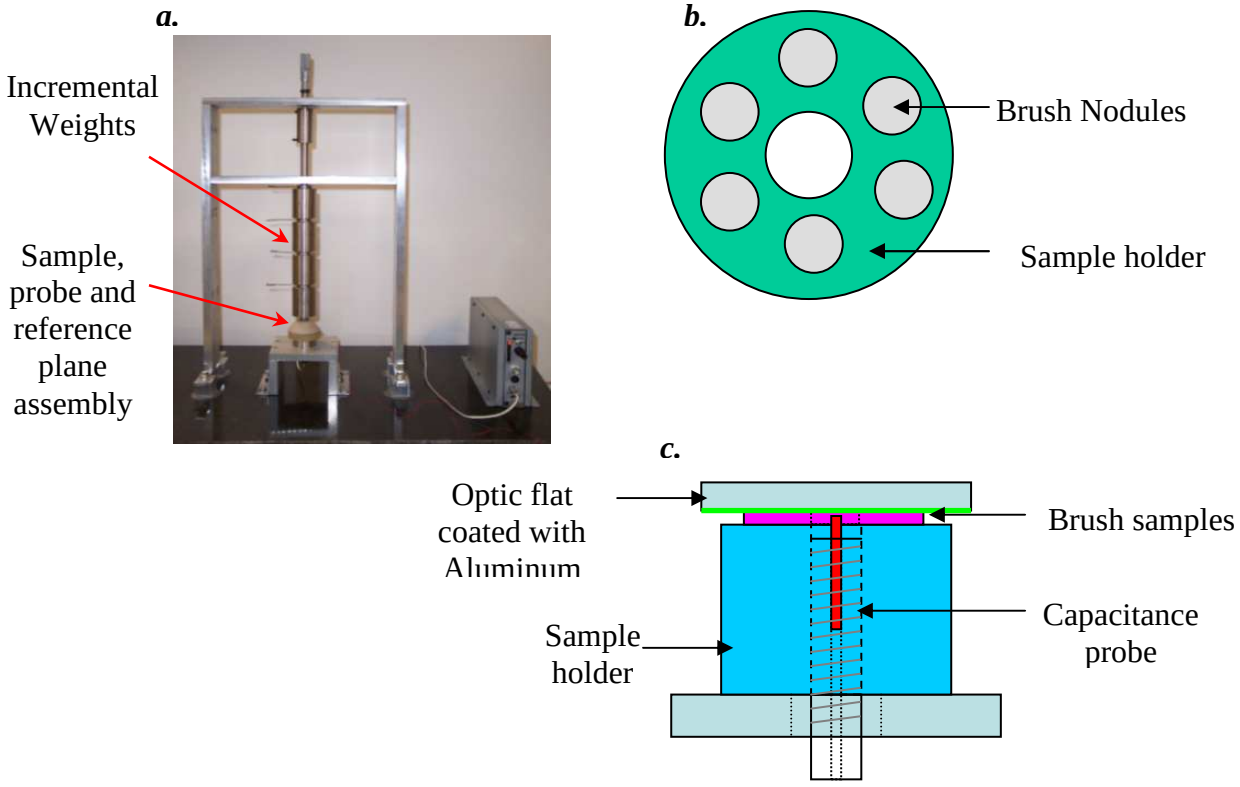

Figure 2. Brush deformation measurement tool: (a) tool picture; (b) top view of brush nodule sample arrangement on the sample holder; (c) schematic drawing of sample, probe and reference plane assembly

ESH Impact:

- Extend PVA brush life by better understanding the wearing mechanism, thereby help to reduce the use of material.

Next Year Plan:

- Develop a model to explain the power dependence of COF on sliding velocity.
- Wear the brush for 48 hours and perform brush deformation measurement before and after the wear test to understand the failure mechanism of PVA brushes during post-CMP scrubbing.

In-Situ Slurry Thickness and Friction Measurements during Chemical Mechanical Planarization

Personnel:

PI:

- Chris Rogers: Mechanical Engineering (Tufts University)
- Vincent P. Manno: Mechanical Engineering (Tufts University)
- Robert White: Mechanical Engineering (Tufts University)

Graduate Students:

- Nicole Braun: Mechanical Engineering (Tufts University)
- Caprice Gray: Mechanical Engineering (Tufts University)
- Andrew Mueller: Mechanical Engineering (Tufts University)
- James Vlahakis: Mechanical Engineering (Tufts University)

Objectives:

The Objective of this project is to acquire in-situ data during chemical mechanical planarization (CMP) including slurry film thickness and flow, wafer-pad contact, wafer scale friction, and small scale force measurements. Our goal is to correlate experimental data to modeling predictions to gain a better physical understanding of material removal rate (MRR) and polish quality during CMP.

Background:

A variety of techniques are used in this task. We visualize the slurry layer between the polishing pad and the wafer using a technique called Dual Emission Laser Induced Fluorescence (DELIF). We are able to image the slurry layer because we have replaced the standard wafer carrier and wafer with an optical glass disk. A major focus of our current work using DELIF is to develop reliable measurements of contact during polishing. We have also initiated an exploratory effort to determine if Particle-Image-Velocimetry (PIV) is a viable way to measure particle-asperity scale flow fields. We utilize a force table in our data acquisition setup that is capable of measuring integral (i.e. wafer scale) forces and moments on 3 axes. We also add a second exploratory investigation to use MEMS-based sensors to measure small scale asperity and fluid shear stresses. The overall goal of these efforts are to correlate changes in friction and MMR that accrue from process parameter changes to small scale physical mechanisms.

Method of Approach:

The principle experimental platform used in this work is a modified Struers RotoPol-31 table top polisher in which the wafer carrier has been replaced by a motor-driven shaft supported by an aluminum frame, which is coupled to an optical glass wafer. The polisher sits atop a 3-axis force table, which measures the friction force and moments between the wafer and the platen. The force table is on top of a steel table, which dampens external vibrations. The force table has a resolution of 0.006N/bit on the x and y axis, and 0.097 N/bit on the z-axis. The sample rate is 2 kHz. This facility is used for both

the DELIF-based contact and wafer-scale friction work. The MEMS shear sensor and PIV feasibility efforts are being pursued in ancillary facilities.

DELIF-based Contact Measurements – Dual Emission Laser Induced Fluorescence (DELIF) is an imaging technique that has been used to attain three dimensional maps of thin fluid films. Previous investigations of pad-wafer interactions using DELIF include in-situ measurements of average fluid layer thickness and asperity layer compressibility, surface roughness measurements and polishing pad rebound into etched wells. It is becoming increasingly clear that understanding the small scale polishing mechanisms operating during CMP requires knowledge of the nature of the pad-wafer contact. One goal for this research is to use DELIF to attain instantaneous measurement of in-situ pad-wafer contact.

Wafer-Scale Friction Measurements – During the past year, we have adjusted our general experimental process parameters and processes to be more closely aligned with industrial practices. The most significant changes are:

1. Wafer rotation rates of 60 - 120 rpm, which translate to approximately 0.5 – 1 m/s.
2. Polishing down forces equivalent to pressures of 1.7 PSI (11.7 kPa) and above.
3. Standard baseline slurry dilutions of 3 parts DI water to 2 parts slurry.
4. Exclusive use of grooved polishing pads.

In addition, refinements to our setup and procedures have allowed us to generate more consistent and reproducible data.

MEMS Shear Stress Measurements – A new exploratory effort was initiated this year to determine the feasibility of developing MEMS based shear stress sensors as in-situ measurement devices in the table top polishing facility. The goals of this sensor work is to measure shear stresses typical of both pad-wafer, i.e. asperity force, contact and fluid (slurry) shear forces. Both PDMS and floating sensor options are to be in this effort. Sensor fabrication will initially utilize facilities available at MIT with the ultimate goal of fabricating the sensors in the new microfabrication facilities at Tufts University.

PIV Feasibility – An optical system different than that used in DELIF is needed to carry out the PIV feasibility study. In PIV, it is imperative to eliminate any overlap with the wavelengths produced by the pad's emission, rather than utilize it as is done in DELIF.

Highlights of Results and Accomplishments:

DELIF-based Contact Measurements: Much of the past year has been spent re-examining DELIF and optimizing the optical setup such that we make accurate fluid layer thickness measurements as well as attain pad-wafer contact measurements. We have increased the magnification 1.6X from last year and we now have a resolution of 2.6 μm/pixel. In addition, we have added a 5-axis positioner, depicted in Fig. 1, for the dichroic beam splitter that splits the incoming light into two signals going to each camera. This 5-axis positioner provides a hardware alignment of the two images, which is advantageous over software alignment of the two images with a loss of resolution and imaging area. Both filters and the dichroic beam splitter have been replaced by higher efficiency band pass filters and splitter from Chroma Technology Corp. The filter and beam splitter replacements have improved fluorophore signal isolation.

Figure 1. The 5-axis beam splitter positioner provides hardware alignment.

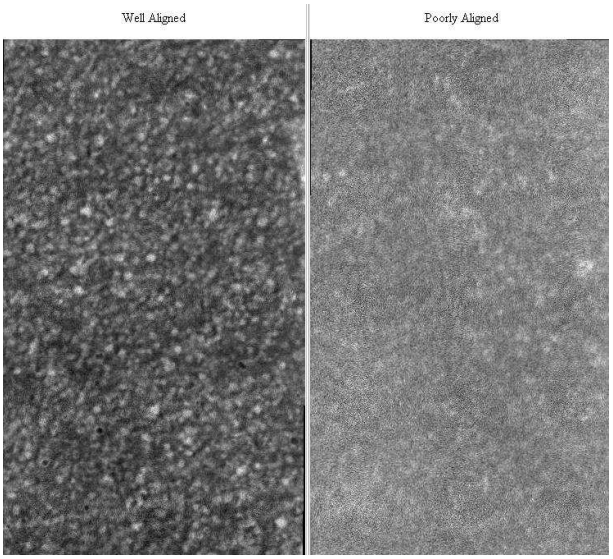

Figure 2. A well-aligned DELIF image (left) compare to a poorly aligned image (right) of a Freudenberg FX9 polishing pad.

We have started to compare DELIF to other visualization methods. Figure 2 shows that when the optics are well aligned DELIF has excellent resolution, but if the optics are slightly misaligned, we lose resolution. Figure 3 shows an SEM and an optical microscope image of the same type of polishing pad (Freudenberg FX9), which was imaged in Fig. 2 using DELIF. The well-aligned DELIF image shows similar features to the SEM image and seems to resolve the pad features better than optical microscopy. SEM and optical microscopy can only give us a qualitative feel for how well DELIF is resolving pad features because these methods can not resolve depth. In an attempt to resolve depth into the pad, we also compared our DELIF images to fluorescent confocal microscopy as shown in Fig. 4. The confocal microscope image compares well to the highly resolved DELIF image. However, there is still some difficult resolving depth with the confocal microscope. If the pad sample being imaged is not entirely level, the image

data will show a slope from one side of the image to the other. For instance, the right side of Fig. 4 is brighter and in better focus than the left side, suggesting that the confocal imaging planes were not parallel to the pad sample.

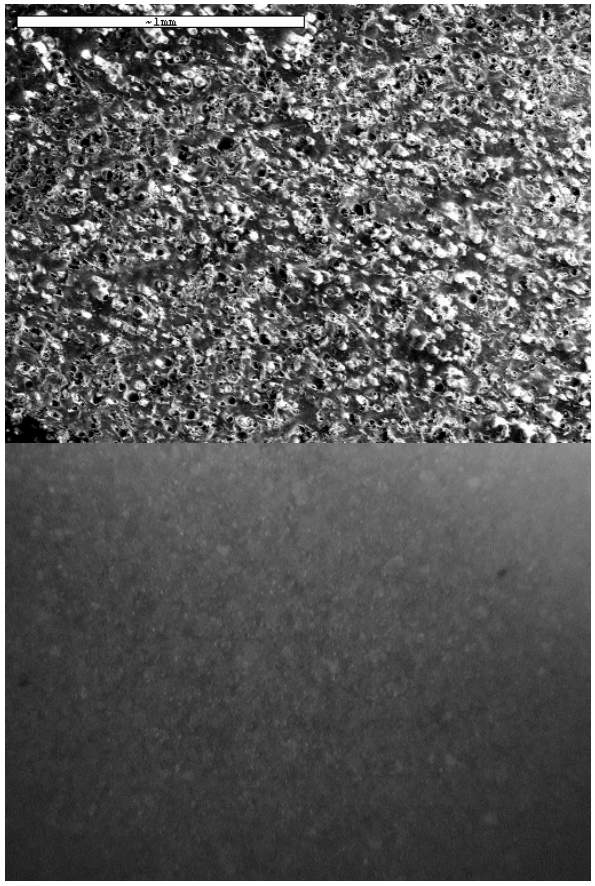

Figure 3: An SEM image (left) and an optical microscope image (right) of a Fruedenburg FX9 polishing pad at resolution similar to DELIF.

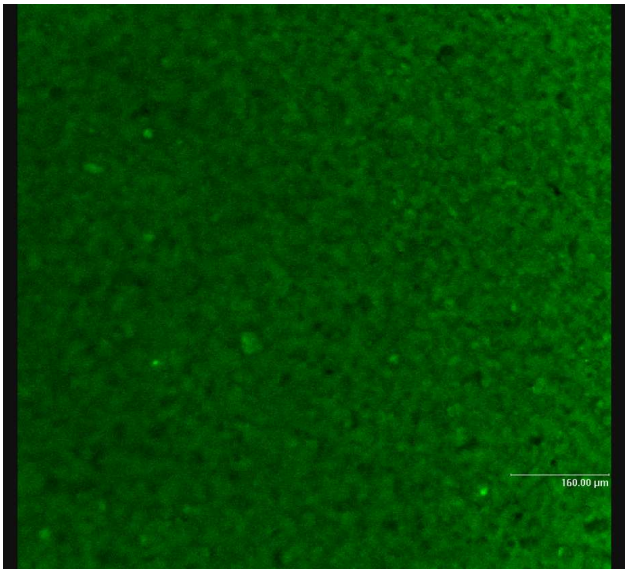

Figure 4. A confocal microscope image of a Freudenberg FX 9 polishing pad a similar resolution to a DELIF image.

Wafer-Scale Friction Measurements: During the past year we have continued our investigation of the frictional behavior of various pads and various process conditions. Results are shown in Fig. 5.

In addition, we have generated spectral data for the various experimental conditions a shown in Fig. 6. The spectral data are from direct measurements of the normal (F_z) forces. The figure on the left is typical of the spectral signatures of test conditions which yield stick-lip conditions. Note that the reduction of the high frequency content in the plot on the right (120 rpm) which exhibits smoother polishing and no apparent stick-slick phenomena.

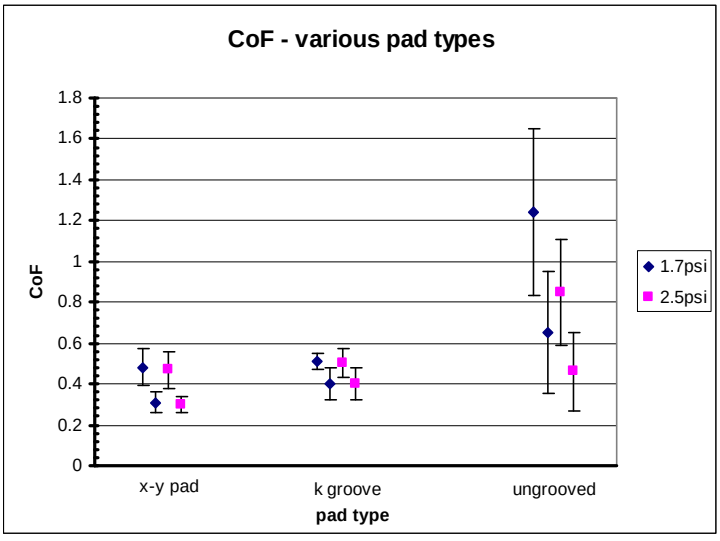

Figure 5. Coefficient of friction data for various pad types with down forces of 1.7 PSI (11.7 kPa) and 2.5 PSI (17.2 kPa).

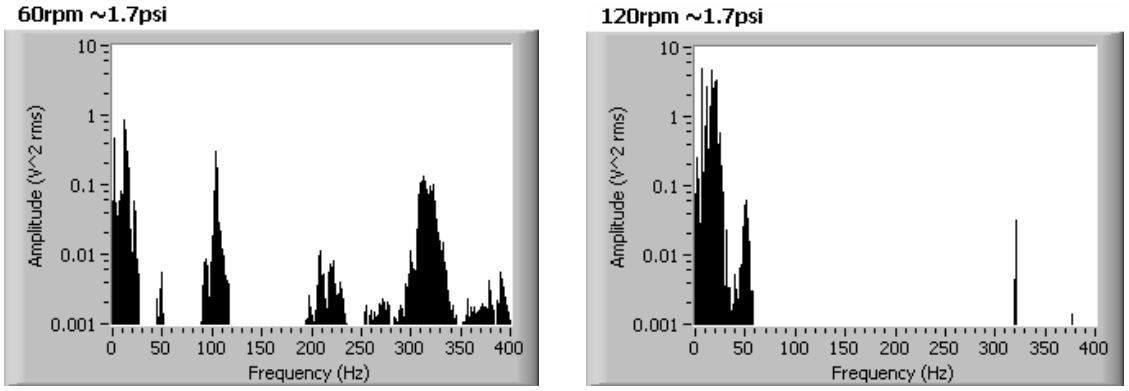

Figure 6. Measured spectra of down force data.

A number of experiments have been performed to ascertain the relationship between COF and slurry particle concentration. Figure 7 is a representative data set. Data acquired to date indicate three regimes in this data range – high COF with pure slurry, moderate and stable COF at dilutions ranging from 1:5 to 9:1 (pH controlled water : slurry), and low COF with pure water. It should be noted that chatter and apparent stick-slip conditions begin to occur in the midrange dilutions around 3:2 and continue to 9:1. The pure water case appears to be in a distinctly different regime.

MEMS Shear Stress Measurements: Preliminary design and testing of the shear sensors followed dual tracks; both post arrays, fabricated from PDMS, and floating element sensors were examined to determine which might best meet the design specs. Although both designs are possible, fabrication of the PDMS structures can proceed more rapidly. Hence we are currently focusing on the PDMS sensors only.

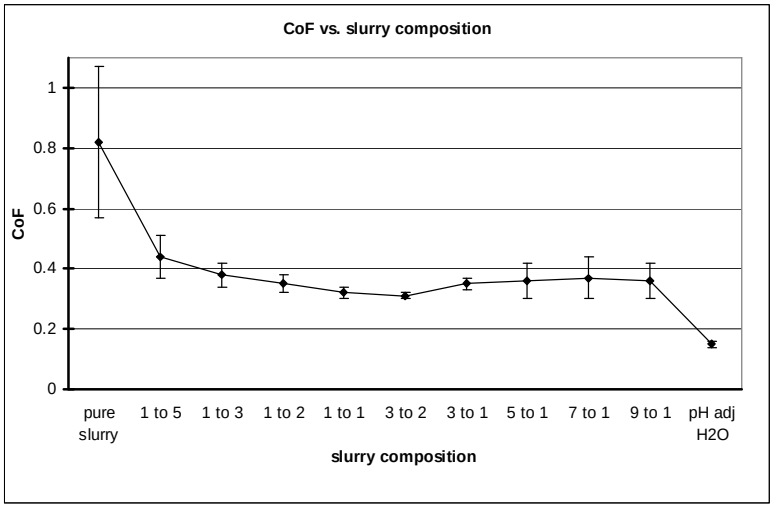

Figure 7. Coefficient of friction at different slurry dilution ratios.

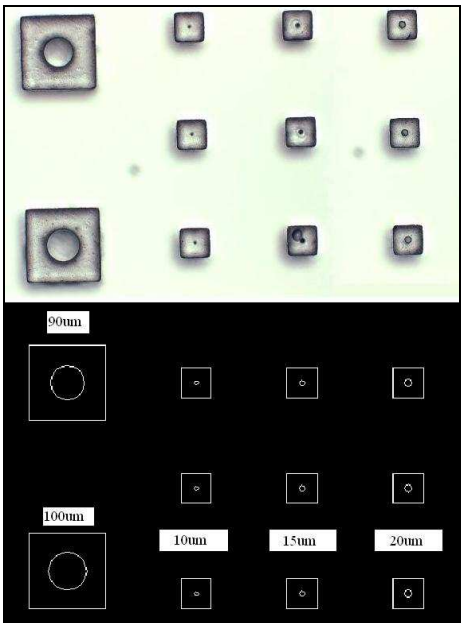

Figure 8. 83 µm thick SU-8 mold for PDMS posts. The SU-8 blocks are circular in the final design creating circular wells in the PDMS sensors.

We have completed the modeling and design of an initial PDMS post array stress sensor that will indicate stresses due to asperities and fluid flow. PDMS posts are recessed in wells (their top surfaces are co-planar with the surface of the sensor) and their deflection indicates the shear stress present at sensor/pad interface. We have successfully fabricating these sensors by using an SU-8 base mold in which to cure the PDMS sensors (see Fig. 8). Fabrication limitations on PDMS post diameters have been determined at 30µm. An image of the SU-8 mold for the initial PDMS sensor design is shown in Fig. 9. Sensor sensitivities are expected to be 0.1 - 10 µm/µN. Based on rough estimates of asperity contact forces, we expect sensor deflections between 0.5 and 500 µm due to interactions with individual asperities. Fluid forces are expected to be considerably lower than those from asperities and result in expected deflections of 0.1 to 3 µm. These small deflections may not be measurable with current optics; higher resolution optics are being pursued.

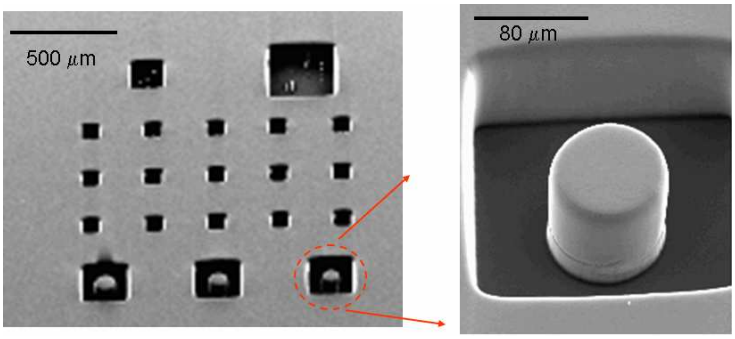

Figure 9. SEM images of successfully fabricated initial PDMS asperity and fluid shear sensors. Inset shows 80µm diameter asperity shear sensor.

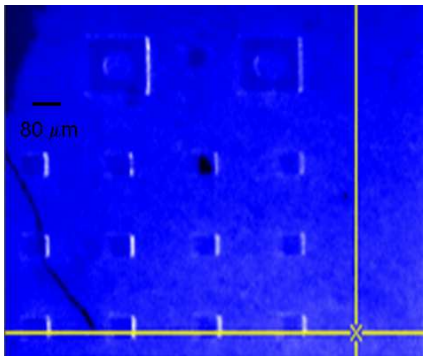

Figure 10. Image from RB dye experiment to aid in PDMS post deflection detection in. Right edges of the wells are illuminated by the dye.

To aid in deflection detection of the PDMS posts, we are experimenting with dyeing the sensors with Rhodamine B (RB) dye. Images from preliminary dye experiments are shown in Fig. 10. The right edges of the wells are illuminated relative to the rest of the wafer. The final goal is to have the edges of the wells and posts illuminate to view relative deflections between the two. Calibration of asperity sensors will be conducted first using a Veeco Dektak 6M Stylus Profilometer. Depending on the success of these calibrations, a Dimension 3100 atomic force microscope may also be used to calibrate asperity sensors. Design and fabrication of the calibration chamber to determine sensitivity to fluid flow induced stresses is ongoing.

PIV Feasibility: To track particles, FluoSpheres Fluorescent Microspheres in Nile Red by Invitrogen will be utilized. The FluoSpheres are comprised of fluorescence dye encased within a polystyrene shell. Excitation of the FluoSpheres, which is shown in Fig. 11 by the dotted green line, will be initiated using Lumex LED lightbulb arrays in Ultra Pure Green, shown in the checkered green area. Very little of the FluoSpheres will be excited by the pad emission. The emission of the FluoSpheres occurs at a higher wavelength than the other components of the system and can be easily separated from the other phenomena and their wavelengths.

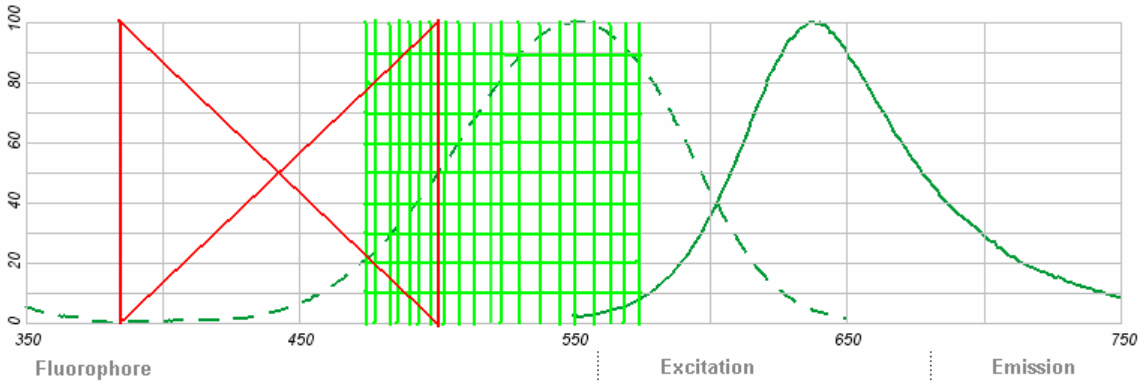

Figure 11: The dye emission compared to LED light and pad emission.

With careful selection of a filter, most of the excitation source signal and noise from the pad can be eliminated. Figure 12 shows the bandpass filter in purple. It is centered at 650 nm and has a +/- 40 nm range. By placing the filter directly in front of the camera, only the wavelengths between 610 and 690 nm will be captured.

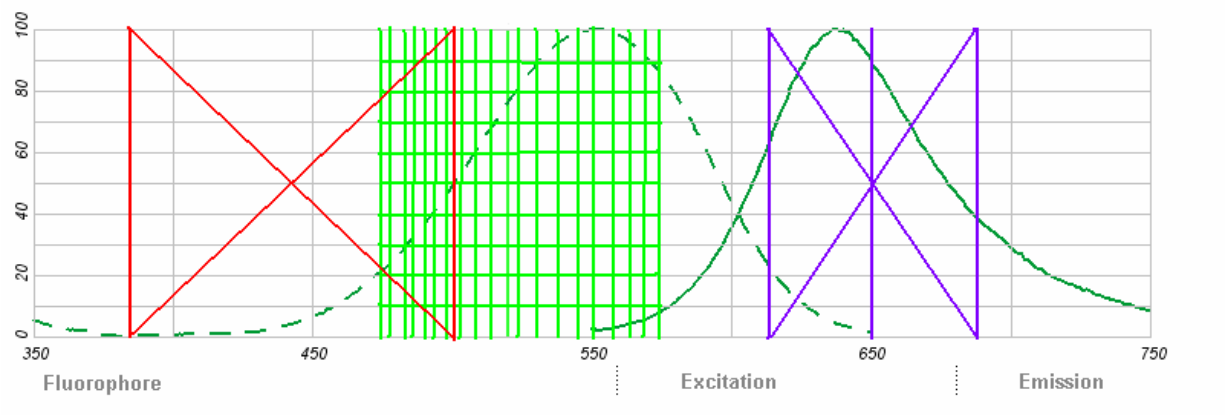

Figure 12: Filter detection of the system.

LED lights are to be used more in PIV as they have several advantages over UV and laser illumination sources. Compared to both sources, LED's are extremely cheap and easy to use. LEDs can be purchased for thousands of dollars cheaper than UV or laser illumination sources and will last for more than 100,000 hours. In addition, LED lights do not produce any heat and eliminate the problem of pad burning caused by laser and UV. Furthermore, there are no associated handling or safety concerns.

Next-Year Plan:

- Re-qualify the DELIF system and take pad-wafer contact measurements on the following polishing pads: Fruedenburg FX9, CMC D100, CMC D200, and IC1000.
- Optimize DELIF contact measurements by assessing the efficacy of three different slurries with different particle loadings.
- Develop a laser based sensor to measure wafer vertical position and angle of attack in situ and attempt to correlate these data with stick-slip phenomena.
- Develop a method for measuring material removal rate (MMR) utilizing the equipment available here at Tufts University.
- Use CoF and MRR data to develop a working model of CMP that connects small scale mechanical and chemical phenomena to wafer scale measurements.
- Demonstrate first in-situ applications of MEMS sensors.
- Continue feasibility study of floating element shear stress sensors.
- Acquire equipment and conduct PIV proof of concept experiments.

Surface Characterization and Flow Resistance Estimation of CMP Pads

Personnel:

PIs:

- Ara Philipossian: Chemical and Environmental Engineering (UA)

Other Research Personnel:

- Len Borucki: (Araca Incorporated)
- Yun Zhuang: Chemical and Environmental Engineering (UA)

Graduate Students:

- Ting Sun: Chemical and Environmental Engineering (UA)

Objectives:

The objective is to investigate the fluid carrying capacity of CMP pads by quantifying their surface topography through both contact and non-contact methods. By better understanding how pad surface asperities resist or assist slurry flow during CMP, pads with engineered surfaces can be produced to yield lower slurry flow rate processes.

Background and Method of Approach:

Both contact and non-contact methods were used to analyze surface properties of Rohm and Haas IC1000 and psiloQuest Cu 4870 pads. A custom-made incremental and cyclic loading device (ILD) was used to measure the gap between a reference plane in contact with the pad sample surface and a stationary capacitance probe under different loads.

The ILD uses a contact method to measure the mechanical response of pad surfaces to periodic loading and unloading (i.e. cycles that are similar to the loading cycle of a fixed area of the pad surface as it passes under the wafer during CMP). The method is based on the fact that the bulk modulus of a hard pad (i.e. < 500 MPa) is much larger than the apparent modulus of its surface (i.e. 1 to 20 MPa). This difference is due to the fact that CMP pads have rough surfaces in the order of tens of microns consisting of asperities which compress easily under the loads typically used in CMP. In our studies, an annular pad sample with fixed area of one square inch is used for convenience. The sample is mounted on a flat, polished cylinder and a metal-coated optical flat is placed on the top surface. A capacitance probe is positioned through the hole in the sample until the surface of the flat can be detected. When a load is applied, the capacitance probe measures the change of the gap between the flat and the tip of the probe. Under the conditions described above, nearly all of the measured displacement can be attributed to pad asperity deformation. Before starting the test, a light preload (~ 0.25 lb) with a centering ball is placed on the optical flat. This is to flatten the sample, which usually is slightly distorted after being cut from the pad, and to deform any edge burrs that might be present. After the system has stabilized, a series of triggers are used to drop weights onto the sample at fixed time intervals. Each weight is 1 lb, so individual weights increment the pressure on the surface by 1 PSI. To avoid large oscillations, the weights are dropped only a few tens of microns. The drop distance can be adjusted using a micrometer at the

top of the load stack. During the experiment, the deformation of the surface is continuously recorded as a function of time.

Separate from ILD tests, optical interferometry is used to probe the pad surface without contact and produce a visible surface height probability density function (PDF). This information is used to not only validate the data obtained from the ILD, but to also estimate the load carrying capacity in the land area of the pad samples.

Highlights of Results and Accomplishments:

In incremental loading analysis, when loads are applied to, or released from, the pad sample surface, the gap changes and a load-displacement relationship can be measured that shows evidence of pad surface elastic/plastic deformation as well as rebound and creep. The elastic/plastic data display nonlinear features characteristic of a rough surface response rather than a bulk response. Pad surface height PDFs obtained from interferometry have exponential tails on the side that contacts the wafer. This tail can be characterized by a decay length λ (defined as the distance over which the tail drops by a factor of 1/e). Based on the Greenwood –Williamson rough surface contact model, the load-displacement relationship is also exponential if contact remains within the exponential tail of the pad surface height histogram. For both Rohm and Haas IC1000 and psiloQuest Cu 4870 pads, the decay length λ is extracted from the log plot of the pressure ratio vs. the change in displacement obtained through incremental loading measurements. The decay length λ is also extracted independently from non-contact interferometry data (Table I). Results show that values of λ are consistent for both pads using these two methods.

Table I. Results from Incremental Loading Device and Interferometry

Pad Type		Decay Length λ, ILD (μm)	Decay Length λ, Interferometry (μm)	Pad Surface Standard Deviation σ (μm)
PsiloQuest Cu 4870	1	7.0	6.9	29.2
	2		6.0	28.8
Rohm and Haas IC1000	1	5.4	4.9	7.9
	2		5.0	6.9

Slurry flow under the wafer in the land areas can be modeled with the Reynolds equation with roughness correction. Pressure flow factors and shear flow factors were then calculated from PDF data using the method of homogenization to estimate the flow resistance and fluid carrying capacity for both Rohm and Haas IC1000 and psiloQuest Cu 4870 pads as a function of wafer loading.

Pad surface topography can present an obstacle to fluid flow when pressure differences exist in the fluid. Resistance to pressure-driven flow can be quantified by pressure flow factor which has a value is 1 when the surface is perfectly smooth and drops to zero when no flow occurs. The pressure flow factor depends on the location of the wafer, which varies with loading. The flow factor generally decreases as the load increases. It should be noted that pressure-driven flow is not important for grooved pads,

since there is very little fluid pressure development during CMP when grooved pads are used.

Valleys in the pad surface topography carry fluid directly. The effect of valleys on fluid transport can be quantified by the shear flow factor. Shear flow factors are estimated for both psiloQuest Cu 4870 and IC1000 pads, and are plotted against H (location of the reference plane divided by the pad surface height standard deviation), as shown in Fig. 1. Each interferometry image yields two estimates of the flow factors. Flow factor curves from all images are averaged. The value is 0 for a smooth surface and increases as valleys become deeper. The shear flow factor curve associated with the psiloQuest Cu 4870 pad increases with H up to a certain point then decreases with H. This implies that direct transport of fluid by valleys in the land areas of the pad is enhanced up to a point as the surface is compressed. For IC1000 pad, the same trend shows in shear flow factor curve, except that the enhancement of fluid transport by valleys is not as large as psiloQuest Cu 4870 pad.

Combined with ILD data, H can be related to specific applied processing pressures, as shown in Fig. 1 with dotted vertical lines. It can be seen that the psiloQuest Cu 4870 pad has higher shear flow factor than IC1000 pad at a certain applied load. The total fluid flux is proportional to the product of the shear flow factor and the surface height standard deviation (see Table I). Therefore the psiloQuest Cu 4870 pad has about 5 times more capacity to transport fluid in topographical valleys relative to the Rohm and Haas IC1000 pad. This suggests that much lower slurry flow rates might be possible with psiloQuest Cu 4870 pad.

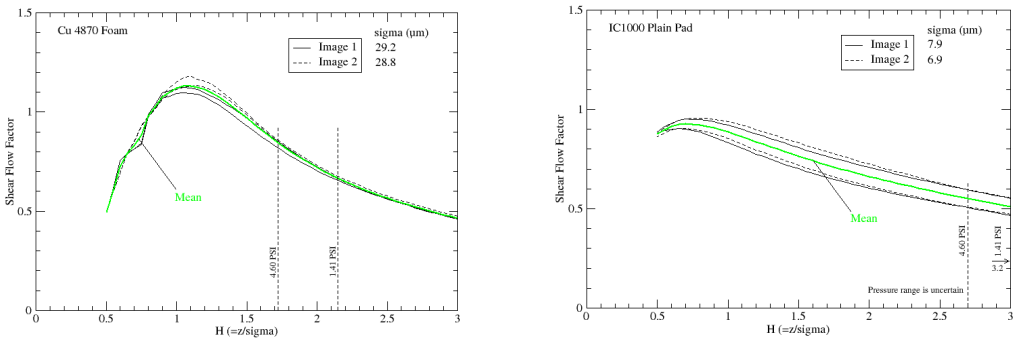

Figure 1. (a) Shear Flow Factor of psiloQuest Cu 4870 Pad; (b) Shear Flow Factor of IC1000 Pad

Industrial Interactions and Technology Transfer:

- Dan Marks (psiloQuest)
- Tony Clark (psiloQuest)
- Jam Sorooshian, Darren DeNardis and Don Hooper (Intel)

ESH Impact:

- A method was developed to study fluid flow features on the land areas of pad surfaces. This method can be used to assess and novel designs of pad

materials and surface texture, which would reduce slurry usage. As a result, the waste volume produced by CMP process would be reduced.

Conference Presentations:

- 'Surface Characterization and Flow Resistance Estimates for CMP Pads' T. Sun, L. Borucki, Y. Zhuang, D. Marks, T. Clark and A. Philipossian. 210th Meeting of the Electrochemical Society, Cancun, Mexico, October 29 - November 3 (2006).

Next-Year Plan:

- Determine whether ILD can be used with moist pad samples. Study of moist pad samples is more realistic, and not possible with interferometry. Quantify and explain differences between moist and dry pad samples.
- Modify the ILD to allow samples to be analyzed at different temperatures.
- Investigate the effect of temperature on pad surface topography.

Mechanistic Study and Modeling of Novel Orbital Motion Polisher for Copper CMP Process

Personnel:
PI:

- Ara Philipossian: Chemical and Environmental Engineering (UA)

Other Research Personnel:

- Leonard Borucki: (Araca Incorporated)
- Yun Zhuang: Chemical and Environmental Engineering (UA)

Graduate Student:

- Hyosang Lee: Chemical and Environmental Engineering (UA)

Objectives:

The objectives of this task are to (1) characterize the by-product build up on the pad surface and investigate how process parameters affect by-product build up and polishing performance for orbital polishers for copper CMP, and (2) perform numerical simulations to simulate copper removal with the incorporation of local pad staining.

Background:

Orbital polishers have a 'through-the-pad' slurry distribution and injection system. This approach can greatly reduce slurry use and enhance slurry utilization efficiency during polishing since all of the slurry is injected under the wafer. While orbital polishers have a potential benefit of 3-5X reduction in slurry consumption compared with conventional rotary tools, various effects can reduce or offset this benefit in specific CMP processes. For example, non-uniform slurry distribution, wear ring - pad interaction and sub-optimal pad grooving can lead to by-product build up on the pad surface and cause low, non-uniform and unstable polish rates during the process. These concerns may be addressed through fundamental mechanistic studies to understand slurry transport, slurry chemistry, and the tribological, thermal and kinetic characteristics of the polishing process.

Method of Approach:

A polishing tool was constructed using a scaled polisher modified to allow injection through the center via a peristaltic pump with flow rate buffering. A 5-mm hole was drilled through the platen center and the pad for slurry delivery. All polishing was done with a stationary pad and a rotating polishing head aligned co-centrically with the pad. 100-mm blanket copper wafers were polished on IC1000 XY-groove pads. Copper wafers were mounted on a 4-inch optical flat, which in turn was attached to a gimbaling polishing head. Conditioning was performed *ex situ* using a 3M A165 4-inch disc co-rotating with the pad and having a 2-cm axial offset. Polishing was performed for various time, pressures, rotational speeds and slurry injection rates. Cabot Microelectronics Corporation iCue 5001 slurry was used. Injection rates were consistent with commercial practice on orbital polishers. Removal rates were determined using a 4-point probe. Stain

intensities were quantified by photographing the pad with a high resolution digital camera and converting the images to grey scale.

Highlights of Results and Accomplishments:

Figure 1 indicates that staining on XY-groove pads was found to increase with applied pressure, wafer rotation rate, time, and slurry injection rate. Removal rates were found to increase approximately linearly with distance from the injection point at the flow rate of 50 ml/min in Fig. 2, consistent with a mechanically-limited, Prestonian mechanism. However, at a lower flow rate of 25 ml/min and high rotation rate (Fig. 2, upper right), the rate was found to level out and tool vibration occurred, suggesting onset of a chemical limitation or incomplete lubrication.

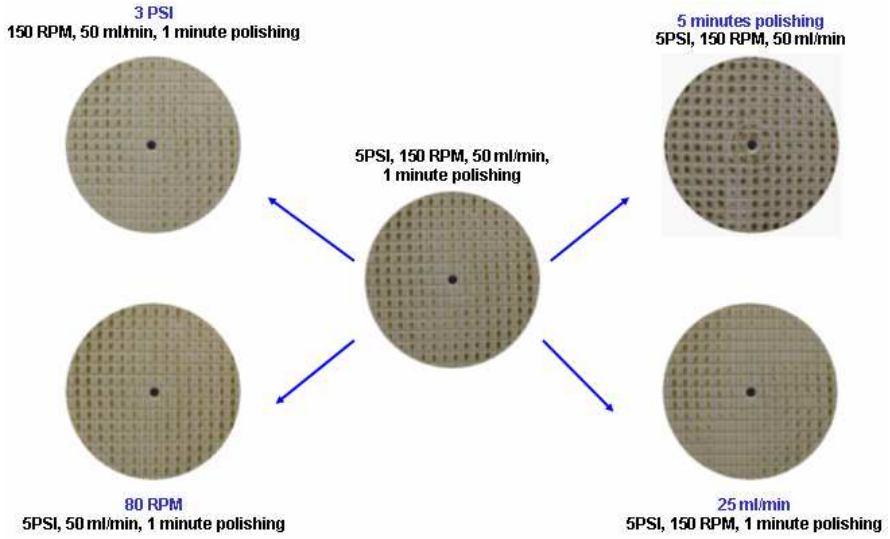

Figure 1. Effect of pressure, velocity, time and flow rate on pad staining.

A key question was whether the stain itself affected the rate in a feedback mechanism. An experiment was performed in which the pad was cleaned and conditioned, and then wafers were polished in succession without further dressing under two conditions differing only by pad staining (Fig. 3). In one condition, the pad was cleaned with oxalic acid between wafers. In the other, the pad was cleaned and restored but there was no further treatment between wafers. In both cases, the mean rate was found to decrease with each successive wafer polished (Fig. 4). The decay in removal rate was approximately the same in both cases in spite of large differences in pad staining. An observed difference in rates between the first wafers was probably due to variation of the initial surface topography. These results suggest that if stains from the slurry affect rate at all, then the effect is smaller than experimental error. A visually observed increase in glossiness of the pad surfaces with time (sometimes interpreted as glazing) suggested that the observed rate decay was caused by plastic flow or abrasion of contacting surface asperities. This, rather than staining, would then be the main factor affecting rate on orbital tools, which do not allow *in situ* conditioning.

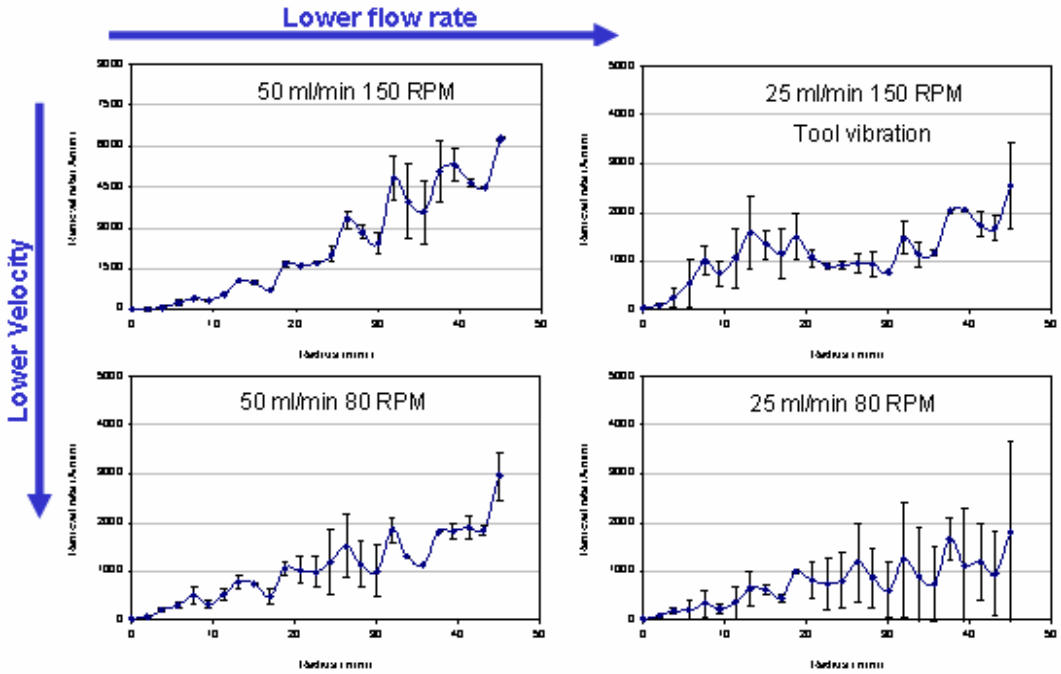

Figure 2. Removal rate vs. wafer radius under different flow rates and wafer rotational rates

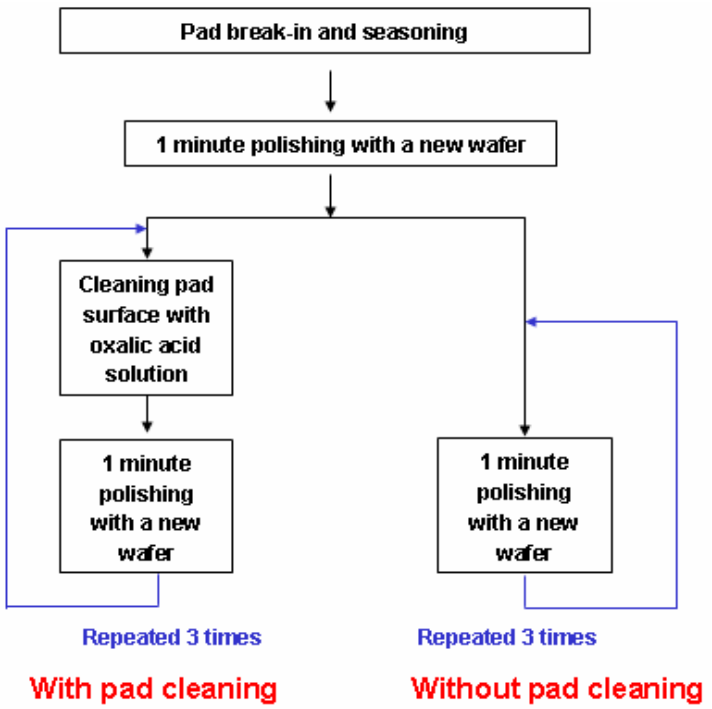

Figure 3. Experimental procedures for investigating the effect of staining on removal rate.

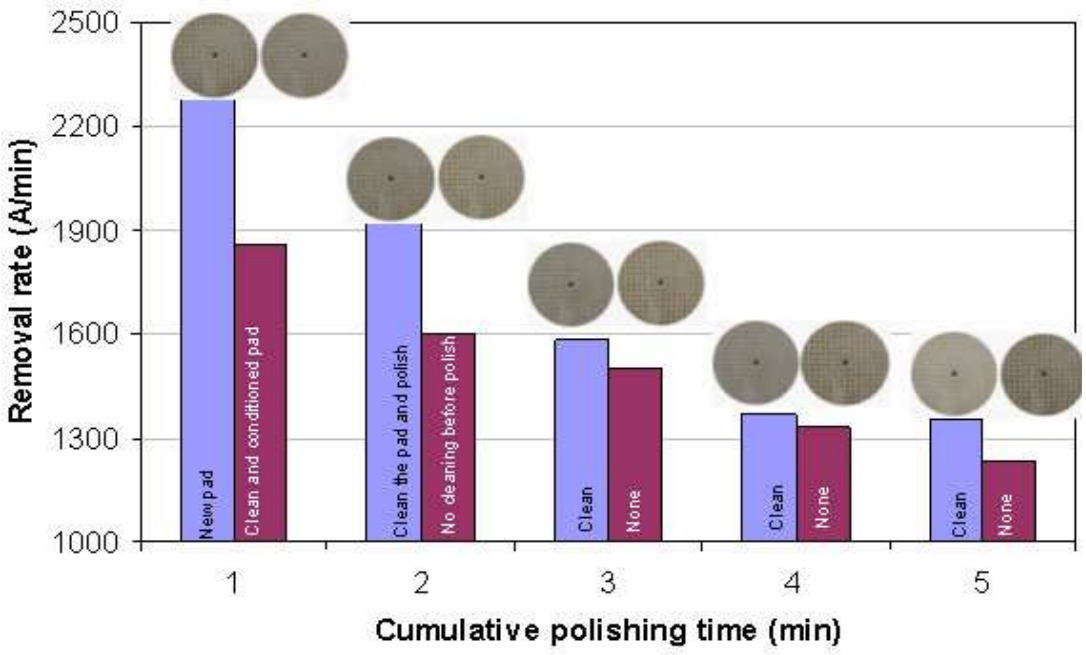

Figure 4. Effect of staining on removal rate.

A model was developed to simulate stain formation on the pad surface. The model consisted of the incompressible Navier-Stokes equations, the heat equation with advection, a material removal rate model, a model for generation, transport and deposition of the polishing byproduct that produces the stain, and load and moment balance. The Navier-Stokes equations for the slurry flow were solved only in the grooves and on the land areas. COMSOL software was used to solve the Navier-Stokes equations in order to find slurry flow in XY-groove pad. The simulated result was shown in Fig. 5. The simulated result indicated that there were shear flow on the land areas and wafer-driven circulation in the grooves.

The heat equation is being solved in the slurry using the velocity field from the Navier-Stokes equations in the advection term. The heat equation is solved in the surrounding solid materials (e.g., pad, sub-pad, wafer) using the appropriate rigid body velocities in the advective terms. The source flux for the heat equation applies only on the land areas and has the form

$$Q = \mu_k p_s V \tag{1}$$

where μ_k is the coefficient of friction, p_s is the local solid contact pressure and V is the sliding velocity. The heat equation is also solved on COMSOL software.

The above considerations apply to any CMP system. In the present case, experiments suggest that mechanical removal is necessary for staining to occur. For systems in which copper polishing can be described with a three-step chemical-mechanical model with static etching via surface complexing, the flux of mechanically removed surface oxide from the wafer surface into the slurry is

$$D_{ox}\nabla c_{ox}\cdot\vec{n}=\frac{k_1k_2}{k_1+k_2+k_3} \tag{2}$$

where c_{ox} is the concentration of stain-producing by-product in the slurry, D_{ox} is the diffusivity, $\vec{n}$ is a unit normal vector to the wafer surface, and k_1, k_2, k_3 are the rate constants for the copper surface oxidation rate, the mechanical removal rate of the oxide, and the rate of surface oxide removal by complexing, respectively. The oxidation and complexing rates depend on the reaction temperature, which comes in part from the heat equation. In general, an additional contribution due to asperity flash heating may also be necessary. Equation (2) is a boundary condition for advective transport of the staining agent in the slurry,

$$\frac{\partial c_{ox}}{\partial t}+\vec{V}_f c_{ox}=\nabla\cdot(D_{ox}\nabla c_{ox})\,. \tag{3}$$

where $\vec{V}_f$ is the slurry velocity field from the Navier-Stokes equations. The staining agent, in accordance with experiments showing that a stain can be deposited from slurry pad transferred from a working pad to a test pad, is assumed to be deposited on the pad according to a first order reaction with rate constant k_s,,

$$-D_{ox}\nabla c_{ox}\cdot\vec{n}=k_s c_{ox}\,. \tag{4}$$

The total accumulation of staining agent on the pad is the integral of the flux with time. Note that color saturation should occur as the thickness of the stained layer increases.

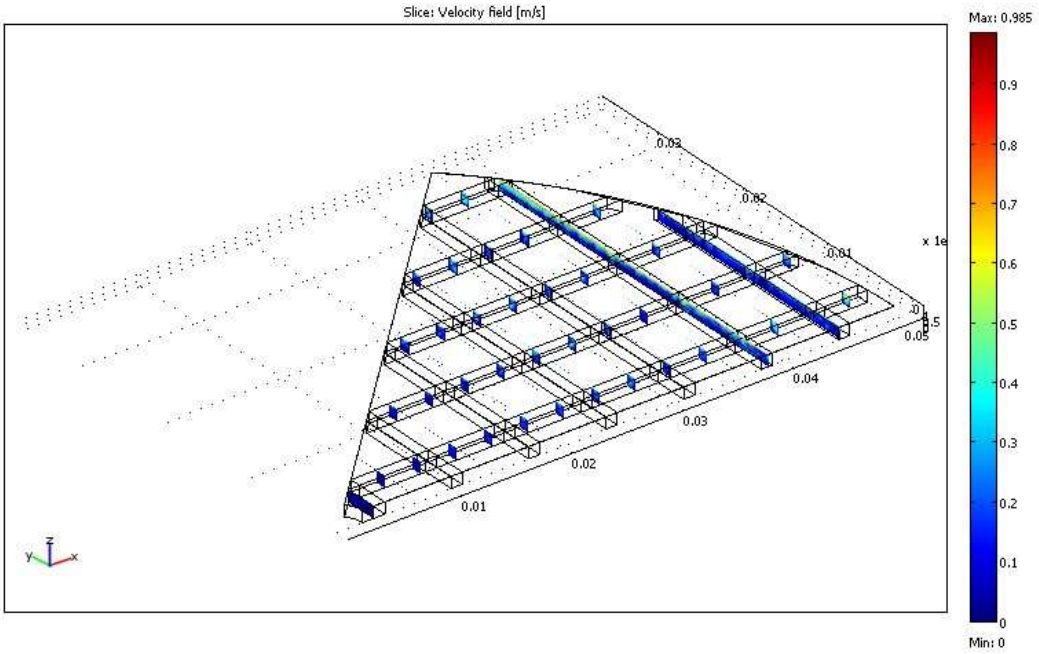

Figure 5. Simulated slurry flow in XY-groove pad.

Industrial Interactions and Technology Transfer:

- Fergal O'Moore: Novellus Systems, Inc.
- Sooyun Joh: Novellus Systems, Inc.

Conference Presentations:

- Yun Zhuang, Hyosang Lee, Len Borucki, Fergal O'Moore, Steve Schultz, Sooyou Joh, and Ara Philipossian, "Investigation of Pad Stain and Its Effect on Copper Removal Rate", *11th International Symposium on Chemical-Mechanical Planarization*, Lake Placid, NY, August 13 – 16, 2006.
- Hyosang Lee, Len Borucki, Yun Zhuang, Fergal O'Moore, Steve Schultz, Sooyou Joh, and Ara Philipossian, "Investigation of Pad Stain and Its Effect on Copper Removal Rate", *2006 International Conference on Planarization/CMP Technology*, Foster City, CA, October 12 – 13, 2006.

Process Optimization and Modeling of Copper and Tantalum Chemical Mechanical Planarization

Personnel:
PI:

- Ara Philipossian: Chemical and Environmental Engineering (UA)

Other Researcher:

- Leonard Borucki: (Araca Incorporated)

Graduate Student:

- Daniel Rosales-Yeomans: Chemical and Environmental Engineering (UA)
- Darren DeNardis: Chemical and Environmental Engineering (UA)

Objectives:

The objective is to analyze the effect of novel groove patterns on the kinetic, thermal and tribological attributes of copper CMP in an effort to reduce slurry and pad consumption.

Background:

Differences in pad grooves can affect the chemical processes in copper CMP by modulating the: (a) net flow under the wafer, (b) process temperature, and (c) reactants and polish debris concentrations. Furthermore, changes in the mechanical abrasion of the passive film may occur due to differences in pad grooving which can in turn affect: (a) slurry film thickness under the wafer, (b) shear force, (c) pad compressibility and (d) pad-wafer contact area. The effective transport of slurry in and out of the pad-wafer interface becomes critical particularly for process in which by-products are detrimental to polishing rates. In this study, novel groove patterns (i.e. a combination of logarithmic and spiral, as well as slanted concentric grooves) were evaluated to effectively control the introduction of fresh slurry into, and the discharge of spent slurry and debris, out of the pad-wafer interface. In addition, a novel 3-step model was implemented to analyze the experimental data and evaluated the effects of these groove designs on the chemical and mechanical mechanisms of the process.

Method of Approach:

Polishing was performed on polyurethane pads divided into two different groups of groove design. Group 1 included combinations of logarithmic and spiral grooves in different directions (positive and negative). Positive grooves were intended to retain the slurry while negative grooves were meant to aid in slurry and by-product discharge. The pads evaluated in Group 1 were: Logarithmic Negative Spiral Negative (LNSN), Logarithmic Positive Spiral Positive (LPSP), Logarithmic Negative Spiral Positive (LNSP), Logarithmic Positive Spiral Negative (LPSN) and concentric grooves (Fig. 1 *left*). Group 2 consisted of pads with concentric grooves slanted at different degrees (zero, 20 and 30 degrees) and directions (positive if leaning towards the edge of the pad, and negative if leaning towards the center of the pad). The pads tested in Group 2 were: Minus 30°, Minus 20°, Zero degrees, Plus 20° and Plus 30° (Fig. 1 *right*). Copper wafers

were polished at applied wafer pressures of 1.0, 1.5, 2.0, 2.5 and 3.0 PSI and sliding velocities of 0.3, 0.75 and 1.20 m/s. Real-time shear force (COF) data were taken simultaneously along with the real-time infrared thermal measurements.

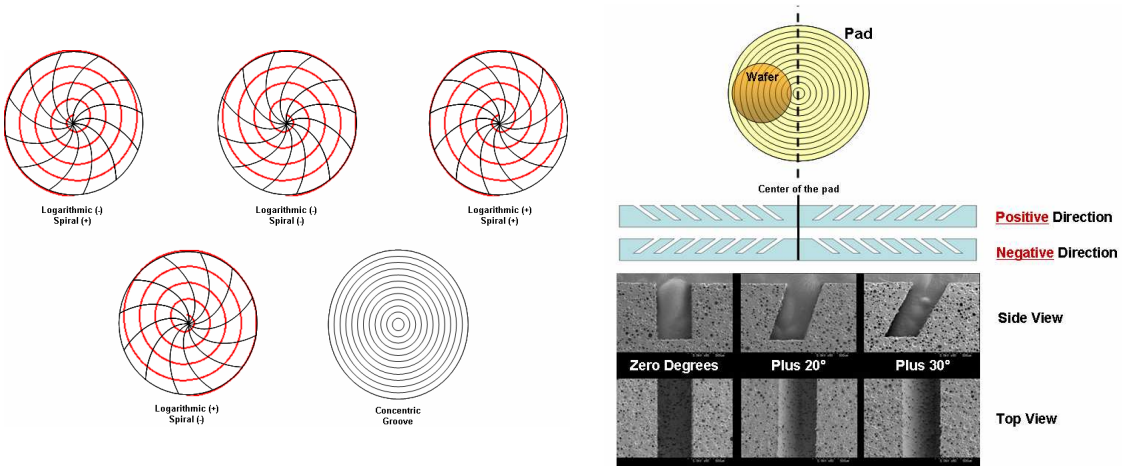

Figure 1: Pad groove patterns evaluated in groups 1(left) and 2 (right).

A novel 3-step model combined with a previously developed flash heating thermal (FH) model is proposed to theoretically evaluate removal rates for all the pads tested in this study. In 'Step-1' copper is oxidized at rate k_1 which is then removed through both mechanical abrasion (i.e. 'Step-2') at rate k_2 and dissolution by complexing agents in the slurry (i.e. 'Step-3') at rate k_3. The governing equation for the removal rate model is:

$$RR = \frac{M_w}{\rho}\frac{k_1(k_2+k_3)}{k_1+k_2+k_3} \tag{1}$$

where M_w and ρ are the molecular weight and density of copper.

The rate constant for the oxide growth is taken from a copper oxidation model based on cation migration to represent measured copper oxide growth profiles as a function of temperature. The rate constant for 'Step-1' is described as follows:

$$k_1 = \frac{\rho_{ox}}{Mw_{ox}} \cdot N\Omega f \cdot \exp\left(\frac{-W}{kT}\right) \cdot \exp\left(\frac{q \cdot a}{2kTx} \cdot E\right) \tag{2}$$

The rate constant used to characterize the dissolution of the copper oxide is extracted from a 1-dimensional model, where the diffusion of the complexant through a by-product film appearing on the wafer surface after etching controls the process. The rate constant for 'Step-3' in the removal rate model is as follows

$$k_3 = \frac{-A\exp\left(\frac{-E_a}{RT}\right)}{(x_c - X)} \quad (3)$$

All variables in Eqs. (2) and (3) are either known constants or have been experimentally determined except for x and $(x_c - X)$, which both represent the thickness of oxide in the wafer surface at a given time.

The mechanical removal rate constant is assumed to be proportional to the frictional power density,

$$k_2 = c_p \mu_k pV \quad (4)$$

where c_p is the proportionality constant with units of mol J^{-1}, μ_k is the average coefficient of friction, p is the applied pressure and V is the pad/wafer relative velocity.

The average reaction temperature at the wafer surface T, used for the rate of oxide growth and the rate of oxide dissolution, is hypothesized to be a combination of the average leading edge pad temperature and the temperature generated by asperity tip flash heating.

$$T = T_p + \Delta T_f \quad (5)$$

where T_p is the measured average leading edge pad temperature at each (p,V) condition and ΔT_f is the mean flash temperature increment. In this study, during the characterization of experimental data we control p and V, measure T_p and μ_k, and extract c_p, β' and e to minimize the RMS error between the model and the measured removal rates.

Highlights of Results and Accomplishments:

Figure 2 shows contour plots of copper removal rates corresponding to Group 1 (*upper*) and Group 2 pads (*lower*). Unlike the Preston plot, the contour plot shows the separate influences of p and V rather than presupposing a dependence of removal rate on pV. Figure 2 shows that at a given sliding velocity (i.e. 0.75 m/s) less pressure is needed in the case of LNSP than in the cases of LPSN or Concentric groove (i.e. 1.5 instead of 2.5 PSI) in order to achieve the same removal rate. Similarly, in Fig. 2 regardless of the direction of slanting, less pressure is needed with the 20° slanted groove pad compared to other slanted configurations (i.e. 2 instead of 3 PSI). The behavior observed for these novel pads is an advantage in polishing ultra low k dielectrics where lower pressures will be required to prevent delamination issues.

Figures 3 and 4 show that the 3-Step removal rate model agrees well with the experimental data. A good fit to the data also allows determination of the chemical and mechanical rate constants. Figures 5 and 6 show the ratio of k_1 to k_2 as a function of pV. In all cases, at values of pV below 5000 W/m^2, the process is more limited by film removal through mechanical abrasion, however, as pV increases, this limitation is reduced and a transition occurs to a more balanced process where the ratio of the rate

constants approaches unity and neither mechanism dominates. In addition, the model allows the establishment of an important correlation between the degree of chemical-mechanical balance and the removal rate achieved for each pad. The amount of copper removal agrees very well with the balance between the chemical and mechanical mechanisms. Figures 5 and 6 show that the faster and closer the ratio of the two constants approaches unity, the higher the removal rate achieved for that pad.

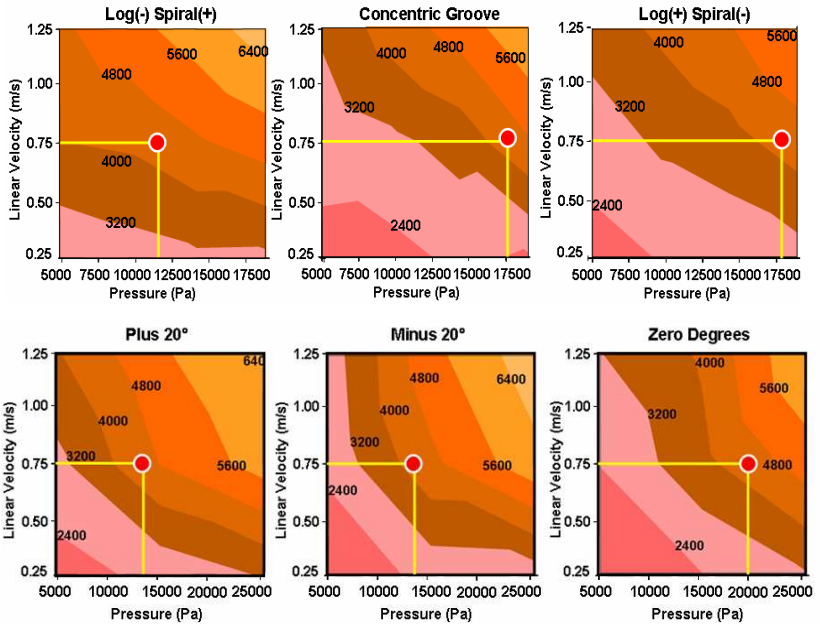

Figure 2: Contour plots of copper removal rates for logarithmic-spiral groove (upper) and slanted groove (lower) pads.

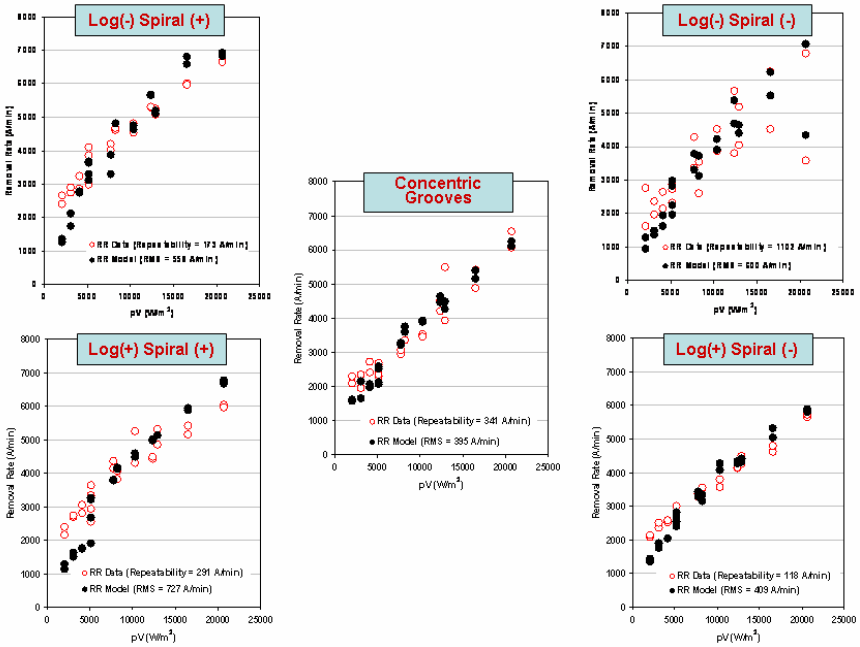

Figure 3: Experimental (open symbols) and modeled (solid symbols) removal rates as a function pV for all pads evaluated in group 1.

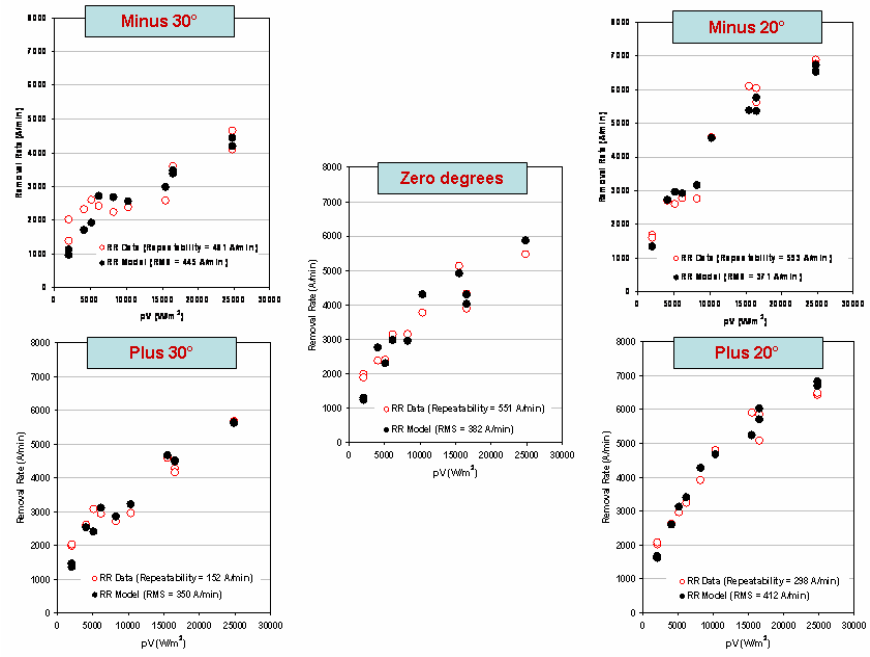

Figure 4: Experimental (open symbols) and modeled (solid symbols) removal rates as a function pV for all pads evaluated in group 2.

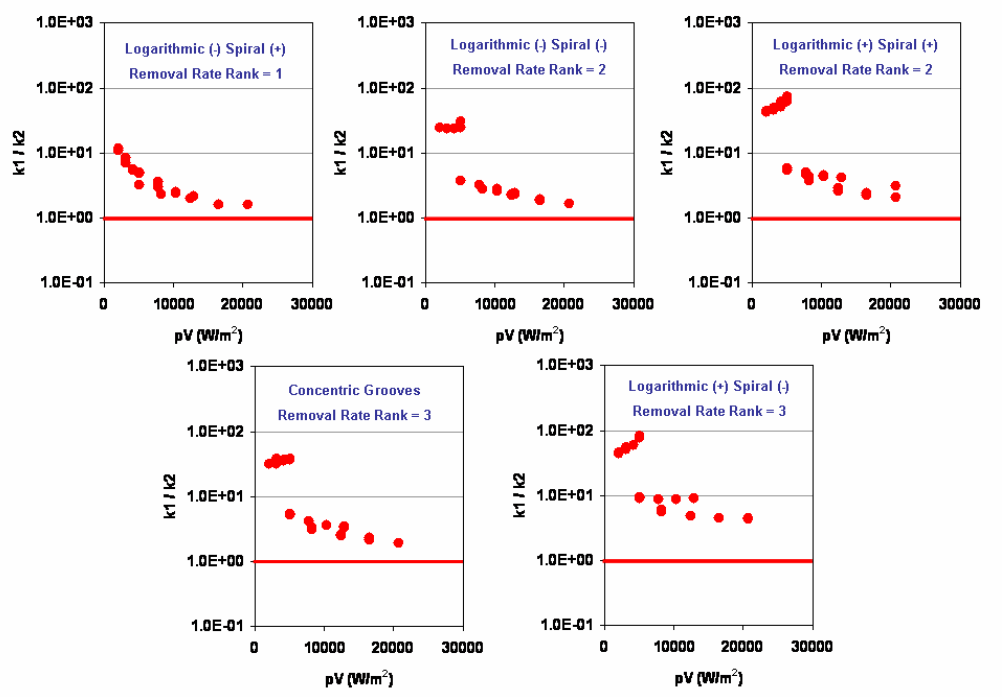

Figure 5: Ratio of k_1 to k_2 plotted as a function of pV for all pads evaluated in group 1.

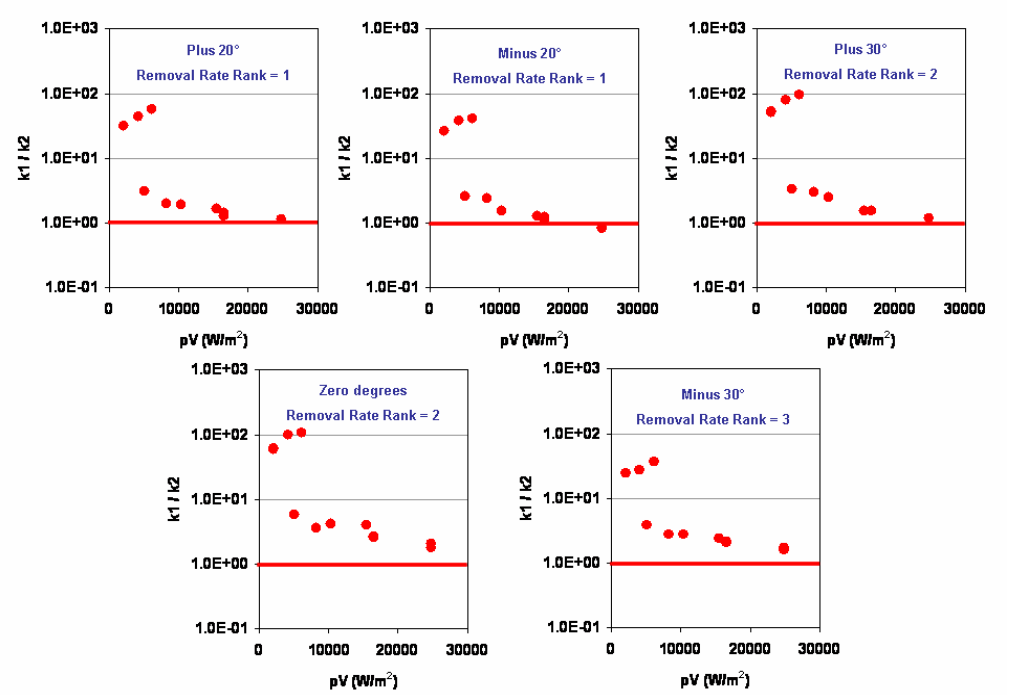

Figure 6: Ratio of k_1 to k_2 plotted as a function of pV for all pads evaluated in group 2.

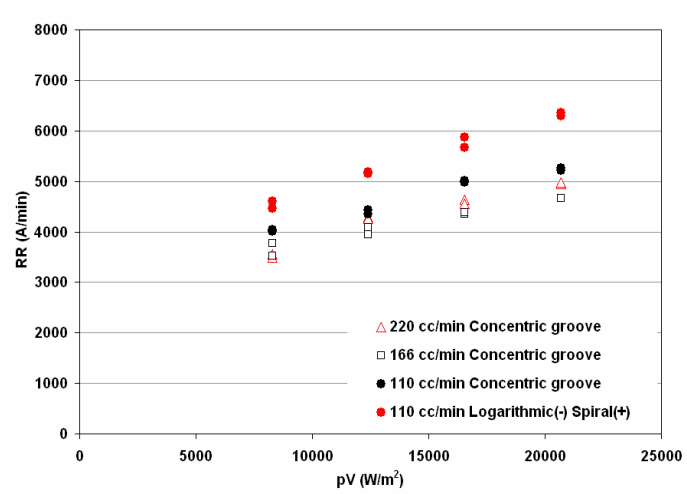

Figure 7: Removal rates as a function of pV during polishing under reduced slurry flow rate conditions for LNSP and Concentric groove pads.

Industrial Interactions and Technology Transfer:

- Tatsutoshi Suzuki: Toho Engineering

ESH Impact:

- Significant increase in pad life as evident from the nearly 50 percent reduction in required applied pressure with certain pad groove designs

- Significant reduction in slurry consumption as evident from Fig. 7 which shows copper removal at reduced slurry flow rates for the LNSP and concentric groove pads. Removal rate increases slightly as slurry flow rate decreases for the pad with concentric grooves. However, the LNSP pad results in much higher rates when slurry flow is reduced by 50 percent.

Publications:

- D. Rosales-Yeomans, D. DeNardis, L. Borucki, and A. Philipossian, "Design and Evaluation of Novel Pad Grooves for Copper CMP", *to be submitted to Thin Solid Films.*
- D. Rosales-Yeomans, D. DeNardis, L. Borucki, and A. Philipossian, "Analysis of Concentric Slanted Circular Groove Pads during Copper CMP", *to be submitted to Thin Solid Films.*

Conference Presentation:

- D. Rosales-Yeomans, D. DeNardis, L. Borucki and A. Philipossian "Design and Evaluation of Novel Pad Grooves for Copper CMP", *210th Meeting of the Electrochemical Society*, Cancun, Mexico, October 29 - November 3, 2006.

Next-Year Plan:

- Extent the learning from this study to ILD CMP on D100 pads manufactured by Cabot Microelectronics Corporation
- Complete analysis and modeling of the effect of groove design under reduced slurry flow rate conditions during copper polishing.
- Perform Dual Emission UV Enhanced Fluorescence (DEUVEF) analysis to evaluate the effect of pads with slanted groove patterns on process hydrodynamics during CMP.
- Expand the 3-step copper removal model by characterizing the dependence of copper oxide film growth on the pad/wafer rotational velocity and conditioning process during CMP.

Sematech/Texas Instruments Custom Project: Environmentally Benign Repair and Sealing of Ultra Low-k Dielectrics

Personnel:

PIs:

- Anthony J. Muscat, Chemical and Environmental Engineering, UA

Graduate Students:

- Eduardo Vhymeister, Chemical and Environmental Engineering, UA and Chemical Engineering, University of Puerto Rico, Mayaguez

Undergraduate Students:

- Lieschen Choate-Hatch, Chemical and Environmental Engineering, UA

Objectives:

This project seeks to develop the science of supercritical fluid processing to restore and cap porous low-*k* films, enabling the integration of ultra low-*k* dielectrics for the 32 nm technology node. Supercritical carbon dioxide ($scCO_2$) could replace conventional solvents used in device fabrication and reduce the environmental costs since CO_2 can be separated from byproducts and reused. Continuous pores present significant integration challenges that may not be addressed satisfactorily by conventional backend cleans based on organic solvents or inorganic acids containing water and modifiers. The goal is to control the chemistry of sealing and repair layers deposited using $scCO_2$ on porous low-*k* materials to produce a thin, robust barrier with good electrical properties. Previous work showed that plasma-damaged film repair and pore sealing were possible using millimolar concentrations of a variety of chlorosilane molecules dissolved in $scCO_2$. This study demonstrates independent control over the thickness of the sealing film and its surface properties, which is a step in achieving narrow line widths with this technology. Texas Instruments and Sematech jointly funded this project.

Background:

Copper metallization was introduced in the later half of the 1990's to reduce the resistance of metal lines, and low-*k* dielectrics are under development to reduce the capacitance. Vapor, liquid, and supercritical phase processes have been investigated to silylate the surfaces of resist materials and porous low-*k* films. A vapor treatment of hexamethyldisilazane (HMDS) followed by heating to 400°C yielded a hydrophobic surface and restored the *k* value of porous methylsilsesquioxane (p-MSQ) films from 3.14 after etching and ashing to 2.43, which was close to the 2.23 nominal dielectric constant of the starting material.[6] Mixtures of HMDS and $scCO_2$ were used to repair H_2 plasma ash damaged porous p-MSQ films. The starting contact angle of 18° was increased to 90°

[6] P. G. Clark, B. D. Schwab, J. W. Butterbaugh, H. J. Hunter, and P. J. Wolf, *Semicond. Int.* 9, 46-48, 50, 52 (2003).

in <1 min.[7] The addition of HMDS, trimethylchlorosilane (TMCS), and other chlorosilanes to $scCO_2$ reduced the dielectric constant of O_2 plasma damaged p-MSQ films from 3.5 after ashing to 2.4 ± 0.2.[8] Methyltrichlorosilane (MTCS) produced only a small decrease in dielectric constant, but polymerized forming a capping layer on the surface.

Supercritical fluids have excellent surface wetting properties, high diffusion coefficients, and solvate a variety of molecules. Moreover, supercritical carbon dioxide is nonaqueous making it compatible with metals and has no surface tension allowing it to penetrate nanometer-sized structures. CO_2 is a green house gas, but approximately 80% of the CO_2 used commercially is a by-product from other industries. Moreover, there are proven technologies to recycle and reuse CO_2. The bulk cost of CO_2 is approximately $0.50/lb.

Previous work in the Center developed an understanding of backend wafer pore capping and film repair chemistries based on supercritical carbon dioxide, as well as demonstrated proof of concept processing sequences.[9] Although commercial development of supercritical CO_2 tools and processes by the semiconductor industry was curtailed significantly in 2005 because of tactical cost analysis and performance requiremetns, understanding the fundamental science of a processing fluid that could enable the fabrication of nanoscale structures has strategic value.

Method of Approach:

Porous methylsilsesquioxane (p-MSQ) films were deposited by International Sematech and Texas Instruments using JSR LKD 5109 spun on 200 mm Si(100) wafers (p-type, 11-20 ohm-cm), cured, and ashed in an O_2 plasma. The porosity of the ashed films was 40% and the nominal film thickness was 3700 Å.[9] Wafers were cleaved into 3.0 cm^2 pieces for processing. The chlorosilane chemistries were TMCS [$(CH_3)_3SiCl$] (99%+) and MTCS [$(CH_3)SiCl_3$] (97%) purchased from Sigma-Aldrich and used without further purification. Samples were processed in a cylindrical high-pressure reactor (16 mL volume) with a quartz viewing window. CO_2 was admitted into the reactor via a tube (0.076 cm ID) on the side of the cylindrical wall at the end opposite the window. An exhaust tube, chemical injection port, and a thermocouple (Omega, KMTSS-062G-6) were located at the end with the viewing window. The chemical injection port consisted of two needle valves (HiP, 15-11AF1) mounted in series creating a volume of approximately 0.25 ml. The cell was wrapped in heating tape (Omegalux, SRT101-040) and insulated to maintain a fixed temperature of 33, 38, or 43^oC, using a PID controller (Omega, CNi3244-C24). Samples were placed in the back of the reactor, and a magnetic stirring bar was positioned in the front before sealing. The reactor was put on a magnetic

[7] B. P. Gorman, R. A. Orozco-Teran, Z. Zhang, P. D. Matz, D. W. Mueller, and R. F. Reidy, *J. Vac. Sci. Technol. B* **22,** 1210-1212 (2004).

[8] B. Xie and A. J. Muscat, *Microelec. Eng.* 76, 52-59 (2004).

[9] B. Xie, and A. J. Muscat, *Microelec. Eng.* 82, 434-440 (2005); B. Xie, *Ph.D. Dissertation, University of Arizona*, August 2005; B. Xie, L. Choate, A. J. Muscat, *Microelec. Eng.* 80, 349-352 (2005).

stirring plate and purged with CO_2 gas, followed by a supercritical CO_2 rinse at 65 bar. CO_2 (>99.99\%, Air Liquide Coleman grade) was admitted into the system using a syringe pump (ISCO, 260D) and controller (ISCO, series D). After the initial rinse, the reactor was refilled with CO_2 at 87±0.5 bar at the reaction temperature. Chemicals (10-60 microliter) were introduced using a syringe into the chemical injection port. CO_2 at 90±0.5 bar was mixed with the chemicals and used to push the mixture into the reactor through a needle valve. Reaction times were defined by the interval between opening the needle valve and purging the reactor. Samples were rinsed with $scCO_2$ at 75 bar at the reaction temperature for 5 min and removed from the cell for post-process analysis. Transmission Fourier transform infrared (FTIR) spectroscopy (Nicolet Nexus 670 with a MTCA detector), ellipsometry (J.A. Woollam Co. M-2000), and contact angle (Rame-Hart Inc. Model 100-00 goniometer) were used to characterize samples before and after processing. Toluene was the probe molecule used for ellipsometric porosimetry analysis. Metal-insulator-semiconductor (MIS) capacitors were fabricated by e-beam deposition of gold dots patterned with a shadow mask and tested electrically with an Agilent 4284A precision LCR meter at 1 MHz and a DC bias of –40V to +40V in a light tight box.

Highlights of Results and Accomplishments:

The thickness of the film added to the surface by chlorosilane treatment increased approximately linearly with the final contact angle (Figure 1). Samples were processed for 3 min with TMCS and MTCS dissolved in $scCO_2$ at 90 bar and 43^{o}C. Three different processes were examined: 1) MTCS and TMCS mixtures; 2) MTCS followed by TMCS; 3) TMCS followed by MTCS. The maximum contact angle is 96-98^{o} using chlorosilanes. The mixture data (open circles) showed that contact angles above 90^{o} could be achieved with film thicknesses above 450 Å. The contact angle is not only a measure of the hydrophobicity of the film deposited on the surface, but also a measure of the pore coverage. The higher the contact angle generally means the better and more uniformly the pores are covered. In contrast, processing sequentially achieved >90^{o} contact angles with film thicknesses as low as 150 Å. Thinner layers are preferred, since films added to the barrier layer decrease the linewidth available for copper metal in a subsequent step. The MTCS is used to form a polymer on the surface depositing a sealing layer. The reaction is complicated by the number and placement of the silanol (SiOH) groups remaining in the film. MTCS produces silanol groups by reacting with water molecules present in the fluid and for this reason is not desirable for repairing the film and decreasing the dielectric constant. TMCS is a monofunctional molecule and reacts readily with SiOH groups present in the p-MSQ and has successfully reduced the dielectric constant of plasma-damaged films to the value of the pristine surface.

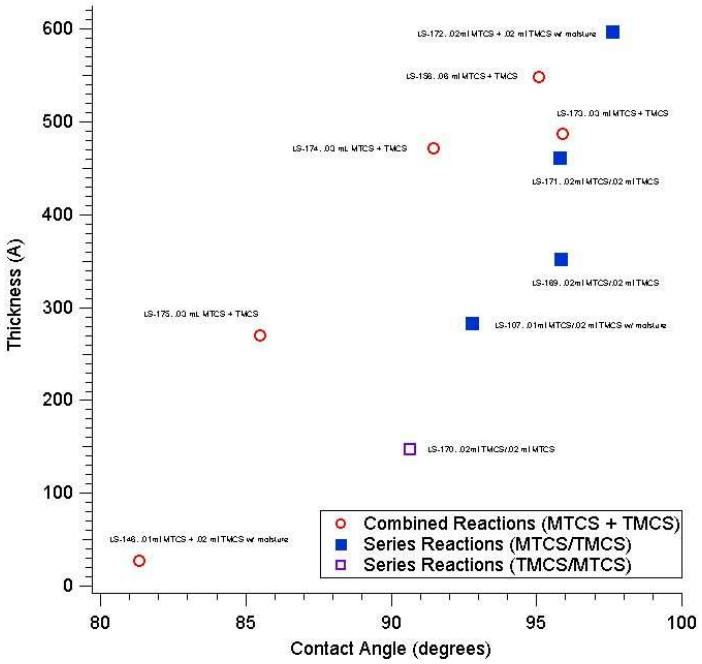

Figure 1. Thickness of the layer added to p-MSQ surfaces by treatment with chlorosilanes dissolved in $scCO_2$ as a function of the contact angle. Three processes are compared: MTCS + TMCS mixture, sequential process MTCS followed by TMCS, and sequential process TMCS followed by MTCS. Samples were processed for 3 min at 90 bar and 43 ^oC.

The results in Figure 1 demonstrate that independent control over the thickness is possible by introducing the MTCS and TMCS in separate steps, rather than mixing the two together. Contact angles from 92-97^o were produced by MTCS followed by TMCS, which were only weakly dependent on film thickness, ranging from 250-650 Å (solid squares). Reversing the sequence and introducing TMCS followed by MTCS yielded a lower contact angle (91^o) and a thinner film (150 Å) compared to the MTCS first process at the same concentrations. The TMCS reacts with surface sites, blocking these sites for further reaction with MTCS. With fewer points of attachment present, the polymer layer formed by MTCS was thinner, decreasing the contact angle. A similar mechanism explains the results for the MTCS and TMCS mixtures, except that reaction occurred in the fluid phase between MTCS and TMCS. Since TMCS has one point of attachment, once it reacts with MTCS, it is no longer available for reaction with the surface and it terminates a polymer chain formed by MTCS. This is the reason that higher concentrations of each chemical were required to achieve similar contact angles compared to the sequential process.

Samples LS-146 (MTCS+TMCS mixture) and 107 (sequential MTCS followed by TMCS) were characterized by ellipsometric porosimetry. These samples were treated with the same chemical concentrations with moisture present in the reactor, differing only in the way that the chemicals were applied. Isotherms measured by toluene adsorption showed that the open porosity was reduced from 40% on the starting, plasma-damaged sample to 32% by the MTCS+TMCS mixture and to 23% by the sequential treatment of MTCS followed by TMCS. The polymer film thickness was less than 50 Å and the contact angle was <82^o after processing with the chlorosilane mixture, whereas the polymer film was approximately 300 Å and the contact angle 93^o after the sequential process. These film thicknesses measured by conventional ellipsometry are representative of the repaired film and the added sealing layer in a probe area of approximately 1 mm. The pore size distribution of these samples obtained from ellipsometric porosimetry

isotherms (Figure 2) shows how the repair and sealing changes the average sizes of the pores. Both the mixture and sequential processes reduced the porosity of the low-k film. The pores after sequential processing (sample 107) were not completely closed off or sealed, but the height of the average pore radius decreased in size from the 1.8 Å of the starting plasma-ashed film producing a stronger secondary maximum at 0.92 nm than the mixture process (sample 146). The exposed pore volumes were reduced by processing with the chlorosilanes dissolved in $scCO_2$. The sequential MTCS followed by TMCS steps had the largest effect.

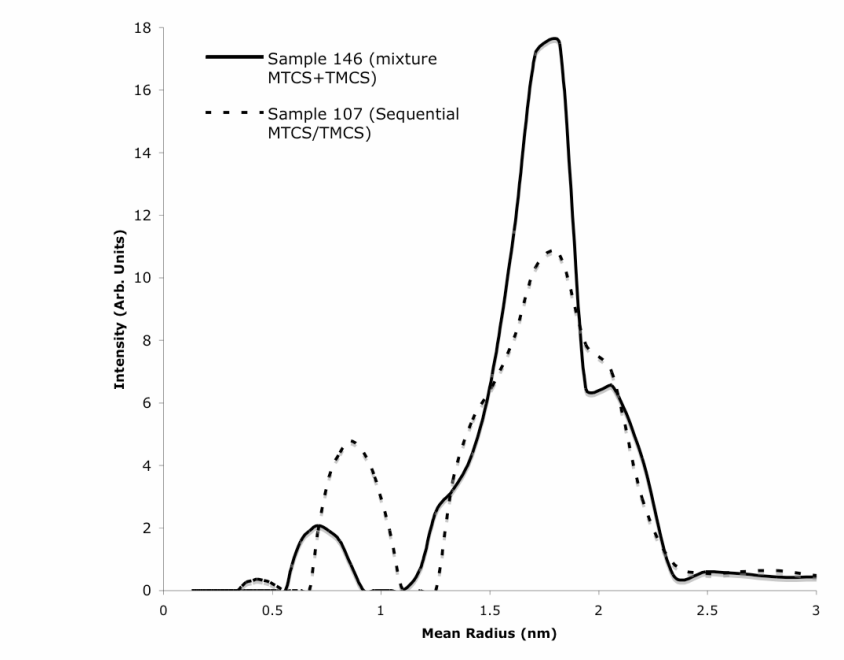

Figure 2. Pores size distribution obtained from Ellipsometric porosimetry analysis od samples LS-146 (mixed MTCS+TMCS process) and LS-107 (sequential MTCS/TMCS processes).

Industrial Interactions and Technology Transfer:

- Phil Matz and J. D. Luttmer, Texas Instruments
- Sharath Hosali and Sitaram Arkalgud, Sematech

ESH Impact:

- The use of CO_2 would eliminate solvents from backend of line processing of low-*k* films.
- Recycling the CO_2 would reduce the waste generated to the byproducts of the additives, which are easily separated from CO_2 by pressure drop.
- Successful implementation of a barrier film formed by chlorosilane addition would eliminate processing steps, since repair, capping, and barrier formation would be done in one reactor.

Publications:

- None

Conference Presentations:

- J. Muscat, "Environmentally Sustainable Process Chemistry at Solid Surfaces using Supercritical CO_2" *61st Northwest Regional Meeting of the American Chemical Society, Reno, NV, United States, June 25-28* 2006, RE06-139.
- L. N. Hatch, A. J. Muscat, B. Xie, "Repair and capping of porous MSQ films using chlorosilanes and supercritical carbon dioxide," *19th Rocky Mountain Regional Meeting of the American Chemical Society, Tucson, AZ, United States, October 14-18* 2006, RM-006.
- E. Vyhmeister, A. Muscat, L. A. Estévez, D. Suleiman, and L. Choate, "Study of low-k film repair and pore sealing using chlorosilanes dissolved in $scCO_2$," *19th Rocky Mountain Regional Meeting of the American Chemical Society, Tucson, AZ, United States, October 14-18* 2006.

Disclosures and Patents:

- Witvrouw, C. Van Hoof, R. C. Hellin Rico, A. J. Muscat, J. Fransaer, J.-P. Celis, "Method for encapsulating a semiconductor device in a microcavity by forming a porous film," patent application US 650,638.

Next-Year Plan:

- Demonstrate optimized sequential process using chlorosilanes to repair and seal ultra low-*k* films with good electrical properties and copper diffusion barrier properties.
- Investigate mechanism of repair and sealing layer deposition using new reactor fitted with *in situ* FTIR spectroscopy to understand fluid and surface chemistry in real time.

Research Report on the Screening of Four Options of PFOS Removal from Litho-Track Wastewater

Personnel:

PI:

- Reyes Sierra, Chemical and Environmental Engineering, UA

Other Research Personnel:

- Fiona L. Jordan, Research associate, Chemical and Environmental Engineering, UA
- James A. Field, Professor, Chemical and Environmental Engineering, UA

Graduate Students:

- Valeria Ochoa, Chemical and Environmental Engineering, UA

Undergraduate Students:

- Beshoy Latif, Chemical and Environmental Engineering, UA

Objectives:

The proposed research will conduct a preliminary assessment of the effectiveness of four different approaches for the removal of perfluorooctane sulfonate (PFOS) in semiconductor effluents, namely: *1)* Anaerobic reductive dehalogenation; *2)* Biomimetic dehalogenation (vitamin B_{12} - Ti(III) citrate); *3)* Activated carbon adsorption; and *4)* Biosorption. The long-term objective is to develop a highly effective, low energy wastewater treatment system to prevent emissions of PFOS to the environment. This research is conducted in the frame of a one-year seed project initiated on June 15, 2005.

Background:

PFOS and related perfluorinated alkyl surfactants (PFAS) are important components in a number of semiconductor operations. Although more environmentally benign chemistries are under development, commercial alternatives to PFOS for critical photolithography uses are still lacking. There is an urgent need for feasible methods to remove PFOS/PFAS from semiconductor effluents in order to minimize environmental release of these emerging pollutants. Application of conventional methods to the removal of PFOS in semiconductor effluents appears to be limited by technical and/or economic considerations.

Method of Approach:

Work conducted focused on:

1) Set up of analytical methods for the detection of PFOS in aqueous and solid matrixes.
2) Assessment of the inhibitory effect of PFOS, perfluorobutane sulfonate (PFBS, a surfactant proposed as a possible PFOS alternative), and tetramethyl ammonium hydroxide (TMAH, a common co-contaminant of PFOS in semiconductors wastewaters) to anaerobic microorganisms.

3) Preliminary assessment of the effectives of microbial reductive dehalogenation for the removal of PFOS in semiconductor effluents.
4) Preliminary evaluation of biomimetic reductive dehalogenation for the removal of PFOS. Initial experiments evaluating the removal of PFOS by sorption onto activated carbon and biosolids (wastewater treatment sludge) are ongoing.
5) Screening of the removal of PFOS by adsorption onto activated carbon and by wastewater treatment sludge

Highlights of Results and Accomplishments:

Analytical Methods: Analytical methods for the determination of PFOS and PFOS degradation products were set up. The approaches explored included: direct injection tandem mass spectroscopy (MS/MS), ^{19}F-nuclear magnetic resonance (^{19}F-NMR), and total dissolved carbon analysis. The relatively high atomic weight of the fluorine as compared to the hydrogen atom common in organic molecules facilitates the detection of different perfluorinated compounds in relatively clean matrices by MS/MS without prior chromatographic separation. Furthermore, two different methods were set up for the analysis of fluoride released from the dehalogenation of PFOS, one based on the use of ion-selective electrodes, the other on ion chromatography with suppressed conductivity detection. While MS/MS and ^{19}F-NMR are useful techniques for the analysis of PFOS in simple mixtures and relatively clean matrices, more specific and sensitive methods, such as liquid chromatography tandem mass spectroscopy (LC/MS/MS) and ion chromatography, are essential for the analysis and identification of PFOS/degradation products. Both analytical methods require expensive and sophisticated equipment that was not available to this project.

Microbial Toxicity: The inhibitory effects of PFOS, PFBS, and TMAH towards methanogenic microorganisms in anaerobic wastewater treatment sludge were tested at concentrations ranging from 5 to 500 mg/l. The highest concentration tested is close to the solubility limit for PFOS. Assays utilized acetate or H_2 as substrate. PFOS lead to a small decrease in the methanogenic activity (20% compared to the control) when present at 500 mg/l (Figure 1). None of the other compounds tested were found to cause significant microbial inhibition in these assays. These results are of significance because methanogenic microorganisms are the most sensitive microorganisms in anaerobic sludge digestors, which is the treatment unit more prone to toxic shocks in municipal wastewater treatment systems.

Anaerobic Biodegradation: Microbial reductive dehalogenation experiments were set up to determine the ability of six different microbial inocula to degrade PFOS. No evidence has been obtained yet that the perfluorinated compound is degraded after 6 months. If microorganisms do exit which are capable to degrade PFOS, they are likely to be found in matrixes exposed to PFOS for extended time periods (e.g. contaminated sediments). Our assays included wastewater treatment sludges previously exposed to PFOS, however, liquid and sludge retention times in wastewater treatment systems are relatively short.

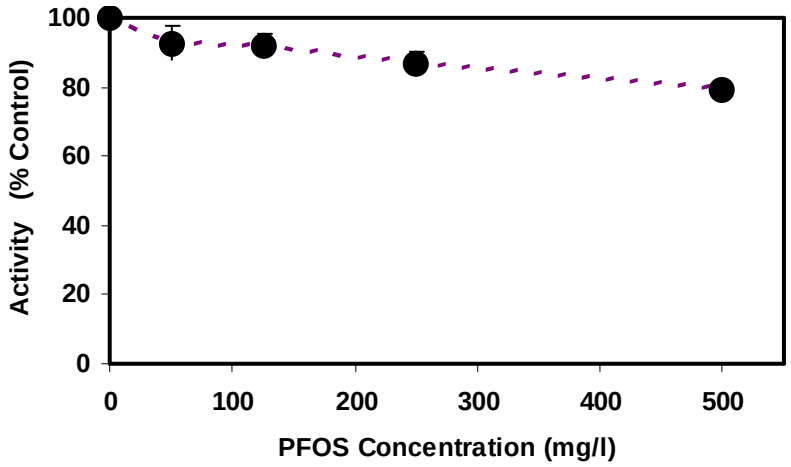

Figure 1. *Effect of PFOS on the methanogenic activity of a mixed anaerobic culture.*

Biomimetic Dehalogenation: Research conducted in the frame of this one-year project has unequivocally demonstrated that vitamin B_{12} (cobalamine) and Ti(III)-citrate can catalyze the reductive defluorination of PFOS. The evidence was based on fluoride release. This finding is highly significant because it is the first report of reductive dehalogenation of PFOS.

Preliminary experiments were performed to optimize the biomimetic dehalogenation of PFOS. The conditions considered included vitamin B_{12} and Ti(III) dosage, pH and temperature. As shown in Figure 2, the rate of PFOS degradation increased considerable with increasing temperature. As much as 18% PFOS defluorination, equivalent to the removal of three fluorine atoms, was obtained in less than one week. Increase of the reaction pH from 7.5 to 9.0 also had a positive impact on the rate of PFOS defluorination, although less marked compared to the results obtained at high temperature. These results have important implications for biodegradation since partially defluorinated PFOS derivatives, comparable to the products expected from reductive defluorination are known to be susceptible to biodegradation by aerobic bacteria (Key et al., 1998).

Additional research should attempt to identify the products formed from PFOS degradation and their characteristics.

Adsorption of PFOS by Activated Carbon: The effectiveness of granular activated carbon (GAC) and wastewater treatment sludge as sorbents for the removal of PFOS from aqueous streams was evaluated. Experiments conducted with PFOS solutions (0 to 150 mg/L) under well defined conditions (T= 30ºC, pH 7.2) showed that PFOS adsorbs readily to GAC. However, the affinity of PFOS for GAC is moderate to low when compared to contaminants traditionally removed by GAC adsorption. The feasibility of utilizing GAC to remove PFOS from semiconductor wastewaters will strongly depend on both the desired target effluent concentration of PFOS and the physico-chemical characteristics of the untreated wastewater.

Adsorption of PFOS by Biosolids: PFOS was shown to adsorb readily to anaerobic wastewater treatment sludge. GAC was more effective at very low equilibrium PFOS concentrations in the aqueous solution, whereas both sludge and GAC were relatively comparable at high equilibrium concentrations. These findings indicate that partial removal of PFOS by sorption to biomass should be expected during biological treatment of semiconductor wastewaters.

Industrial Interactions and Technology Transfer:

- Walter Worth, Sematech
- Tim Yeakley**,** Texas Instruments

ESH Impact:

This research considers different treatment options to reduce environmental releases of PFOS. Development of feasible abatement technologies to remove PFOS and related perfluoroalkyl surfactants (PFAS) from effluent streams would eliminate the main ESH concern associated with the use of PFAS in semiconductor manufacturing.

Publications:

- Ochoa, V. L. 2006. Removal of perfluorooctane sulfonate (PFOS) by sorption onto activated carbon and onto wastewater treatment sludge. August 2006. Environmental Engineering MS report. University of Arizona.

Disclosures and Patents:

- Biomimetic degradation of perfluorinated and highly-fluorinated organic compounds.
  R. Sierra-Alvarez.

Next-Year Plan:

- This was a one-year project. A follow-up project titled "Task ID: 425.015 - *Reductive Dehalogenation of Perfluoroalkyl Surfactants in Semiconductor Effluents*" was selected by ERC/SRC for core funding in the Spring 2006.

References:

- Key, B. D., Howell, R. D. & Criddle, C. S. (1998). Defluorination of organofluorine sulfur compounds by *Pseudomonas* sp. strain D2. *Environmetal Science and Technology*, **32**(15), 2283-2287.